Mantle Sulfides and their Role in Re–Os and Pb Isotope Geochronology

Jason Harvey

Institute of Geophysics and Tectonics
School of Earth and Environment
University of Leeds
Leeds, LS2 9JT
United Kingdom

Jessica M. Warren

Geological and Environmental Sciences
Stanford School of Earth Science
Stanford University
*Stanford, CA 94305-2115*
USA

Steven B. Shirey

Department of Terrestrial Magnetism
Carnegie Institution of Washington
*Washington DC 20015-1305*
USA

INTRODUCTION

Mantle sulfides (Fe–Ni–Cu-rich base metal sulfides or BMS; Fig. 1) play a crucial role in the distribution of Re, Os, and Pb in mantle rocks and are thus fundamental to obtaining absolute ages by direct geochronology using the Re–Os and Pb–Pb isotope systems on mantle samples. Mantle samples exist as hundreds of exposures of peridotites, pyroxenites and diamonds, either brought to the surface as accidental xenoliths and xenocrysts during kimberlitic or alkali basaltic volcanism (for comprehensive reviews, see Pearson et al. 2014; Aulbach et al. 2016, this volume; Luguet and Reisberg 2016, this volume), or as orogenic, ophiolitic and abyssal peridotite obducted at convergent margins and drilled / dredged from oceanic basins (e.g., Bodinier and Godard 2014; Becker and Dale 2016, this volume).

This chapter reviews the occurrence of BMS in mantle samples and the role that they play in controlling the Re–Os and Pb isotope systematics of the mantle. Included in this review is a discussion of the role BMS plays in recording the multiple depletion / enrichment / metasomatic events that the mantle has undergone and the preservation of chemical heterogeneities that are inherently created by these processes. Along with discussions of the utility of Re–Os and Pb isotope measurements, this review will also consider the potential pitfalls and some of the surprises that can arise when analyzing these BMS micro-phases. Specifically excluded from this review is the extensive literature on Re–Os and Pb for the geochronology of sulfide systems in magmatic ores. This study is another field entirely from the study of sulfides in their native mantle hosts because of the complicated magmatic concentration processes occurring at crustal levels.
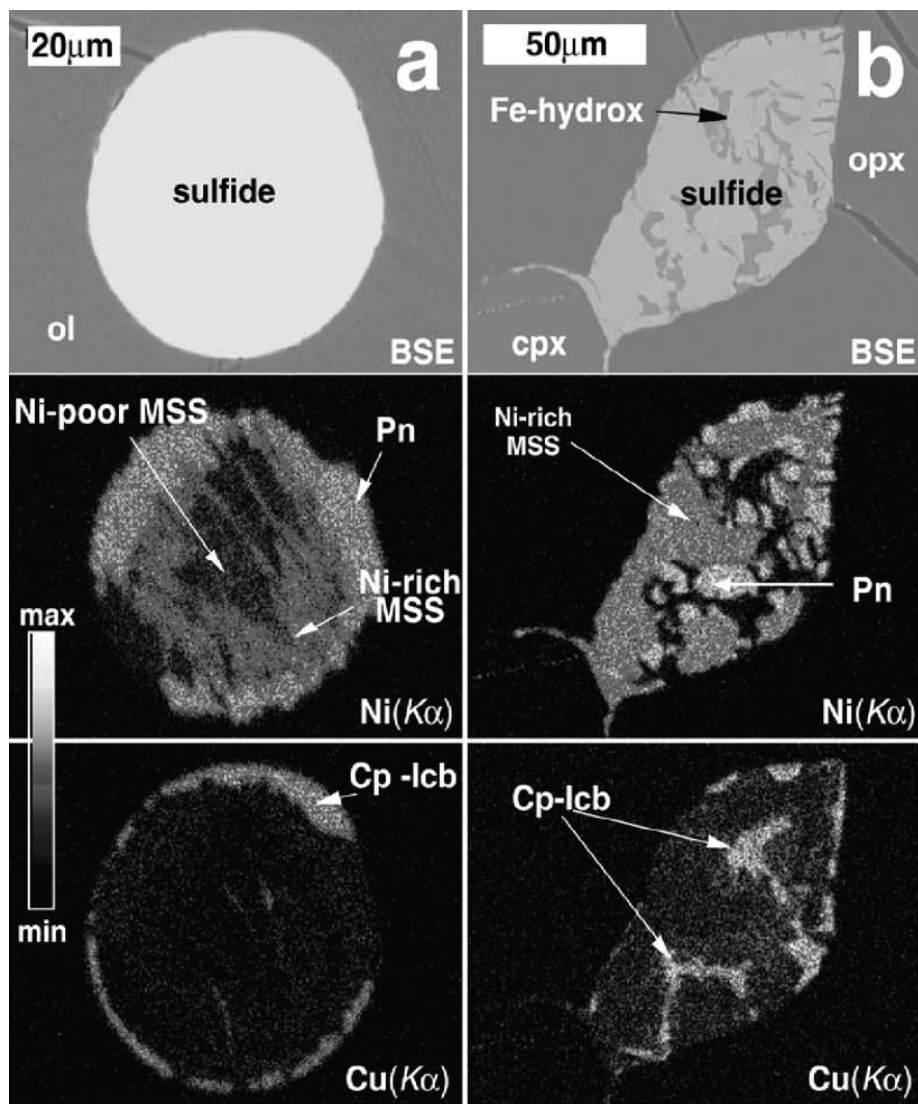
Figure 1. Backscattered electron and chemical maps of typical mantle BMS grains. (a) Enclosed; (b) interstitial BMS, both from Mt Gambier peridotites, SE Australia (Alard et al. 2002); BSE, backscattered electron; MSS, monosulfide solid solution; Pn, pentlandite; Cp-Icb, chalcopyrite–isocubanite. Grayscale indicates the relative abundance of a given element. Reproduced with permission of Elsevier BV from Alard O, Griffin WL, Pearson NJ, Lorand J-P, O'Reilly SY (2002). Earth and Planetary Science Letters 203:651–663.

This review represents the first time that BMS in mantle rocks and diamonds are discussed together for the purposes of age determination. The interested reader should also consult other articles that have discussed these topics individually (e.g., Shirey and Walker 1998; Burton et al. 1999, 2012; Pearson and Shirey 1999; Luguet et al. 2001, 2003, 2004, 2007, 2008; Richardson et al. 2001, 2004, 2009; Shirey et al. 2001, 2002, 2004a,b, 2013; Alard et al. 2002, 2005; Aulbach et al. 2004a,b, 2009a,b,c, 2011; Harvey et al. 2006, 2010, 2011; Pearson and Wittig 2008; Gurney et al. 2010; Shirey and Richardson 2011; Warren and Shirey 2012).
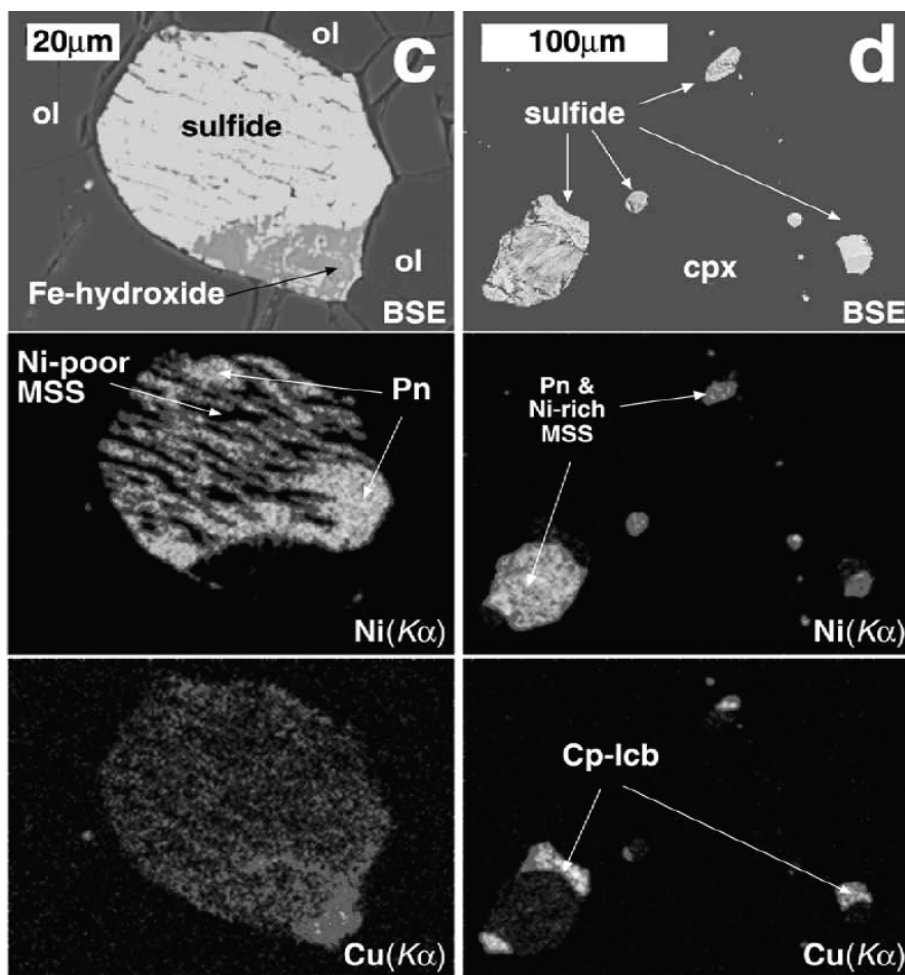
Figure 1 (Cont'd). Backscattered electron and chemical maps of typical mantle BMS grains. (c) intergranular BMS from Montferrier, French Massif Central (Alard et al. 2002); (d) cpx-enclosed BMS from Montboissier, French Massif Central (Alard et al. 2002). BSE, backscattered electron; MSS, monosulfide solid solution; Pn, pentlandite; Cp-Icb, chalcopyrite–isocubanite. Grayscale indicate the relative abundance of a given element. Reproduced with permission of Elsevier BV from Alard O, Griffin WL, Pearson NJ, Lorand J-P, O'Reilly SY (2002) Earth and Planetary Science Letters 203:651–663.

BACKGROUND

Through the 1980s, much of the information obtained regarding mantle composition and its inherent heterogeneity was derived through indirect evidence, i.e., the study of basaltic volcanism and the interpretation of its isotopic signatures and trace element compositions (e.g., Zindler and Hart 1986). This method of studying inaccessible regions of the mantle relies heavily on the fundamental assumption that isotope ratios of a source peridotite are faithfully transferred to the resultant melt. However, isotopic studies of mantle rocks have shown that melts average out some of the variability and extreme depletions present in the mantle, especially when the melting region is larger than the scale of heterogeneity (e.g., Saal et al. 1998; Cipriani et al,. 2004; Harvey et al. 2006; Liu et al. 2008; Maclennan 2008; Warren et al. 2009; Stracke et al. 2011; Day 2013; Lassiter et al. 2014; Gannoun et al. 2016, this volume).

The focus on basalts is not only because of a lack of mantle rocks exposed at the Earth's surface. Problems arise in analyzing mantle samples because of the mobility during melting of the incompatible trace elements upon which early geochronological measurements relied (e.g., Rb–Sr, Sm–Nd, U–Pb, Th–Pb, Lu–Hf isotope systems).

Mantle rocks exposed at the Earth's surface typically undergo melting (i) as a result of adiabatic decompression, such as beneath a mid ocean ridge, continental rift, or in a mantle plume, and/or (ii) by lowering the solidus with CO_2 or water such as when fluid fluxes into the mantle wedge at convergent margins, or carbonated peridotite generates carbonatite and kimberlite. In peridotites, melting is frequently overprinted by melt–rock interaction at a variety of scales and intensities (Warren 2015). Observations from seismic investigations, convection models, and basalt geochemistry also indicate that the mantle is heterogeneous due to prior episodes of melt depletion and enrichment (e.g., Stixrude and Lithgow-Bertelloni 2012; Dalton et al. 2014). The overprint of recent melt addition makes it difficult to "see through" metasomatic processes and determine the nature and, critically, the timing of melt-depletion in the mantle using lithophile elements. In contrast, the highly siderophile elements (HSE), which comprise the platinum group elements (PGE: Ir, Os, Ru, Rh, Pt, Pd) and Re, are compatible at a bulk-rock scale during melting (Re excepted) and have increasingly been used to study mantle composition and processes.

Compared to the Earth's core, HSE in the mantle are highly depleted (around 10 mg·g^{-1} versus 30 ng·g^{-1}, respectively; Palme and O'Neill 2003; Lorand et al. 2008). However, these concentrations in the mantle are still unexpectedly high compared to those predicted by core–mantle separation models (e.g., Borisov et al. 1994). The most likely explanation for the elevated HSE concentrations in the Earth's mantle is the "late veneer" hypothesis - an influx of meteorites impacting the Earth after core–mantle differentiation (Kimura et al. 1974; Chou 1978; Holzheid et al. 2000; Palme and O'Neill 2003; Lorand et al. 2008; Walker 2009).

Two of the HSE, rhenium and osmium, comprise the Re–Os isotope system. Osmium remains in the mantle residue during bulk peridotite melting, while Re behaves incompatibly, so basaltic melts contain relatively little Os. Consequently, metasomatic and refertilization processes involving silicate melts can have little overall effect on the Os isotope ratio of residual mantle, which is fixed by its high Os content. As such, the Re–Os system in ultramafic rocks is generally regarded as the most favorable isotopic system for recovering model ages of mantle melting events (different types of model ages based upon Re–Os isotope systematics are discussed later in this chapter), even though they may contain inherent uncertainties of up to 300 Ma caused by heterogeneity or poor characterization of reference reservoirs such as the mantle (Carlson 2005; Rudnick and Walker 2009). As a result, over the past 26 years Os isotopes have been used routinely to date the melting events that an individual portion of the mantle has experienced, i.e., the transformation of fertile asthenospheric material into a depleted, buoyant lithosphere (e.g., Walker et al. 1989; Snow and Reisberg 1995; Pearson et al. 1995a; Reisberg and Lorand 1995; see also Luguet and Reisberg 2016, this volume, and Aulbach et al. 2016, this volume, for comprehensive reviews).

Partitioning experiments (see Brenan et al. 2016, this volume, for details) have consistently demonstrated that PGE, including Os, on the whole behave as a group of strongly chalcophile and siderophile elements in mantle peridotites, being hosted—in the case of moderately melt-depleted ultramafic lithologies—entirely in accessory Fe–Ni–Cu BMS. As will be discussed in more detail later in this chapter, BMS therefore exert the main control on Re–Os isotope systematics in most ultramafic samples. The high K_d^{Os} $_{sulfide/silicate}$ of ~10^5–10^6 therefore ensures that bulk-rock $^{187}Os/^{188}Os$ is tracked by the behavior and abundance of BMS in the mantle. However, in highly depleted and/or altered peridotites, HSE are often hosted in refractory platinum-group minerals (PGM) and alloys (e.g., Luguet et al. 2007; Lorand et al. 2013) that have formed from BMS as a consequence of reactions involving melts or fluids. Thus, in strongly melt-depleted and/or altered peridotites, the influence of PGM on Os mass balance should not be ignored. Platinum-group minerals are discussed in detail in O'Driscoll and González-Jiménez (2016, this volume).

In the mantle, BMS grains (Fig. 1) are usually present as trace or ultra-trace phases ($\ll 0.1$ modal %; e.g., Luguet et al. 2001). They have been observed as intergranular grains and as inclusions in silicate minerals in spinel lherzolite and spinel harzburgite xenoliths (Fig. 2; White 1966; Vakhrutshev and Prokoptsev 1972; MacRae 1979; Pasteris 1981; Amundsen 1987), garnet peridotite (e.g., Bishop et al. 1975; Meyer and Tsai 1979) and pyroxenite xenoliths (e.g., O'Reilly and Griffin 1987; Wilshire et al. 1988). Similar BMS grains are also found in abyssal peridotites (Fig. 3; e.g., Luguet et al. 2001, 2003; Alard et al. 2005; Harvey et al. 2006; Warren and Shirey 2012; Marchesi et al. 2013), orogenic peridotites (e.g., Reisberg et al. 1991; Luguet et al. 2007; Lorand et al. 2008; van Acken et al. 2010a), and ophiolites (e.g., Luguet et al. 2004). In diamonds they are recognized as a common group of mineral inclusions, although 99% of gem-quality macroscopic diamonds are inclusion-free (Stachel and Harris 2008).

In the last 15 years, the accurate and precise measurement of Re–Os isotope systematics in individual BMS grains has become possible (e.g., Pearson et al. 1998; Burton et al. 1999; Richardson et al. 2001; Shirey et al. 2001; Griffin et al. 2002). The utility of Re–Os measurements for individual BMS grains has become increasingly apparent in light of growing evidence for
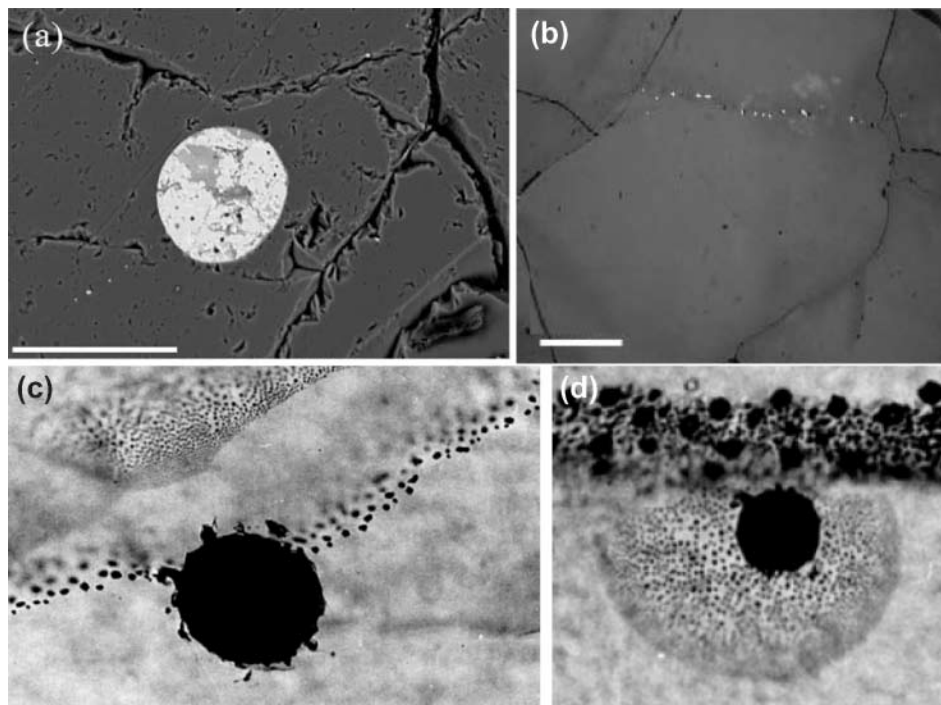
Figure 2. (a) Back scattered electron image of Type-1 BMS enclosed within host olivine grain from a lherzolite xenolith (Harvey et al. 2010). Several tiny BMS grains to the lower left of the main sulfide may be evidence for decrepitation resulting from rapid decompression as host xenolith is brought to the surface. Scale bar 100 μm. (b) Reflected light image of a trail of sulfide inclusions and silicate melt inclusions, precipitated from a C–O–S–H-rich fluid, spanning a fractured olivine grain that was subsequently annealed. Scale bar 100 μm. (c) Transmitted light image of a Type-1 enclosed BMS in a clinopyroxene megacryst, with clear evidence of decrepitation evidenced by trails of minute BMS grains leading away from the main sulfide. Field of view 400 μm. (d) Transmitted light image of a clinopyroxene megacryst containing "exploded" BMS grain surrounded by a cloud of minute BMS droplets which escaped from the main sulfide through decrepitation and decompression (Andersen et al. 1987). Field of view 300 μm. (a) and (b) reproduced from Harvey J, Gannoun A, Burton KW, Schiano P, Rogers NW, Alard O (2010) Geochimica et Cosmochimica Acta 74:293–320, (c) and (d) from Andersen T, Griffin WL, O'Reilly SY (1987) Lithos 20:279–294 with premission of Elsevier BV.
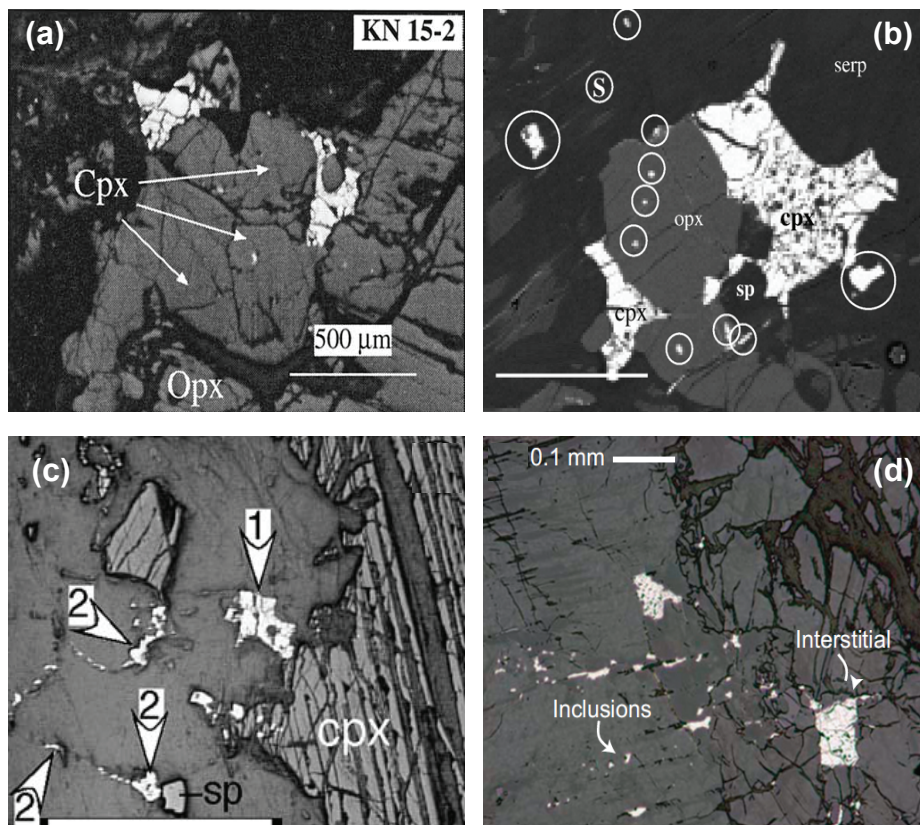
Figure 3. Backscattered electron images of clinopyroxene-spinel-metasomatic BMS associations in abyssal peridotite. (a) Large metasomatic BMS grain (light gray) interlocked with magmatic clinopyroxene (cpx) surrounding a large orthopyroxene porphyroclast (opx) from the Kane Fracture Zone, Mid-Atlantic Ridge. (b) Clinopyroxene (cpx), with strongly arcuate and curvilinear grain margins, intergrown with residual orthopyroxene. A secondary origin for the clinopyroxene is suggested by the non-equilibrium dihedral angles between clinopyroxene grains, the common association of clinopyroxene with secondary BMS grains (S, circled), and the interstitial location of clinopyroxene. From the 15° 20' N Fracture Zone, Mid-Atlantic Ridge. Scale bar 200 μm. (c) Base metal sulfide (arrow 1) along the margins of coarse clinopyroxene, with stringer of metasomatic BMS in close association with spinel, from the 15° 20' N Fracture Zone, Mid-Atlantic Ridge. Scale bar 500 μm. (d) Intergranular BMS at boundary between olivine and pyroxene, and as inclusions in pyroxene from the SW Indian Ridge. (a) reproduced from Luguet A, Lorand J-P, Seyler M (2003) Geochimica et Cosmochimica Acta 67:1553–1570 and (d) from Seyler M, Lorand J-P, Toplis MJ, Godard G (2004) Geology 34:301–304 with permission of Springer-Verlag.

the disturbance of bulk-rock HSE systematics by C–O–H-bearing fluids (e.g., Alard et al. 2011) and sulfur-saturated silicate melts (e.g., Harvey et al. 2015, and references therein). Distinct generations of PGM and BMS grains have different Re–Os isotopic signatures, thus leading to the observation that the mantle has a heterogeneous isotopic composition at various length scales (Rehkämper et al. 1999; Griffin et al. 2002; Alard et al. 2005; Beyer et al. 2006; Frei et al. 2006; Harvey et al. 2006). Moreover, in the last few years, combined Pb–Pb and Re–Os isotope studies of peridotite-hosted sulfides have shed new light on mantle geochronology (Burton et al. 2012; Warren and Shirey 2012).

Whole-rock Re–Os analyses of mantle-derived peridotites almost inevitably reflect the mixing of different generations of BMS because they have experienced multiple generations of

processes. The movement of Os during melting, recrystallization, or metasomatism may occur independently of Re and there can be separate addition of Re (e.g., Alard et al. 2002; Griffin et al. 2002, 2004), making the interpretation of bulk-rock Re–Os isotope data ambiguous in some samples, in the context of the timing of melt depletion (see reviews in Reisberg et al. 2004; Carlson 2005; Rudnick and Walker 2009). For example, in the study of BMS inclusions in the Western Gneiss region of Norway, Beyer et al. (2004) identified at least two generations of BMS with model ages that ranged from 4.0 to < 0 Ga. Similarly, in the study of Marchesi et al. (2010) of BMS grains from the Ronda peridotite, Spain, multiple generations of BMS were detected at the thin section scale, implying that the whole-rock Os isotope composition and model ages of these samples are controlled by the modal abundance and Os contents of distinct generations of BMS. Such variability at the mineral scale overprints the inherent heterogeneity known to exist in mantle reservoirs fostering concerns that the mantle is adequately homogeneous in terms of $^{187}Os/^{188}Os$ to be described by large-scale geochemical reservoir systematics (Meibom et al. 2002). Although unradiogenic $^{187}Os/^{188}Os$ in peridotitic residues often can be adequately explained by ancient melt depletion, using bulk-rock Re–Os isotope systematics indiscriminately can have its drawbacks (Reisberg et al. 2004; Rudnick and Walker 2009). Like the standard caveats in other radiogenic isotopic systems, the Re–Os geochronology of bulk-rock peridotites has two built-in weaknesses: (i) mixing ages can be generated that are not geologically meaningful model ages, and (ii) potential parent (Re)–daughter (Os) mobility either directly or in sulfide liquids at deep-mantle temperatures lead to problems in interpreting Re–Os isotopic composition of sulfides as an absolute age.

The utility of the Re–Os isotope system as a geochronometer thus lies in the ability of BMS to retain an Os isotope ratio that may have been generated billions of years ago. Despite the low closure temperature for Re–Os (e.g., ≤300 °C for pyrrhotite; Brenan et al. 2000), the low diffusivity of Os in silicate materials (Behrens et al. 1990; Cherniak 1995; Ganguly et al. 1998a,b; Burton et al. 1999) means that once Os is contained in BMS, it is difficult to equilibrate the Os isotope ratio of a BMS grain with surrounding silicates. For example, for a BMS inclusion in olivine, if the $K_d{}^{Os}{}_{sulfide/olivine}$ is 1, then at 1200 °C $D_{Fe–Mg}$ in olivine is about 10^{-17} m^2s^{-1} (Chakraborty 1997) and the diffusion distance in 10^6 years is about 1.7 m (using the approximation $x^2 \sim Dt$). However, using a K_d of 10^6 for sulfide/olivine; i.e., a more realistic partition coefficient as derived from experimental data and measurement of natural samples, the diffusional flux drops by 4 orders of magnitude about 10^{-21} m^2 s^{-1}, and the diffusion distance is reduced to less than 0.5 mm. This makes the retention of ancient $^{187}Os/^{188}Os$ in a BMS grain trapped within a silicate much more plausible, irrespective of re-equilibration of silicates with metasomatic events subsequent to BMS grain isolation.

ANALYTICAL METHODS AND PRACTICAL ASPECTS OF SAMPLE PREPARATION

Over the last 15 years or so, two main methods have been developed for the analysis of Re–Os isotopes in BMS grains; (i) *in situ* laser ablation multi-collector inductively coupled plasma mass spectrometry (LA MC ICPMS) and (ii) sulfide extraction, chemical purification, and thermal ionization mass spectrometry (TIMS). Lead isotopes have also been measured using the TIMS technique, as well as by *in situ* secondary ion mass spectrometry (SIMS). There are distinct advantages and disadvantages associated with each analytical method, particularly with respect to sample preparation and interpretation of the information obtained.

Early work on Pb, Re, Os, and other PGE concentrations in BMS grains was performed by *in situ* proton microprobe analysis coupled with a MC ICPMS (Bulanova et al. 1996; Guo et al. 1999). Due to limited availability and because detection limits were higher and standard reproducibility for this method was less precise, *in situ* determination of Re and PGE

concentrations are now routinely performed using LA ICPMS (e.g., Alard et al. 2000, 2002 2005; Lorand and Alard 2001; Luguet et al. 2001; Pearson et al. 2002). For Os isotope ratios, *in situ* LA MC ICPMS typically employs a Nd:YAG 266-nm or 213-nm laser microprobe coupled to the mass spectrometer (e.g., Pearson et al. 2002; Nowell et al. 2008). The new generation of Excimer lasers are also eminently suitable for this purpose and are routinely employed for PGE analysis in metals, BMS grains and PGM (e.g., van Acken et al. 2012).

The spatial resolution achievable by LA MC ICPMS and SIMS, with analytical spot sizes that are typically as small as 50 μm, means that multiple analyses can be made on large (>100 μm) BMS grains, allowing within-grain heterogeneity to be assessed and any contributions from exsolved phases to be examined. Also, it is possible to raster across large BMS grains to search for variability across a larger area. For smaller grains, the entire grain can be analyzed by increasing the beam diameter such that the whole grain and even part of the surrounding host phase are incorporated in the analysis, reducing the likelihood of skewing of data by omitting sub-grain exsolution products. As silicate or oxide phases are unlikely to contain significant amounts of Re or Os, letting the laser overlap small amounts of surrounding silicates in order to capture the entire volume of the sulfide is unlikely to result in any significant interference on the analysis of the sulfide itself. The ability to sample grains of a wide range of sizes is only limited by the amount of Re and / or Os contained in the grain and the resulting analytical precision that will be achieved. Moreover, after ablation, samples can be polished down further to reveal more material for subsequent ablations, as long as the sulfide is large enough. Hence, a benefit of *in situ* analysis is that internal textures of BMS grains can be assessed prior to ablation and that profiles through individual grains are possible.

For the analysis of Re–Os in BMS grains by LA MC ICPMS, a mass bias correction is made by bleeding a dry aerosol of Ir into the gas line between the ablation cell and the ICPMS. Although the values obtained by plasma machines may drift over the course of a day, this can easily be corrected for by analyzing a sulfide standard at regular intervals during the analytical session. Typically, instrument induced drift is limited to 1–2 % over a 24-hour period (Pearson et al. 2002).

However, there are several limitations that have been highlighted regarding the analysis of BMS grains using LA MC ICPMS. The overlap of ^{187}Re on ^{187}Os needs to be corrected for by measuring ^{185}Re and using the natural ratio of ^{187}Re/^{185}Re of 1.6742. This isobaric interference can only be corrected for accurately when the ^{187}Re/^{188}Os is below a certain level. There has been some debate as to exactly what the limit should be for precise ^{187}Os/^{188}Os determination. The early study of Pearson et al. (2002) defined the limit of ^{187}Re/^{188}Os as <1.2 but this was later refined by Nowell et al. (2008), who suggested that the much lower ^{187}Re/^{188}Os value of <0.5 is more appropriate to ensure an accurate correction of the isobaric overlap. Pragmatically, this ^{187}Re/^{188}Os upper limit rules out the analysis of eclogitic sulfides that have been in equilibrium with basaltic and more evolved liquids—leaving peridotitic sulfides to be tractable. LA MC ICPMS only allows the determination of mass ratios, and not Re and Os concentrations, as internal normalization is not possible. Semi-quantitative Os contents in BMS grains can be obtained indirectly by comparing the signal intensity of an unknown to that obtained on the standard that is analyzed throughout the analytical session. There are, however, several potential limitations on the accuracy of these data. For example, it is extremely difficult to manufacture completely homogeneous sulfide standards for LA MC ICPMS. Nanoclusters of PGE alloy may form when the bead is not quenched instantly, resulting in the possibility of tiny, but significant, heterogeneities on an analysis-to-analysis basis. Ablation conditions may also vary. This method cannot make use of an internal standard and optimum signals may not always be obtained when analyzing particularly small unknowns. In BMS grains of sufficient size, it may be possible to ablate a second hole, next to that ablated

for isotopic analysis, for concentration determinations. However, this is only advisable when a large enough area of homogeneous sulfide is available for both measurements.

Where *in situ* methods have a distinct advantages over TIMS analyses is the speed of analysis. A typical analysis of a BMS grain, including laser warm up time, the ablation of the sulfide itself and then wash out to return to the instrumental baseline often takes less than 15 minutes. Sample preparation time is, in general, low compared to the amount of chemical purification necessary for a TIMS analysis, and is limited to the amount of time necessary to cut and polish a thick (ca. 250 μm) section, inspect the section under microscope, and to locate the BMS grains. Significant sample preparation time is also saved as a single polished section may contain several 10s of grains that would otherwise have to be prepared separately for analysis by TIMS. However, care must be taken in the preparation of sulfides for laser ablation analysis as it is possible to inadvertently pluck some phases from the BMS grains. For example, removal of exsolved chalcopyrite will skew measured Re/Os ratios to lower values, as chalcopyrite may preferentially partition Re (Richardson et al. 2001). Nonetheless, several hundred sulfides can be analyzed in the same time it takes to prepare and analyze a single BMS grain by TIMS.

Textural and mineralogical information relating to a BMS grain and its surroundings is preserved using *in situ* measurements. This can be particularly useful in immediately identifying BMS that are enclosed versus interstitial relative to the silicate phases. However, the work of Alard et al. (2002) demonstrated that the simplistic distinction between "enclosed" versus "interstitial" as corresponding to "primary" versus "metasomatic" BMS grains is not appropriate in many cases.

The large datasets obtainable by LA MC ICPMS often have to be heavily filtered for sufficiently low Re/Os ratios and for high enough Os contents to give precise isotopic analyses, meaning that, in some extreme examples, up to 90% of a dataset needs to be cut because the ^{187}Re/^{187}Os isobaric interferences cannot be resolved. If bulk-rock Re–Os ratios are also available, then it is advisable to assess the remaining BMS data points in the context of the data on the bulk rock. One of the benefits of being able to rapidly generate large datasets is that probability density plots of Os isotope ratios and model ages (see section on the utility of sulfide Re–Os and Pb isotope geochronology below) can be generated. The large number of analyses required to produce meaningful probability density plots often, but not always, precludes this type of study using TIMS analyses alone (cf. Pearson and Wittig 2008).

The TIMS method is conceptually much simpler than LA MC ICPMS—simply physically remove the sulfide grain by picking or drilling it out from surrounding silicate minerals. There also are some distinct advantages of analyzing individual BMS grains by TIMS. The level of precision and accuracy attainable for Re–Os–Pb isotope analysis is substantially higher, allowing precise measurements at the picogram level for Os and Re and at the tens of picogram level for Pb. This level of sensitivity makes TIMS the more desirable method for the analysis of Re–Os isotope systematics of diamond-hosted BMS, which tend to be very small. By adding enriched spike solutions (^{185}Re ^{190}Os ^{205}Pb) to samples during their dissolution, precise elemental abundances can be obtained in addition to isotope ratios. Without prior knowledge of the paragenesis of a sulfide grain, it can be difficult to accurately spike a sulfide and only an estimate can be made in advance. In practice, the accuracy of a TIMS measurement compensates for under- or over-spiking, except when either excess is catastrophically large. Weighing errors can artificially influence the measurement, particularly for smaller sulfide grains that may have a mass of only a few micrograms, but the use of mixed spike solutions minimizes uncertainty in the analysis.

Sample preparation is by far the greatest drawback of TIMS analysis. Extraction of the sulfide from the host rock, dissolution and purification are time consuming. If the sulfide is being extracted from a polished block, then this represents an additional step in the sample

preparation compared to LA MC ICPMS. As with the polishing of samples for laser ablation, the problem exists of incomplete extraction of grains. When a sulfide is extracted from a host diamond or a thick section, the hole can be inspected to check that no sulfide phase remains. However, if sulfides are handpicked from a peridotite crushate or magnetically separated from an aggregate, then this check is not possible and the possibility exists of fractionating Re from Os in an individual BMS grain and producing an artificially low Re/Os ratio (e.g., Harvey et al. 2010, 2011). The advantage of hand picking or magnetically separating sulfide grains is that no material is lost compared to polishing down through a sulfide to identify a large enough grain to analyse. However, individual grains could become broken and grains can be fractured and entire fragments of a sulfide lost. Handpicking of sulfides from a crushate may also result in the preferential selection of interstitial grains that are easier to liberate from a bulk rock crushate.

For the analysis of diamond-hosted sulfides (Fig. 4), the distinction between an eclogitic or peridotitic origin for the sulfide is important because of the large Os concentration differences
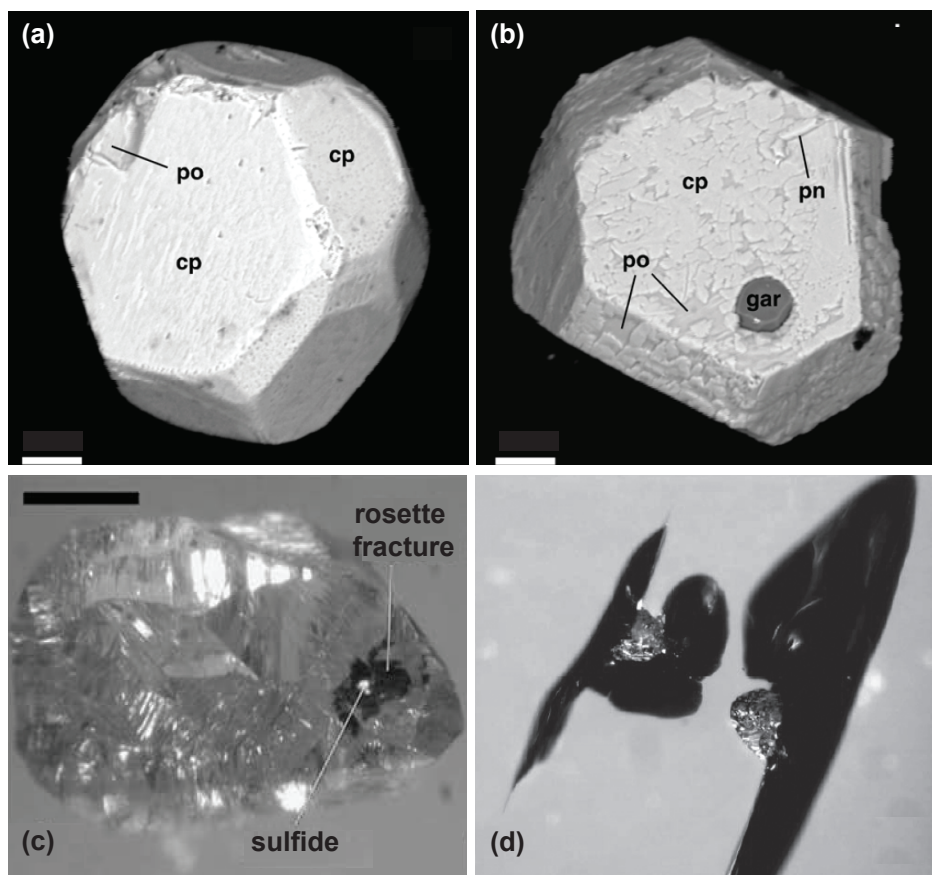
Figure 4. Eclogitic (a) and (b) and peridotitic (c) and (d) diamond-hosted BMS inclusions. (a) and (b) Back-scattered electron images of eclogitic BMS inclusions liberated from Jwaneng diamonds, Kaapvaal craton (scale bar in μm). Pyrrhotite (po), chalcopyrite (cp), and pentlandite (pn). (c) and (d) Visible light images of peridotitic BMS inclusions (~150 μm diam) surrounded by rosette fracture systems in a diamond recovered from Panda, Slave craton, Canada. Reproduced from Aulbach S, Stachel T, Creaser RA, Heaman LM, Shirey SB, Muehlenbachs K, Eichenberg D, Harris JW (2009) Lithos 112:747–757 with the permission of Elsevier BV and Gurney JJ, Helmstaedt HH, Richardson SH, Shirey SB (2010) Economic Geology 105:689–712, under the Fair Use provision.

that can be up to 1000 times less in the eclogitic sulfides. This distinction is typically made by placing the sulfide on a conducting carbon sticky disk in a scanning electron microscope and analyzing the grain for Fe, Ni, Cu, Co, and S. Exsolution features and grain surfaces can also be examined to determine if multiple BMS phases are present (Fig. 4a-b) and to check if the grain has been fractured. This technique could also be applied to BMS grains separated from bulk rock by magnetic separation in order to determine BMS paragenesis, but the textural context that is retained using *in situ* methods is still lost through the disaggregation of the bulk rock.

Two recent studies (Burton et al. 2012; Warren and Shirey 2012) have presented Pb isotope and concentration data for individual BMS grains from abyssal peridotites, measured using TIMS analytical methods. Burton et al. (2012) measured Pb compositions in sulfides from the same section of peridotite drill core that was previously analyzed by Harvey et al. (2006) for Re–Os compositions. Warren and Shirey (2012) measured Pb, Re, and Os isotopic compositions and concentrations in the same grain by extracting all three elements during the chemical purification procedure and employing spikes. Lead isotopic compositions have also been measured *in situ* by SIMS, using either a Sensitive High-Resolution Ion Microprobe (Eldridge et al. 1991; Rudnick et al. 1993b) or a Cameca IMS 1280 ion microprobe (Blusztajn et al. 2014). The main drawbacks of this technique are that [204]Pb concentrations are too low to be detected and Pb concentration data have large uncertainties due to the lack of low concentration sulfide standards.

## BASE-METAL SULFIDE OCCURRENCE, MAJOR ELEMENT GEOCHEMISTRY AND PETROLOGY

For nearly half a century, BMS have been identified in a number of mantle-derived materials, including: peridotite and pyroxenite xenoliths entrained in basaltic and kimberlitic rocks (Fig. 1; e.g., Meyer and Brookins 1971; Desborough and Czamanske 1973; Frick 1973; Vakhrushev and Sobolev 1973; Bishop et al. 1975; De Waal and Calk 1975; Meyer and Boctor 1975; Mitchell and Keays 1981; Lorand and Conquéré 1983; Dromgoole and Pasteris 1987; Fleet and Stone 1990; Szabó and Bodnar 1995), disaggregated clinopyroxene, garnet and diamonds preserved as megacrysts (Figs. 1 and 4; e.g., Peterson and Francis 1977; Gurney et al. 1984; Andersen et al. 1987; Fleet and Stone 1990; Rudnick et al. 1993b; Deines and Harris 1995; Bulanova et al. 1996); and tectonically exposed ultramafic sequences derived from the upper, mostly oceanic, mantle (Fig. 3; e.g., Lorand 1985, 1987; Luguet et al. 2004; Alard et al. 2005).

The interest in sub-mm BMS in ultramafic material stems from early, broad scale investigations into the behavior of BMS under magmatic conditions and sulfide liquid immiscibility in mafic and ultramafic rocks (Figs. 5 and 6; Bell et al. 1964; Kullerud et al. 1969; Naldrett 1969; Skinner and Peck 1969; Craig 1973; Misra and Fleet 1973; Haughton et al 1974; Usselman 1975; Buchanan and Nolan 1979; Fleet and Pan 1994; Karup-Møller and Makovicky 1995). More recently, experimental investigations into the behavior of BMS and, in particular, the HSE and strongly chalcophile elements that they contain, have provided a more comprehensive overview over a wide range of mantle *P–T–X* conditions (e.g., Bockrath et al. 2004; Ballhaus et al 2006; Holzheid 2010; and, in particular, see the review of experimental methods of Brenan et al. 2016, this volume). The most impressive, and economically interesting examples of the redistribution of BMS through magmatic processes are the large Fe–Ni–Cu-sulfide ore deposits such as Sudbury in Canada, Norilsk in Russia, and the Duluth Complex in the USA. Highly siderophile and chalcophile element-bearing ore deposits are reviewed in this volume by Barnes and Ripley (2016).

The major sulfide phases observed in mantle rocks are generally pentlandite ((Fe,Ni)$_9$S$_8$), chalcopyrite (CuFeS$_2$) ± pyrrhotite (Fe$_{1-x}$S) and, in isolated instances,
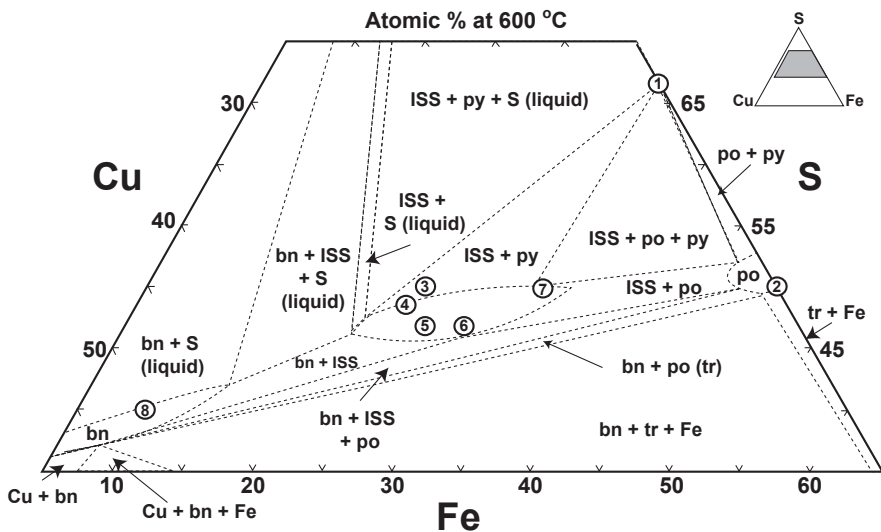
Figure 5. Phase relations in the central portion of the Cu–Fe–S system at 600 °C. Numbered circles represent the stoichiometric compositions for the minerals (1) pyrite, (2) troilite, (3) chalcopyrite, (4) talnakhite, (5) mooihoekite, (6) haycockite, (7) cubanite and (8) bornite. All phases and phase assemblages coexist with vapour. Modified after Cabri (1973).
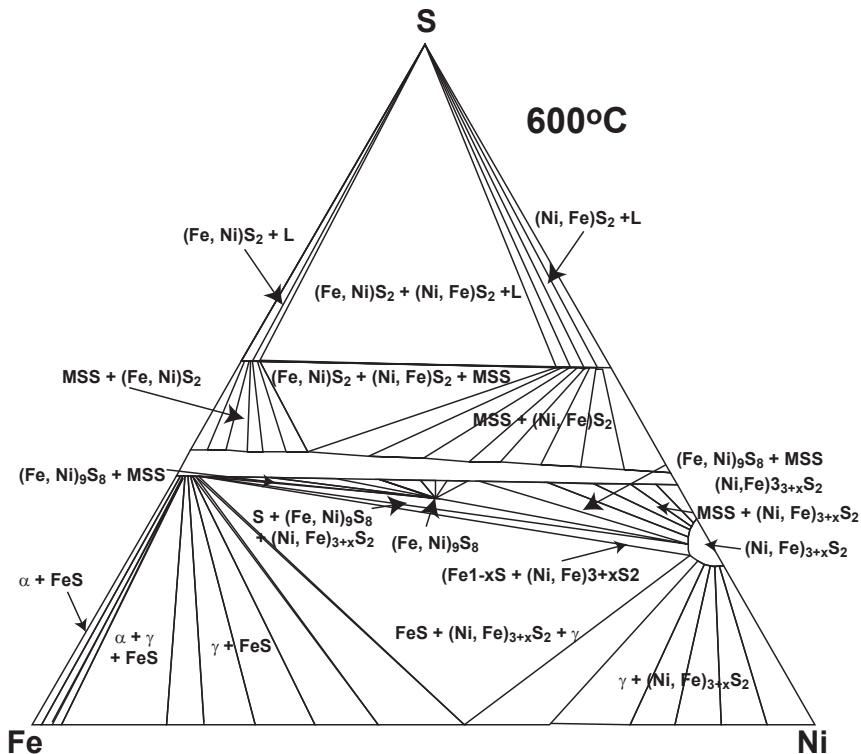

Figure 6. 600 °C isothermal section of the condensed Fe–Ni–S system (modified after Naldrett et al. 1969). All phases are in equilibrium with vapor.

bornite (Cu_5FeS_4), shown on phase diagrams for the systems Ni-Fe-S (Fig. 6) and Cu-Fe-S (Fig. 5). These phases are interpreted as representing the low-temperature ($< 300\,°C$) subsolidus assemblages formed first from monosulfide solid solution ($MSS = Fe_{1-x}, Ni_{1-x}\,S$; Fig. 6) and later from intermediate solid solution (ISS) of the Cu–Fe–S system (Fig. 5), and heazlewoodite (Ni_3S_2) solid solution (HzSS) of the Ni–Fe–S system (e.g., Cabri 1973; Lorand and Conquéré 1983; Dromgoole and Pasteris 1987; Szabó and Bodnar 1995; Guo et al. 1999; Fleet 2006; Lorand and Grégoire 2006). Bornite, if present, likely crystallizes from bornite solid solution (BoSS), which is shifted toward a higher Cu content (and higher metal/sulfur ratio) than chalcopyrite. At the ambient, high pressure and high temperature conditions of the mantle, BMS forms either a homogeneous sulfide melt (known as a *matte* if it is high abundance) or is only partially molten (Bockrath et al. 2004). Experimental work suggests that MSS is the main stable BMS phase in the uppermost convecting mantle (Bockrath et al. 2004). Independent of their tectonic origin, the BMS found in peridotites, i.e., MSS/pyrrhotite–pentlandite–chalcopyrite, are the result of fractional crystallization from a high temperature sulfide melt followed by sub-solidus re-equilibration. At 1192 °C, MSS with a composition close to FeS crystallizes, leaving a Cu–Ni-rich residual sulfide liquid at 1192 °C. As temperature decreases towards 1000 °C, the MSS field extends toward Cu and Ni-richer compositions. With continued cooling (between 800 and 900 °C, the ISS and HzSS fractionally crystallize from the Cu–Ni-rich residual sulfide liquid. This is often manifested as an outer rim on BMS grains or sometimes as veinlets escaping intergranular BMS. Subsequently, at ca. 600 °C, HzSS and the MSS may react and crystallize pentlandite, while chalcopyrite crystallizes from the ISS shortly afterwards at ca. 560 °C. Below 300 °C further exsolution into a Ni-poor MSS, Ni-rich MSS (>30 wt% Ni) and pentlandite takes place. However, when MSS–pentlandite–chalcopyrite melts, it does so incongruently, producing a Ni–Cu-rich sulfide melt, leaving behind a Ni–Cu-poor sulfide.

Peridotitic BMS represent ca. 0.1 vol% of the upper mantle, which corresponds to a S concentration of $250 \pm 50\,µg·g^{-1}$ (Lorand 1990; O'Neill 1991; Palme and O'Neill 2003), and therefore, typically, sulfides are exhausted from the mantle after 12–30% partial melting (Luguet et al. 2003; Lorand and Grégoire 2006; Alt et al. 2007). The extent of sulfide exhaustion depends on local sulfur abundance, pressure of melting (Mavrogenes and O'Neill 1999) and melt composition. These reactions with melting result in the formation of PGM that become the major carriers of the PGE, as discussed in detail in this volume by O'Driscoll and González-Jiménez (2016). During melting, Ir and Os are strongly partitioned into the MSS, whereas Cu, Pt and Pd are partitioned into the coexisting melt (Brenan et al. 2016 this volume). Monosulfide solid solution at 900–1100 °C can accommodate $>10^4\,µg·g^{-1}$ of Os, Ir, Ru, and Rh (Li et al. 1996; Alard et al. 2000; Brenan 2002; Mungall et al. 2005; Ballhaus et al. 2006), while pentlandite, chalcopyrite, and pyrrhotite can accommodate from $10^2–10^3\,µg·g^{-1}$ of each PGE (e.g., Peach et al. 1990; Fleet et al. 1996; Fonseca et al. 2011).

Alteration of primary BMS occurs by supergene weathering (Fig. 7), in the case of continentally derived non-cratonic peridotites and by hydrothermal alteration / seawater interaction, in the case of oceanic peridotites. These processes typically increase the number of sulfide minerals observed in ultramafic assemblages. For example, during serpentinization at low temperature ($<250\,°C$) and reducing conditions, BMS can experience desulfurization or, conversely, metal enrichment, to S-poor BMS such as heazlewoodite (Ni_3S_2), jaipurite (CoS), violarite ($FeNi_2S_4$), millerite (NiS, covellite (CuS), digenite (Cu_9S_5) and ultimately native metals or alloys such as copper or awaruite ($Ni_2Fe–Ni_3Fe$; Lorand and Conquéré 1983; Lorand 1987; Luguet and Lorand 1998; Alt and Shanks 2003; Bach et al. 2004; Marchesi et al. 2013; Schwarzenbach et al. 2014; Foustoukos et al. 2015). Continental supergene weathering also results in a loss of sulfur but, under oxidizing weathering conditions, it tends to produce Fe oxy-hydroxides at the expense of primary sulfides (Fig. 7; Dromgoole and Pasteris 1987; Lorand et al. 2003a).
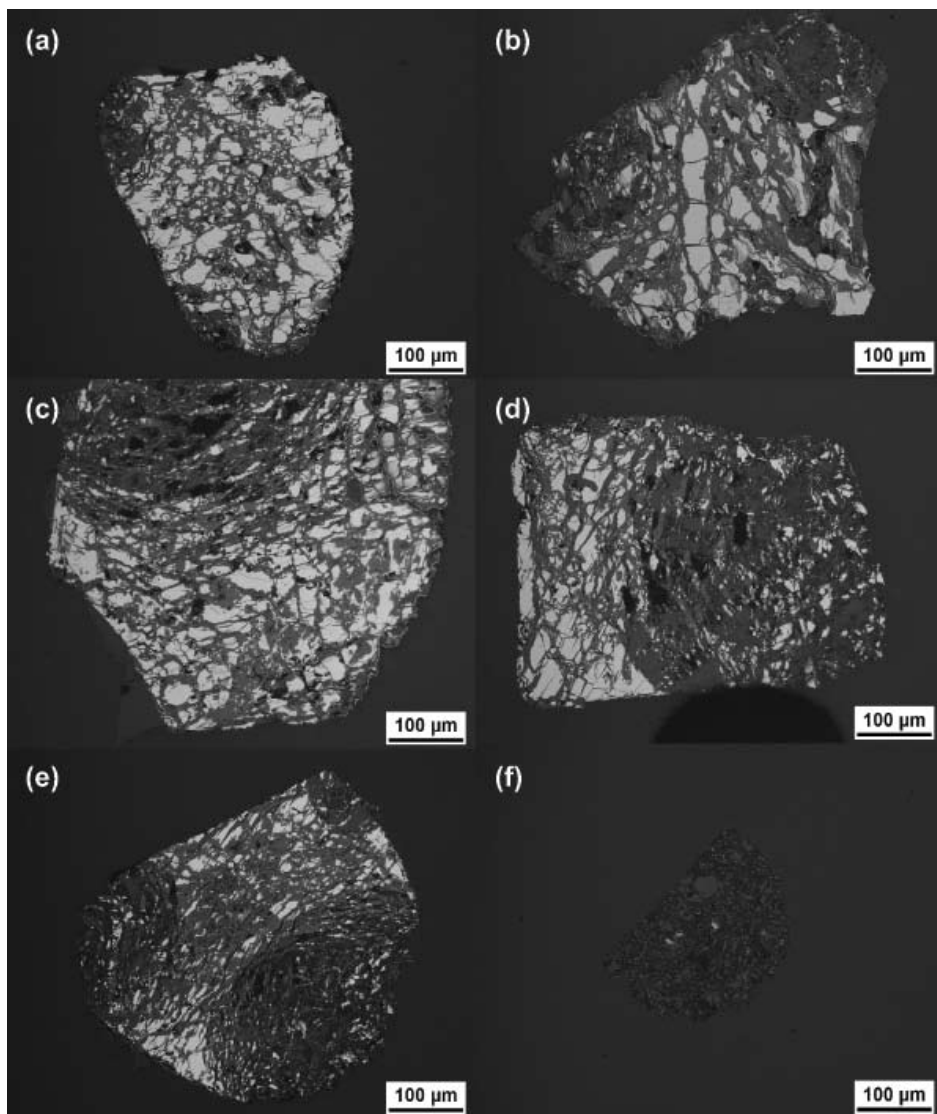
Figure 7. Progressively weathered BMS grains recovered from a Kilbourne Hole (NM, USA) peridotite xenolith (Harvey, unpublished data). Supergene weathering, resulting from interaction of interstitial BMS with meteoric water become increasingly weathered to Fe-oxyhydroxides (Lorand et al. 2003a) from (a) to (e), as sulfide oxidizes to sulfate, leading to loss of sulfur and oxidation of Os.

Peridotite-hosted sulfides

Mantle-derived BMS can be divided into those that are peridotite-hosted, pyroxenite-hosted, and diamond-hosted. Most primary BMS grains found in mantle peridotites have a diameter of 10–50 μm (Figs. 2 and 3; e.g., Guo et al. 1999), although in exceptional cases this may extend to 200 μm for sulfides enclosed in silicate grains (e.g., Beyer et al. 2004) and up to 500 μm for sulfides in intergranular interstices (e.g., Gonzáles-Jiménez et al. 2014). Sulfide commonly resides as a discrete inclusion within a silicate grain, but rarely within spinel (Ferraris

and Lorand 2008). Alard et al. (2000, 2002, 2011) and Lorand and Alard (2001) define Type-1 sulfides as sulfides enclosed in olivine, orthopyroxene and garnet that have MSS compositions with minor amounts of pentlandite and chalcopyrite. The Type-2 BMS of Alard et al. (2002) have compositions dominated by pentlandite and chalcopyrite, with little or no pyrrhotite or MSS. These BMS tend to be intergranular and restricted to grain boundaries, fractures and pockets interstitial to the silicate minerals, as well as metasomatic BMS encapsulated within secondary (i.e., melt-crystallized) clinopyroxene. Type-2 sulfides may be derived by crystallization from a melt or liquid that was trapped during partial melting (Frick 1973; Mitchell and Keays 1981; Hamlyn and Keays 1986; Dromgoole and Pasteris 1987; Szabó and Bodnar 1995; Fig. 1) or introduced after melt depletion as a metasomatic melt or volatile-rich fluid (e.g., Alard et al. 2002, 2011; Luguet et al. 2008; Harvey et al. 2011, 2015; Lorand and Luguet 2016, this volume). These sulfides are the most common BMS population in peridotites, whereas Type-1 sulfides are rare and generally restricted to peridotite xenoliths (e.g., Alard et al. 2002).

The original Type-1 and Type-2 definitions of Alard et al. (2002) encompass not only the geochemical, but also the petrological and textural contexts of BMS grains. Historically, the sub-division into Type-1 versus Type-2 BMS has served the BMS community well, yet the last decade of investigations has highlighted increasing difficulties with dividing mantle BMS into only two categories. In some instances, a third population of BMS may be present where limited mixing of Types 1 and 2 has occurred, resulting in a hybrid sulfide population that shares characteristics of both of its precursors (e.g., Griffin et al. 2002; Wang et al. 2009; Harvey et al. 2010). As will be discussed in the following sections, simple discrimination between "primary" versus "metasomatic" and "enclosed" versus "interstitial" can be difficult. In off-craton xenoliths, sulfide precipitation has also been attributed to sulfidation reactions between S-rich fluids and olivine, or metals dissolved in highly alkaline, volatile-enriched melts. Sulfides related to sulfidation have been identified in xenolith suites from the Kerguelen archipelago (Lorand et al. 2004), the Western United States (Lee 2002), and the Massif Central, France (Lorand et al. 2003b) and Languedoc, France (Alard et al. 2011).

A first order approximation of the nature of the BMS hosted in a particular peridotite, i.e., the balance of BMS composition resulting from melt depletion versus metasomatism, can be made based upon sulfide modal abundance. Sulfur, like Al, is moderately incompatible during partial melting (e.g., Burnham et al. 1998). A sulfide mode of 0.1 % is the approximate theoretical maximum that could be expected from primitive mantle, i.e., a portion of mantle that has not undergone any melt extraction. This is based upon a fertile mantle S abundance of $250 \pm 50 \, \mu g \cdot g^{-1}$ S (Lorand 1990; O'Neill 1991; Palme and O'Neill 2003) and assumes a metal:sulfur ratio of 2:1. Modal abundances of BMS can be determined by careful point counting (e.g., Luguet et al. 2001, 2003, 2004), which is often made difficult by the low abundance and heterogeneous distribution of BMS in peridotite. The preparation of several thin sections is often required in order to ensure a realistic estimate of BMS abundance has been achieved. Although this is not an infallible means for detecting peridotites that have experienced extensive metasomatism, sulfide modal abundances in excess of 0.1 % are unlikely to be the result of melt depletion alone and may signify melt addition. For example, Aulbach et al. (2004a) reported unusually abundant BMS in garnet spinel lherzolites from the Slave craton, which could only be attributed to a secondary influx of sulfur accompanying a silicate melt. This conclusion was also supported by silicate melt patches in nearby spinel lherzolites, half of which comprised aggregates of polygonal pentlandite. Wang et al. (2009) also reported high BMS modal abundances in Taiwanese spinel lherzolite xenoliths as being the result of extensive metasomatism. The modal BMS contents of their lherzolites from Penghu Island range from 0.1–1 modal % sulfide, far in excess of that preserved in peridotite that has only experienced melt depletion.

Peridotite-hosted BMS are predominantly derived from a MSS precursor which was in equilibrium with a sulfide melt (e.g., Craig 1973). Its occurrence is commonly interpreted

as representing a residuum after partial melting (Helz 1977; Lorand 1987). Lherzolite-hosted BMS are typically polyphase assemblages of pentlandite±chalcopyrite±Ni-poor MSS±cubanite±heazlewoodite±millerite±bornite. The experiments of Kullerud et al. (1969) in the Cu–Fe–Ni–S system demonstrated that Fe-rich MSS, with a composition close to FeS, crystallizes at 1192°C, i.e., at the temperatures at which most non-cratonic peridotite xenoliths equilibrated (<1200°C; e.g., Galer and O'Nions 1989; Zangana et al. 1997; Alard et al. 2002). Therefore MSS is a solid sulfide phase at equilibration depths of non-cratonic sub-continental lithospheric mantle (SCLM), and probably for those cratonic xenoliths with the highest equilibration temperature (e.g., ca. 1400°C; Rhyzenko and Kennedy 1973). Below 1192°C, Ni and Cu partition into FeS to form MSS, which at 1100°C accommodates up to 14 wt% Ni, but <5 wt% Cu. Continued cooling results in an expansion of the MSS field toward Cu, with MSS containing up to 7.5 wt% Cu at 935°C (Fig. 5; Cabri 1973). Nickel, on the other hand, may be present at concentrations up to 46 wt% at 1000°C, increasing to a maximum of 60 wt % in MSS at ca. 900°C, which can be retained during cooling to 700°C (Fig, 6; Kullerud et al. 1969; Guo et al. 1999).

Irrespective of the equilibration temperature and cooling rate of the peridotite host, sulfides do not preserve the high-temperature phase relations observed under experimental conditions. Instead, they recrystallize to low-temperature assemblages such as pyrrhotite±pentlandite±chalcopyrite (Ballhaus et al. 2001, and references therein). This means that it can prove difficult to determine the high-temperature composition of an individual BMS grain as exsolution requires reconstruction of the original composition. Using rounded or polygonal BMS grains trapped within silicate phases, Aulbach et al (2004a) reconstructed the high-temperature composition of multi-phase BMS inclusions that exsolved from high-temperature solid solutions, despite the presence of exsolved flames of pentlandite in pyrrhotite and thin rims of chalcopyrite (cf. Guo et al. 1999). Precursor MSS was identified by its microstructure and bulk composition, which plots in the MSS-field of Craig (1973) at 300°C and a cut-off of 5 wt% Ni was applied to distinguish MSS from pyrrhotite (the maximum solubility of Ni in the pyrrhotite at this temperature; Cabri 1973).

Another example of how high temperature phases can be reconstructed from their exsolved and / or recrystallized products is demonstrated by Wang et al. (2009). These authors reported several peridotite-hosted sulfides as having Cu contents >7.5 wt% and up to 41 wt%, clearly in excess of the Cu solubility limit in residual MSS, indicating that these BMS grains are not residual MSS but, in fact, ISS. The cut-off of 7.5 wt% Cu serves as a convenient geochemical indicator for the distinction between ISS and MSS. In this instance, it is probable that the ISS exsolved from Cu-rich sulfide melts (e.g., Lorand et al. 2003b; Wang et al. 2009). Ni-rich (>46 wt% Ni) BMS in these same samples exceed the solubility limit of Ni in residual MSS at 1000°C. One possibility suggested by Wang et al. (2009) is that these high-Ni BMS crystallized from sulfide melts at up to 1000°C (Ni<54 wt%).

The interpretation of BMS produced metasomatically through sulfidation reactions (Lorand et al. 2004; Delpech et al. 2012) is based on their morphology (high dihedral angle and sharp-straight BMS grain contours), textural relationships (associated with carbonates), and mineralogy (low Cu/Cu+Ni (<0.1) and low-Ni, pyrrhotite-dominated assemblages; Lorand et al. 2013). These BMS are always derived from small fractions of alkali melts that have experienced extensive reaction with the host peridotite in the uppermost SCLM (Menzies and Hawkesworth 1987; Bedini et al. 1997; Alard et al. 2011). Such melts have the potential to be particularly effective metasomatic agents as they are enriched in C–O–H–S and remain liquid, and therefore mobile, to low temperatures (Fig. 8; e.g., Menzies and Dupuy 1991; Moine et al. 2004).

In addition to the compositional heterogeneity preserved in BMS as a result of magmatic or metasomatic processes, many intergranular BMS grains preserve varying intensities of dendritic veinlets of Fe-oxyhydroxides (Fig. 7), or can be partially or completely replaced by magnetite. Both of these features are commonly interpreted as resulting from the oxidation of sulfide at sub-
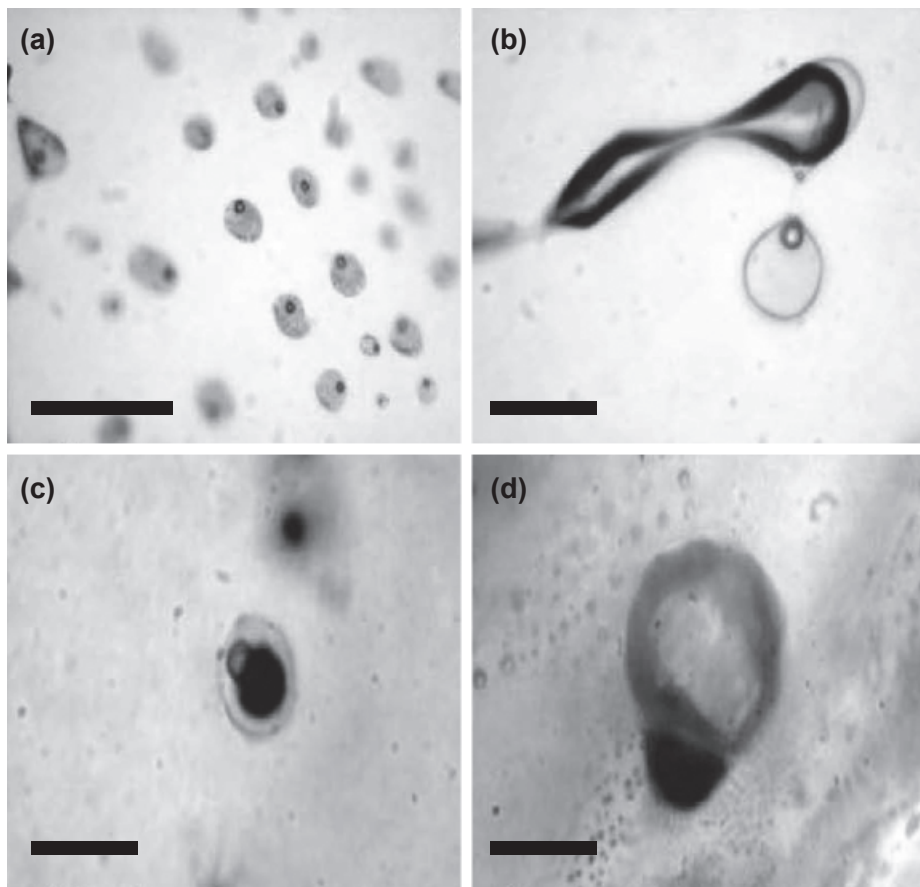
Figure 8. C–O–S–H-rich melt inclusions in peridotite xenoliths from Mont Briançon, French Massif Central (modified after Harvey et al. 2010). (a) Plane polarized light image of a plane of melt inclusions trapped within an annealed olivine grain. Scale bar 20 μm. (b) CO_2-fluid inclusion (top) with co-genetic, silicate melt inclusion beneath. The two phases are joined by a narrow neck ca.1 μm wide. Scale bar 10 μm (c) Co-genetic silicate and BMS grains preserved as immiscible liquids within the same inclusion. Scale bar 10 μm (d) CO_2-fluid inclusion with co-genetic sulfide bleb in olivine. Scale bar 5 μm. Reproduced from Harvey J, Gannoun A, Burton KW, Schiano P, Rogers NW, Alard O (2010) Geochimica et Cosmochimica Acta 74:293–320

magmatic temperatures (e.g., Luguet and Lorand 1998). Sulfide grains in mantle xenoliths may have been partially oxidized by fluids released from the host melt during degassing associated with eruption (e.g., Ryabchikov et al. 1995). Supergene weathering is another cause of oxidation of BMS to oxy-hydroxides (Fig. 7), which results in the selective removal of S in its more soluble sulfate form (Dreibus et al. 1995; Lorand et al. 2003a). This also provides a mechanism for at least partial oxidation of Os and its mobilization, resulting in sub-chondritic Os/Ir in many peridotite xenoliths (Handler and Bennett 1999; Lorand et al. 2003a; Pearson et al. 2004). Such oxidation may even extend to those BMS grains that resided at depth armored within a silicate host grain. For example, Lorand (1990) reported the loss of sulfur and Fe en route to the surface due to the fracturing of host olivine grains during decompression. Finally, metasomatic BMS grains that contain high amounts (>4 wt%) of Si have been attributed to silicate melt inclusions (Aulbach et al. 2004b). Some sulfides also have unusually high-O abundances (up to 16 wt%), which has also been ascribed to oxidation and alteration of the sulfides (Aulbach et al. 2004b).

Despite a narrow range of starting compositions, the large range of processes that can effect peridotite-hosted BMS results in a great potential for morphological and compositional heterogeneity. This variability is also expressed in the HSE and Re–Os isotope systematics of BMS, which may be a function of primary composition, cooling history, metasomatism and mixing of different populations of sulfides. Alard et al. (2002) described peridotite-hosted BMS as being either Type-1 (MMS enclosed within a silicate host), or Type-2 (dominated by Cu-rich pentlandite, commonly interstitial, but also occurring enclosed within metasomatic minerals such as secondary clinopyroxene) and resulting from either precipitation from a sulfur-saturated silicate melt or the introduction of a metasomatic sulfide melt. It is within this context that the Re–Os and Pb isotope systematics of peridotite-hosted BMS are now reviewed, using primarily the nomenclature of Alard et al. (2002). However, this nomenclature is modified as necessary in the examples that follow, where this division fails to adequately describe the petrogenesis of the BMS in question.

The origin and nature of "Type-1" sulfides. Many mantle peridotites contain at least two generations of BMS (Alard et al. 2000; Fig. 1). As discussed in the previous section, Type-1 BMS are mixtures of MSS (with minor pentlandite and chalcopyrite), whereas Type-2 BMS comprise pentlandite + chalcopyrite ± pyrrhotite that exsolved from the higher temperature MSS or due to reaction between MSS and HzSS. The two sulfide types have very different Re and Os contents, and consequently Re/Os and $^{187}Os/^{188}Os$, which in turn have implications for their utility in Re–Os geochronology.

The underlying assumption regarding Type-1 BMS is that they formed during a melt depletion event. This produced a sulfide melt which was lost from the original peridotite and a residual Ni-rich MSS (Type-1 BMS), which was retained within the residual peridotite (e.g., Holzheid 2010 and references therein). Enclosed BMS can exhibit a wide range of shapes that range from polygonal cross-sections with straight contacts to spheroids, but all have habits consistent with entrapment. In harzburgites and dunites, the increase in olivine modal abundance that occurred during melt depletion (70–90 %) could have trapped pre-existing BMS (Lorand 1987).

Osmium concentrations of Type-1 BMS typically range from 1–10s of $\mu g \cdot g^{-1}$ in non-cratonic peridotites (e.g., Burton et al. 1999; Alard et al. 2000; Wang et al. 2009; Harvey et al. 2010, 2011) but this extends to 1000s of $\mu g \cdot g^{-1}$ in cratonic peridotites (e.g., Griffin et al. 2002; Aulbach et al. 2016, this volume), as summarized in Fig. 9; see also *Supplementary Information*. Type-1 BMS are Os-rich because their mineralogy is dominated by MSS. This is a function of the greater number of octahedral sites in Ni-rich MSS (Mackovicky et al. 1986; Cabri 1992; Ballhaus and Sylvester 2000), which are capable of accommodating Os, Ir, and Ru. Osmium isotope ratios (Fig. 10; see also Supplementary Information.) in undisturbed Type-1 BMS are typically less radiogenic than the upper limit estimated for Primitive Upper Mantle (PUM, $^{187}Os/^{188}Os \leq 0.1296 \pm 8$, Meisel et al. 2001) or mean chondrite meterotites ($^{187}Os/^{188}Os \leq 0.127$, Shirey and Walker 1998).

Rhenium concentrations, on the other hand, tend to be much lower (<1 $\mu g \cdot g^{-1}$ in many instances; Fig. 9) with typical $^{187}Re/^{188}Os$ for Type-1 BMS being equal to or lower than the upper value for chondrite meterotites ($^{187}Re/^{188}Os_{chon} \leq 0.40186$; Shirey and Walker 1998). The host phase for Type-1 BMS is most frequently olivine (e.g., Griffin et al. 2002; Aulbach et al. 2004a; Harvey et al. 2006), but occasionally orthopyroxene or garnet (e.g., Beyer et al. 2004). Base metal sulfide included in clinopyroxene with unradiogenic Os isotope ratios (e.g., Burton et al. 1999; Harvey et al. 2011) are likely to be Type-1 BMS, whereas BMS in clinopyroxene with radiogenic Os ratios ($^{187}Os/^{188}Os > 0.1270$, e.g., Warren and Shirey 2012) are probably Type-2 BMS. Base metal sulfides contained in clinopyroxene megacrysts and in pyroxenitic samples have very different Re/Os and $^{187}Os/^{188}Os$ systematics, which are a consequence of a different petrogenesis. These are discussed in the following section along with the potential pitfalls of associating unradiogenic Os isotope ratios exclusively with Type-1 BMS enclosed within primary silicates.
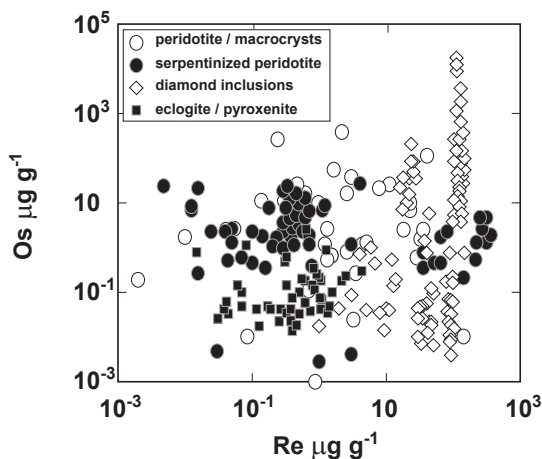
Figure 9. Rhenium and osmium concentrations in BMS grains hosted in abyssal peridotites, continentally derived peridotites and diamonds. See text and supplementary data for data sources.
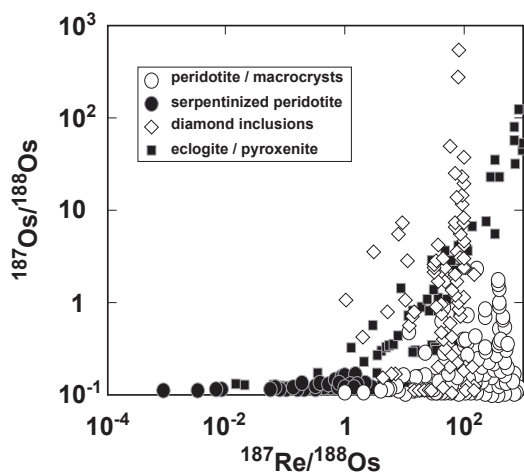
Figure 10. ^{187}Re/^{188}Os and ^{187}Os/^{188}Os in the same BMS grains from Figure 9. See text and supplementary data for data sources.

The identification of unequivocally wholly enclosed BMS can be problematic. Minute (<10 μm) inclusions can often be seen along healed fractures associated with many Type-1 BMS (Fig. 2), for example in patterns that radiate out along former fractures in the host grain. Other sulfide trails intersect larger BMS inclusions in the host mineral (Fig. 2). These trails may originally have been sulfide droplets controlled by cleavage planes, in the case of pyroxenes, or trapped along olivine sub-grain boundaries (Frick 1973). Once these fractures, or sub-grain boundaries annealed, the sulfide droplets become discrete inclusions in the silicate (Andersen et al. 1987). An alternative hypothesis for the trails of minute inclusions that often surround larger (50–100 μm) inclusions is that, just like silicate melt and fluid inclusions (e.g., Bodnar 2003), BMS inclusions hosted within peridotite xenoliths may experience a degree of decrepitation. This could be induced by the rapid drop in pressure associated with entrainment of a xenolith and transport to the surface within the host basalt (e.g., Andersen et al. 1987). Griffin et al. (2002) noted that many BMS grains in Siberian craton peridotite xenoliths, especially the larger ones, show radiating expansion cracks lined with films of sulfide. Critically, sulfide exposed in a thin section or grain mount that may appear to be distant from any grain boundary in the two observable dimensions may in fact intersect a grain boundary in the third dimension.

Following melt depletion, any residual BMS that becomes trapped within a silicate host grain has the potential to evolve in a low-Re environment indefinitely. The radiogenic decay of ^{187}Re to ^{187}Os ($\lambda = 1.666 \times 10^{-11}$ year^{-1}; Shen et al 1996; Smoliar et al 1996; Selby et al. 2007) is the primary control on the long term evolution of ^{187}Os/^{188}Os in the mantle. Therefore, undisturbed Type-1 BMS may preserve important geochronological information pertaining to ancient melt depletion events, as the lack of subsequent ^{187}Os ingrowth due to the near absence of Re that was partitioned into the melt preserves the original ^{187}Os/^{188}Os of the BMS in presumed isotopic equilibrium with the silicate melt at the time of melt depletion.

Burton et al. (1999) discussed the significance of the closed-system behavior of enclosed BMS versus the open system behavior of the silicate phases and interstitial BMS. They noted that Os isotope disequilibrium between an enclosed BMS in a silicate grain and its surrounding phases does not occur simply as a function of the enclosure of the sulfide. Osmium isotope ratios that differ between the enclosed BMS and the other peridotite phases can only be produced by (i) partial re-equilibration of the interstitial BMS and silicates with the host basalt during xenolith eruption or (ii) by diffusional equilibration of the xenolith matrix phases (silicates, spinel and interstitial BMS) with a high-pressure mantle melt originally in equilibrium with a peridotite assemblage. In the absence of any strong petrographic or geochemical evidence for host basalt infiltration during transport and eruption of a xenolith (preserved in either the sulfide or silicate phases), interaction and re-equilibration with a subsequent high pressure melt seems the most likely source of Os isotope disequilibrium. Basaltic melt can form an interconnected network even at low melt fractions (e.g., Kohlstedt 1992; Faul 2001) through which diffusion is rapid (e.g., Ganguly et al. 1998a). This facilitates the re-equilibration of silicate and sulfide phases, i.e., the overprinting upon the silicate phases of the osmium isotope signature of the metasomatic melt. If such interactions are responsible for the re-equilibration of the silicate phases and Type-2 BMS, then bulk-rock Re–Os isotope systematics will not necessarily preserve the age of a single event.

These interpretations are supported by the wide range of Os isotope ratios and Re–Os isotope systematics that can be preserved in a single peridotite xenolith. For example, in SCLM xenoliths from non-cratonic settings (e.g., Massif Central, France; Kilbourne Hole, New Mexico, USA), Harvey et al. (2010, 2011 respectively) demonstrated that in several samples, bulk-rock peridotite ^{187}Os/^{188}Os was significantly more radiogenic than enclosed BMS recovered from the same xenolith. This suggests that the bulk-rock only preserves mixtures of primary and re-equilibrated Os isotope ratios and Re–Os isotope systematics. In contrast, BMS that are armored within a silicate grain and protected from open-system behavior preserve the ^{187}Os/^{188}Os associated with the original melt depletion event. The different model ages derived from single enclosed BMS at these localities can be as much as 0.4 Ga older than their corresponding bulk-rock model ages. This phenomenon has also been reported in oceanic peridotites, where an individual Type-1 BMS preserved an age 0.5 Ga older than the abyssal peridotite that hosted it (Harvey et al. 2006). The potential offset between individual BMS model ages and that of their corresponding bulk-rock has been observed, to even greater effect, in peridotite xenoliths from the Kaapvaal craton (e.g., Griffin et al. 2004), where the age of an individual enclosed BMS was shown to be up to 1.5 Ga older than its host peridotite.

The origin and nature of Type-2 BMS. Depending upon the degree of sulfur saturation, a predominantly silicate metasomatic melt may dissolve or precipitate BMS in interstices between and as inclusions within silicate minerals (e.g., Alard et al. 2002). The S-saturation concentration of lavas increases with decreasing pressure/depth (Mavrogenes and O'Neill 1999), allowing S-undersaturated intra-plate basaltic lava to pass through the SCLM and thus remove any sulfide not enclosed in silicates (e.g., Lorand and Alard 2001; Lorand et al. 2003a,b, 2004; Reisberg et al. 2004, 2005). This effect may be enhanced by ongoing open-system melting associated with reactive porous flow at increasing melt/rock ratios, as this has the effect of diluting S in the percolating melt. On the other hand, an upward decrease

of porosity and temperature in the SCLM can result in sulfide precipitation in the uppermost SCLM (Bedini et al. 1997). This occurs when metasomatic silicate melts reach S-saturation after/during precipitation of metasomatic clinopyroxene and spinel, leading to the formation of a sulfide melt. If a percolating melt undergoes fractional crystallization, MSS will crystallize first, concentrating incompatible chalcophile/chalcogenide elements (critically Re, but also Pd, Cu, Se, Te, Bi, Sb) in a still mobile Cu–Ni-rich sulfide melt (Alard et al. 2000; Luguet et al. 2003; Bockrath et al. 2004; Ballhaus et al. 2006), while retaining Os in the MSS. Where this MSS crystallization occurs, it is generally a smaller amount than observed in Type-1 BMS, and it would react (possibly completely) with HzSS to produce coarse grains of pentlandite often described as Type-2 BMS. The Cu–Ni-rich sulfide melt remains fluid above 900 °C, but ultimately crystallizes as pentlandite ± chalcopyrite (Lorand and Alard 2001; Powell and O'Reilly 2007). A percolating, S-saturated silicate melt will therefore deposit BMS within the host peridotite (Fig. 1), which corresponds to the Type-2 BMS of Alard et al. (2002).

The occurrence of Type-2 BMS is not restricted to intra-plate continental tectonic settings, as the textural association of clusters of secondary clinopyroxene, spinel and metasomatic BMS has also been described in abyssal peridotite dredged or drilled from mid-ocean ridges (e.g., Luguet et al. 2001, 2003; Seyler et al. 2004; Alard et al. 2005; Harvey et al. 2006; Warren and Shirey 2012; Fig. 3). In extreme examples, i.e., at high melt–rock ratios, the distinction between primary versus secondary and enclosed versus interstial BMS becomes difficult to sustain. If the volume of melt is large, it may be possible to completely replace the original silicate phases and crystallize new ones (e.g., modification of harzburgite into dunite; Büchl et al. 2002, 2004; Lorand et al. 2004; Delpech et al. 2012; González-Jiménez et al. 2014), which may lead to a significant, if not complete, mobilisation and dissolution of the enclosed BMS. Type-2 BMS are often associated with a silicate glass from which the sulfide melt exsolved, as well as with (and sometimes enclosed within) the secondary clinopyroxene and secondary spinel whose fractional crystallization may have triggered S-saturation. Aulbach et al. (2004b) also reported the co-existence of pentlandite (which contained silicate inclusions) with secondary spinels contained in patches of metasomatic glass in cratonic peridotite xenoliths recovered from Buffalo Hills kimberlites, Alberta, Canada.

An alternative hypothesis for the presence of Type-2 BMS in peridotite xenoliths, consistent with their mineralogical association with metasomatic glass, secondary clinopyroxene and spinel, is that they are related to contamination by the melt (basaltic or kimberlitic) that brought the xenolith to the surface. However, several lines of evidence suggest that this is a rare occurrence: (1) BMS derived from host lavas are present as stringers or veinlets that are only ever interstitial. This contrasts with the presence of some Type-2 BMS that are located in the secondary silicates with which they co-precipitate. (2) The major element composition of the interstitial BMS (<27 wt% Ni) is distinct from the BMS found in host basalts (<1.0 wt% Ni), as described in xenoliths from Kilbourne Hole (Dromgoole and Pasteris 1987) and Mt. Gambier, Australia (Alard et al. 2002). (3) Bulk-rock and mineral major and trace element abundances are not consistent with the infiltration of REE-enriched basalt. Several early investigations into the relationship between peridotite xenoliths and their host basalts demonstrated that the silicate glass found inside the xenoliths is not derived from the lava. The glass typically has a chemical signature that requires the participation of a hydrous accessory phase (e.g., phlogopite or amphibole), suggesting that the source of the metasomatic melt may be hydrated SCLM (Green et al. 1968; Cooper and Green 1969; Kleeman et al. 1969; Frey and Green 1974; Dasch and Green 1975; Yaxley and Kamenetsky 1999). (4) Textural and mineralogical evidence for pyrometamorphism is absent in the majority of peridotites that contain Type-2 BMS (e.g., Burton et al. 1999).

The preferential partitioning of Re into sulfide melt compared to Os (Brenan 2002, 2008; Brenan et al. 2016, this volume and references therein), combined with Re behavior that is both chalcophile and lithophile, results in a much wider and ubiquitously higher range of Re/Os than

those seen in undisturbed Type-1 BMS (Handler et al. 1997; Burton et al. 1999; Harvey et al. 2010, 2011; Fig. 9). With time, high Re/Os will evolve into ^{187}Os/^{188}Os that is more radiogenic than Type-1 BMS in the same peridotites (Fig. 10). Type-2 BMS are S-poor (relative to MSS), and have Ni and/or Cu-rich bulk compositions—like the sulfide melt from which they crystallize. These features, taken together, demonstrate that they are produced by mantle processes that are distinct from the large-scale melt depletion events associated with the formation of Type-1 BMS.

Deficiencies in the "Type-1" versus "Type-2" nomenclature. The nomenclature used in the previous two sections works very well for peridotites that have experienced a simple petrogenesis. However, when peridotites have experienced multiple events, both chemical and thermo-tectonic following an original melt depletion episode, the simple distinction between "melt depleted" and "metasomatic" BMS becomes somewhat inadequate and simple categorization into "primary" versus "secondary" and "enclosed" versus "interstitial" becomes unwieldy. For example, based upon Re/Os, Os/Pt, ^{187}Re/^{188}Os and ^{187}Os/^{188}Os, Griffin et al. (2002) further subdivided peridotite-hosted BMS populations included in olivines from the Siberian craton into five groups (1, 2, 3A–3C). Like the Type-1 BMS of Alard et al. (2002), the Re–Os isotope systematics of Group 1 BMS were consistent with derivation after small percentages of melt extraction from a fertile mantle source under sulfur-saturated conditions. Group 2 BMS were described, based on modelled compositions derived from the experimental literature (see Brenan et al. 2016, this volume), as mixtures of MSS and PGE-rich alloy phases, also formed at low degrees of melting, but under sulfur-undersaturated conditions (Griffin et al. 2002). This was supported by the observation of Pt-rich micronuggets that were apparent only during laser ablation ICPMS. Group 3C BMS were described as broadly analogous to the Type-2 BMS of Alard et al. (2002), appearing to have crystallized from evolved sulfide liquids, whereas Group 3A and 3B BMS were interpreted by Griffin et al. (2002) as reaction products between the MSS found in Groups 1 and 2, and liquids of Group 3C.

Similarly, distinctions based on "enclosed" versus "interstitial" morphologies has already been demonstrated to not uniquely account for where residual versus metasomatic BMS are found. Griffin et al. (2002) demonstrated that inclusions of different BMS groups may occur within an individual olivine grain. This can only occur if the host peridotite has experienced the repeated introduction of sulfide melts and subsequent recrystallization of the surrounding silicates. Group 1 and 2 BMS of Griffin et al. (2002), and some Group 3A BMS yield ages that appear geologically reasonable, i.e., they are at least consistent with the age of the Earth (≤ 4.6 Ga). However, the majority of the Group 3 BMS had particularly high ^{187}Os/^{188}Os, similar to those observed in the Type-2 BMS of Alard et al. (2002), and consistent with a long-term evolution in a high Re–Os environment. The interpretation of the Re–Os isotope systematics of an individual sulfide and its geochronological implications can often be convoluted, requiring a sequence of several events to account for the composition and "age" that it yields (see section below on pitfalls in Re–Os geochronology).

Since 2002, several studies investigating the mobility of sulfide phases during grain boundary migration and metasomatism have been performed, with contrasting conclusions being reached. In some instances, the reaction of primary silicates with interstitial metasomatic melt/fluids may expose BMS grains that were formerly enclosed (Type-1) to percolating metasomatic fluids, disturbing their Re–Os isotope systematics (Aulbach et al. 2004a; Griffin et al. 2004; Wang et al. 2009; Harvey et al. 2010; Alard et al. 2011). In contrast, Marchesi et al. (2010) observed that, irrespective of subsequent metasomatism, BMS from the Ronda peridotite massif preserve ancient magmatic signals. Powell and O'Reilly (2007) and Greau et al. (2013) have suggested that sulfides can still retain their original Os isotope signature if they are only transported over relatively short distances during metasomatism. Because of the high concentration of Os, particularly in Type-1 BMS, they may be able to buffer against the

effects of metasomatism. This contrasts with the interpretation of Harvey et al. (2010), where enclosed BMS share some of the Re–Os isotope characteristics of interstitial BMS (and vice versa) in a similar manner to that reported by Griffin et al. (2002).

In a recent study of peridotite xenoliths from Calatrava (Spain) by González-Jiménez et al. (2014), ancient $^{187}Os/^{188}Os$ model ages were derived from BMS that bore no consistent relationship to their textural location in the peridotite host. This was interpreted, like Griffin et al. (2002), Wang et al. (2009), and Harvey et al. (2010), as the result of fluid/melt interaction with Type-1 and Type-2 BMS. The ancient model ages are interpreted to result from a Type-1 BMS (which have high Os concentrations and unradiogenic $^{187}Os/^{188}Os$) with a smaller amount of radiogenic Os derived from the subsequent interaction with metasomatic Type-2 BMS. González-Jiménez et al. (2014) went on to question the validity of the original Type-1 versus Type-2 categorization. Similar to the examples from Calatrava (González-Jiménez et al. 2014), Penghu Islands, Taiwan (Wang et al. 2009), Mont Briançon, French Massif Central (Harvey et al. 2010), and the Siberian craton (Griffin et al. 2002), the Type-1 and Type-2 categories do not adequately describe the populations of BMS present.

Additional complications associated with BMS from oceanic peridotite. In addition to the effects of melt depletion and subsequent metasomatism discussed in the previous sections, oceanic peridotites, i.e., abyssal peridotites and ophiolitic ultramafic assemblages, may also be affected by seafloor weathering (e.g., Bischoff and Seyfried 1978; Snow and Dick 1995), serpentinization (Miyashiro et al. 1969; Wicks and Whittaker 1977; Komor et al. 1985; Janecky and Seyfried 1986; O'Hanley 1996), and other hydrothermal processes (Boudier and Nicholas 1991; Mével and Stamoudi 1996; Alt et al. 2007). Each of these processes may affect the preservation or modification of Re–Os isotope systematics retained in oceanic BMS.

Serpentinization involves the reaction of water with primary silicate minerals (principally olivine) at low to moderate temperatures (generally <400 °C) to form hydrous phyllosilicates such as lizardite, chrysotile and antigorite, along with brucite and magnetite (e.g., Bach et al. 2004). In the shallow oceanic mantle, the replacement of primary silicates by hydrous minerals can extend up to 100 %, i.e., no olivine or orthopyroxene remains. For example, the degree of serpentinization in oceanic peridotite exposed at the seafloor in the 15° 20'N Fracture Zone of the Mid Atlantic Ridge ranged from 40 % at the surface to 100 % at 100 m depth in the drill hole (Bach et al. 2004). The consequences for the pre-existing populations of sulfide can be profound under these circumstances. Osmium abundance in seawater is extremely low (1.1×10^{-14} g·g^{-1} Os; Levasseur et al. 1998), but also extremely radiogenic ($^{187}Os/^{188}Os \sim 1$; Levasseur et al. 1998) compared with PUM (0.1296, Meisel et al. 2001). Rhenium, on the other hand, is enriched in seawater by approximately 740 times compared to Os (Anbar et al. 1992). The high Re/Os of seawater means that peridotite that interacts with large volumes of seawater during serpentinization has the potential to rapidly evolve to radiogenic $^{187}Os/^{188}Os$. For example, bulk-rock abyssal peridotites from the Southwest Indian Ridge (SWIR) and American-Antarctic Ridge, analyzed by Snow and Reisberg (1995), possessed elevated $^{187}Os/^{188}Os$ ($^{187}Os/^{188}Os = 0.1305$ to 0.1321) for the weathered sample rim compared to the interior of the sample ($^{187}Os/^{188}Os = 0.1224$ to 0.1253). While absolute Re concentrations were not reported in this study, Harvey et al. (2006) reported a rapid increase in Re abundance with proximity to the surface of the seafloor in drilled abyssal peridotites from the 15° 20'N Fracture Zone (up to 4.9 ng·g^{-1}, i.e., enriched by up to 3 orders of magnitude compared to similarly serpentinized samples deeper in the drilled core).

The ultimate fate of Type-1 BMS in serpentinized abyssal peridotite depends upon a number of factors. Their MSS-dominated mineralogy has the potential to limit the amount of Re-addition through seawater/sulfide interaction due to the negligible uptake of Re in typically enclosed BMS grains. In addition, the absolute amount of extremely radiogenic Os contained in seawater is unlikely to have any significant effect at seawater/sulfide ratios <10^6. Under the reducing conditions of serpentinization, sulfide is generally stable (Snow and Schmidt 1998;

Rehkämper et al. 1999) so even highly serpentinized abyssal peridotites have the potential to preserve highly unradiogenic Os isotope ratios (e.g., Parkinson and Pearce1998; Alard et al. 2005; Harvey et al. 2006; Liu et al. 2008; Warren and Shirey 2012).

Highly siderophile element mobility during serpentinization is controlled by several factors, including oxygen and sulfur fugacities (Bell et al. 2009), pH and temperature (Wood 1987), and fluid chlorinity (Fleet and Wu 1987). Marchesi et al. (2013) recently examined the T, pH, f_{O_2}, and f_{S_2} conditions of serpentinization at Hole 1274A near the 15° 20' N Fracture Zone in the context of HSE mobility. They concluded that HSE mobilization may be minimal overall, being limited to some mobilization of Pt and Pd, in agreement with experimental studies of Gammons and Bloom (1993) and Pan and Wood (1994). Under the reducing conditions of serpentinization (Seyfried and Dibble 1980), it is unlikely that interstitial BMS will be dissolved or physically advected from their host peridotite. It is more likely that, during serpentinization and late stage seawater interaction, interstitial BMS will accumulate Re. If this occurs recently the Os isotopic composition would not be affected. But over time, this grain would evolve to a more radiogenic $^{187}Os/^{188}Os$. For example, Harvey et al. (2006) observed skeletal interstitial BMS with unradiogenic Os isotope ratios ($^{187}Os/^{188}Os \sim 0.117$), but high Re/Os ($^{187}Re/^{188}Os \leq 10$). These sulfides must have recently acquired their high Re/Os signature as otherwise their high Re/Os would have resulted in radiogenic $^{187}Os/^{188}Os$ ratios.

Seafloor peridotites may undergo mutliple episodes of alteration at a range of conditions. For example, some abyssal peridotites from the 15° 20' N Fracture Zone contain cross-cutting serpentine veinlets, some of which contain valleriite ($4(Fe,Cu)S_3(Mg,Al)(OH)_2$), indicating late-stage alteration at higher f_{O_2} conditions (Alt et al. 2007). Less reducing conditions result in higher Pt and Pd mobilization (Gammons and Bloom 1993), while reducing conditions have the potential to break down Ni-rich MSS to awaruite, heazlewoodite, and magnetite (Klein and Bach 2009; Foustoukos et al. 2015). In highly altered peridotites, BMS grains dispersed throughout a serpentine matrix are often partially replaced by veinlets of magnetite, minor awaruite, and occasional native copper. This assemblage is common in partly serpentinized peridotites from the Ronda massif (e.g., Marchesi et al. 2010). While the increase in metal/sulfur ratio of BMS has obvious consequences for the sulfur budget of serpentinites, the effect is also significant for the HSE in BMS (e.g., Foustoukos et al. 2015). These BMS are ultimately transformed into alloys, such as awaruite, with the greater mobility of Re and Pt in seawater resulting in these elements becoming fractionated from Os, although the extent to which this will affect Os isotope heterogeneity in the mantle remains uncertain. However, the preferential removal of Re has the potential to preserve the original Os isotope ratio present in the BMS in the newly formed alloy.

In addition to serpentinization, higher temperature hydrothermal alteration of pyroxenes to talc and amphibole-rich assemblages has the potential to moderate the BMS and HSE budgets of abyssal peridotite. A pervasive, high temperature (ca. 350 °C) hydrothermal overprint superimposed onto a low temperature (100–200 °C) serpentinite assemblage has been documented in some Mid-Atlantic Ridge (MAR) peridotites (Paulick et al. 2006; Boschi et al. 2008; Harvey et al. 2014). The fluids involved are silica rich, having partially equilibrated with local gabbro intrusions, and have Sr and B isotope ratios consistent with a strong seawater influence. While these rocks contain up to 2 wt% S (Paulick et al. 2006), the only BMS identified in these serpentinites are secondary pyrites (Bach et al. 2004), although pyrrhotite, chalcopyrite, pentlandite, and marcasite may also be hydrothermal phases in similar rocks (e.g., Luguet et al. 2004; Alard et al. 2005). Neither bulk-rock nor BMS Re–Os data are available for these samples, but the absence of primary BMS and the presence of hydrothermal BMS makes it likely that these rocks are very radiogenic due to the high $^{187}Os/^{188}Os$ ratio of seawater. The spatial extent of Si-metasomatized rocks along mid-ocean ridges is not well constrained, but the eventual subduction of oceanic

lithosphere containing highly radiogenic BMS has implications for the Re–Os and $^{187}Os/^{188}Os$ heterogeneity of the convecting mantle and for the mantle wedge underlying subduction zones, where radiogenic Os isotope ratios are common (Brandon et al. 1996; Becker and Dale 2016, this volume).

Overall, studies of oceanic peridotite-hosted BMS indicate that serpentinization, hydrothermal alteration and seafloor weathering can add a number of unwanted variables to the interpretation of Re–Os geochronological data for BMS. However, these studies also indicate that the high-temperature mantle history of abyssal peridotites can be recovered from BMS, provided the degree of alteration is not too extreme, as constrained by careful analysis of sulfide composition and petrography.

Pyroxenite-hosted sulfides

Base metal sulfides have been observed in pyroxenites in several studies over the last 40 years from continental localities as diverse as Australia, the French Massif Central, SW USA and Taiwan (e.g., Irving 1974; Peterson and Francis 1977; Andersen et al. 1987; Dromgoole and Pasteris 1987; Luguet et al. 2008; Wang et al. 2009). Several groups of workers have attributed the formation of Al-augite pyroxenite-hosted BMS, and BMS hosted within clinopyroxene megacrysts and clinopyroxenites, to sulfur-saturation resulting from fractional crystallization of mafic magmas at mantle depths (e.g., Andersen et al. 1987; Dromgoole and Pasteris 1987; Guo et al. 1999). However, Re–Os isotope data for pyroxenite-hosted BMS are scarce and are restricted to a handful of studies (Luguet et al. 2008; Wang et al. 2009; Ackerman et al. 2013).

Pyroxenite-hosted BMS grains are usually pyrrhotite with subsidiary pentlandite ± chalcopyrite, which are the low-T ($\leq 300\,°C$) re-equilibrated products of high-T MSS (Guo et al. 1999; van Acken et al. 2010a). In addition, chalcosite (Cu_2S) and Ni- and Co-rich BMS coexisting with MSS and pentlandite have been reported in pyroxenites from the Canadian Shield (Aulbach et al. 2004a). Base metal sulfides measured in pyroxenites from the Penghu Islands, Taiwan (Wang et al. 2009) were reported as having Fe-rich MSS cores, surrounded by a Ni-rich MSS mantle and a Co-rich rim, while a small number of BMS grains contained Cu-rich phases such as chalcopyrite, chalcopyrrhotite and bornite, similar to the range of BMS described from the Bohemian Massif by Ackerman et al. (2013).

The shape of pyroxenite-hosted BMS and their relations to growth planes in pyroxenes suggest that some of them were trapped as drops of immiscible sulfide melt which nucleated on the surfaces of pyroxene crystals growing synchronously from a silicate melt. For example, an x-ray crystallographic study of a clinopyroxene megacryst from Nunivak Island, Alaska demonstrated that BMS grains are aligned along the growth planes (111) and (221), and are not associated with cleavage or exsolution planes (Peterson and Francis 1977). Sulfide shapes include spheroidal, elongated rods and squares, and multi-facetted polygons, suggesting that their shape is controlled epitaxially by the host pyroxene (Dromgoole and Pasteris 1987; Andersen et al. 1987; Guo et al. 1999). While individual pyroxenite-hosted BMS can have sizes up to 500 μm diameter (Guo et al. 1999), more typically they range from 20 to 80 μm (Dromgoole and Pasteris 1987; Wang et al. 2009). However, many enclosed BMS are of a questionable origin. Their association with fractures and with trails of fluid and sulfide inclusions is more consistent with either their introduction sometime after the initial crystallization of the pyroxene host, or by remobilization of pre-existing sulfide (Andersen et al. 1987; Dromgoole and Pasteris 1987). As typically seen for large BMS inclusions in mantle peridotites, it is common to find BMS-bearing inclusion arrays that radiate from sulfides enclosed in magmatic pyroxenes. These sulfides, in extreme examples, have an "exploded" appearance (Fig. 2), which may have resulted from melting and expansion of the sulfide—similar to fluid inclusions that have undergone rapid decompression during their ascent to the surface following entrainment of their host xenolith (Andersen et al. 1987; Dromgoole and Pasteris 1987).

The modal abundance of BMS in pyroxenites tends to be greater than in peridotites (Frick 1973; DeWaal and Calk 1975; Irving 1980; Garuti et al. 1984). Of the pyroxenite suites studied by Irving (1980; BVSP 1981), samples from Kilbourne Hole contained as much as 0.5 modal % BMS, based on bulk-rock sulfur analyses. This is likely to represent a minimum given the susceptibility of BMS to partial or complete oxidation and removal by supergene weathering (Lorand et al. 2003a). Peterson and Francis (1977) described an extreme example of 1 vol% BMS in a clinopyroxene megacryst from Nunivak Island, Alaska. Alternatively, the high abundance of BMS in pyroxene megacrysts may be attributed to the volatile-rich nature of the parent liquid. For example, Harvey et al. (2010) identified compound CO_2–silicate–sulfide inclusions in Massif Central peridotite xenoliths (Fig. 8).

The dearth of direct Re/Os elemental and $^{187}Os/^{188}Os$ isotope measurements of pyroxenite-hosted BMS stems from the fact that (i) pyroxenites make up only around 10% of ultramafic lithologies exposed at the surface (e.g., Frey and Prinz 1978), and (ii) these BMS grains tend to be small ($<100\ \mu m$) and possess very little Os compared to peridotite-hosted BMS, making precise isotopic measurement difficult. For example, Luguet et al. (2008) reported Re and Os abundances (Fig. 9), $^{187}Os/^{188}Os$ ratios, and $^{186}Os/^{188}Os$ modelled from Pt/Os ratios in 3 pyroxenite-hosted BMS from Beni Bousera, Morocco. Osmium concentrations ranged from 262 ng·g^{-1} to 1.1 µg·g^{-1}, with supra-chondritic Os isotope ratios ($^{187}Os/^{188}Os=0.130$ to 0.145) and significantly lower Re abundances (65 ng·g^{-1} to 101 ng·g^{-1}). For BMS grains of $<100\ \mu m$ in diameter, this corresponds to Os amounts of 10s–100s pg. As a result, the Re–Os isotope systematics of pyroxenite-hosted BMS are more typically inferred from the measurement of bulk-rock pyroxenite in which abundant BMS grains have been observed and petrographically described.

The Re–Os isotopic composition of bulk pyroxenite may not always reflects the source melt composition but rather that of the mantle into which the pyroxenite melt has infiltrated. In this situation, the former Re–Os elemental and isotopic fingerprint of the peridotite may not have been entirely overprinted. Distinguishing the $^{187}Os/^{188}Os$ of a pyroxenite magmatic source from that of Type-2 peridotite-hosted BMS that may have been scavenged during the transit and emplacement of the host pyroxenite is practically impossible. For example, BMS grains with radiogenic $^{187}Os/^{188}Os$ may be derived from interstitial BMS in a peridotite body prior to the infiltration of large volumes of silicate melt or be derived from the silicate melt itself during the formation of pyroxenite. If pyroxenite represents the interaction between melt generated by a mafic precursor and peridotite, then the melt derived from the mafic component will already have a high Re/Os elemental ratio and time integrated $^{187}Os/^{188}Os$ ratio compared to the peridotite that surrounds it. If the generation of silicate melt at asthenospheric depths results in a S-undersaturated melt, this melt has the capacity to dissolve interstitial peridotite-hosted BMS as it ascends. These Ni-Cu-rich sulfides have significantly lower melting temperatures than residual Fe–Ni-rich MSS and, as long as the ascending melt remains S-undersaturated, interstitial peridotite-hosted BMS will become incorporated into the melt, mixing their high Re/Os and radiogenic $^{187}Os/^{188}Os$ with that of a mafic-derived melt with similar Re–Os characteristics (e.g., Sen et al. 2011). However, what seems more likely is that melting of, for example, eclogite at asthensospheric depths will generate a sulfur-saturated melt that is capable of precipitating sulfide with a high, time-integrated Re/Os, leading to the deposition of radiogenic sulfide.

The model for pyroxenite formation favoured by Sobolev et al. (2005, 2007) invokes the reaction of eclogite-derived melt with peridotite, where eclogite would begin melting at a greater depth than peridotite (Hirschmann and Stolper 1996). As eclogites are the metamorphosed equivalent of MORB, they should have high S contents (few hundreds to >1000 µg·g^{-1} S), thus melting at depths where the S solubility of basaltic melt is relatively low. This melt would therefore be S-saturated, with the potential for precipitation of eclogite-derived BMS when the pyroxenites crystallize. This would result in pyroxenite-hosted BMS with similar Re–Os isotope characteristics to MORB itself, notwithstanding any interaction with peridotite-hosted BMS during pyroxenite formation.

The complexity of progressive melt infiltration, increasing melt/peridotite ratios, pyroxenite formation and sulfide compositional evolution was investigated in two suites of ultramafic rocks from the South China craton by Wang et al. (2009). They demonstrated that changes in HSE distribution and Re–Os isotope systematics of peridotite- and pyroxenite-hosted BMS could be accounted for by the progressive percolation of melts. In porphyroclastic and partly metasomatized peridotites, Wang et al. (2009) reported subchondritic to suprachondritic $^{187}Re/^{188}Os$ and $^{187}Os/^{188}Os$ in BMS grains, which likely reflected fluid/melt interaction at low melt/rock ratios with residual MSS and/or crystallization of fractionated sulfide melts. This resulted in elevated Cu, Ru, Rh and Pd, and high Re/Os. At intermediate melt/rock ratios, peridotites displayed equigranular textures, were extensively metasomatized and contained sulfur-rich Ni–(Co)-rich MSS, with subchondritic to chondritic $^{187}Os/^{188}Os$ and subchondritic $^{187}Re/^{188}Os$. At the highest degrees of melt/rock interaction, i.e., where spinel-pyroxenite formed, pyroxenite-hosted BMS possessed the lowest HSE contents, had subchondritic to suprachondritic $^{187}Os/^{188}Os$ and subchondritic $^{187}Re/^{188}Os$, and were interpreted as having precipitated from sulfide melts that segregated from basaltic melts under S-saturated conditions. With the exception of the subchondritic $^{187}Re/^{188}Os$, this process is similar to that observed during the formation of dunites at high melt / rock ratios in the Troodos ophiolite by Büchl et al. (2002, 2004) and in Shetland, Scotland (O'Driscoll et al. 2012).

In the Totalp Massif, Switzerland, in garnet–spinel-clinopyroxenites and spinel-websterites contained within melt-infiltrated Jurassic ocean-floor peridotites, van Acken et al. (2008, 2010a,b) identified pyroxenite-hosted pentlandite and godlevskite ((Ni,Fe)$_8$S$_9$) as being the major hosts of HSE. In the host lherzolites, up to 20% of the observed BMS grains had been derived from a mafic melt, resulting in substantial enrichments of Re, Pd and Pt, whereas Ir, Os, and Ru remained largely unaffected. Heterogeneous HSE abundances within individual pyroxenite-hosted BMS were attributed to subsolidus processes, such as exsolution, not resolvable using LA ICPMS, due to small sub-grain sizes. Large grain-to-grain variations were likely caused by multiple events of melt–rock interaction and sulfide precipitation, which demonstrate the potentially complex Re–Os isotope systematics that may occur in pyroxenites and that bulk-rock Re–Os isotope systematics are unlikely to preserve geochronological information pertaining to a single incidence of melt–rock interaction. van Acken et al. (2010a) reported cm-scale heterogeneity amongst pyroxenite-hosted BMS, corresponding to both residual-peridotite and melt-like HSE signatures, suggesting that the prior Re–Os signature of the original peridotite may not have been completely erased. Over time, the enrichment in Pt and Re and depletion in Os of the Totalp pyroxenites would be expected to develop radiogenic ^{187}Os and ^{186}Os, compared to ambient mantle.

In a recent study of Horní Bory, Bohemian Massif, Ackerman et al. (2013) demonstrated that the relationship between bulk-rock Fe-wehrlites, wehrlite-clinopyroxenites, websterites, clinopyroxenite and olivine clinopyroxenite, and the BMS grains they contain are also convoluted and result from the interaction between a melt-depleted peridotite residue and a sulfur-undersaturated melt generated in a subduction setting. Here, the bulk-rock pyroxenites are depleted in Os, Ir, and Ru, enriched in Pd, Pt, and S, and have radiogenic $^{187}Os/^{188}Os$. They interpret the origin of these pyroxenites as melt–rock reaction between peridotite and subduction-related melt at high melt/rock ratios, which resulted in primary BMS grains being replaced by radiogenic (high $^{187}Os/^{188}Os$) but HSE-poor BMS. Bulk-rock Os abundances are highly variable (0.08–9.3 ng·g^{-1}) but generally low (<1 ng·g^{-1}), while Re abundances are less variable (1–4 ng·g^{-1}), corresponding to high $^{187}Re/^{188}Os$ (up to 198) and radiogenic $^{187}Os/^{188}Os$ (0.139–1.23). However, most of the pyroxenite-hosted BMS have exceptionally low Os and Re, typically below detection limits (<0.01 μg·g^{-1}), with the result that Ackerman et al. (2013) calculated that the PGE mass balance was not wholly dependent upon the BMS present. Only 28% of the pyroxenite HSE budget was hosted by BMS, with the remainder contained in

micron-scale PGM. Despite the small-scale heterogeneity, wehrlite, dunite and pyroxenite rocks yielded a Re–Os errorchon age of 334 ± 19 Ma (MSWD = 1318), which is consistent with the age of other high temperature/pressure rocks from the Bohemian Massif, and likely represents the time of melt–rock reaction and subduction. However, it should be remembered that this "age" is derived from a complex mixture of PGM, secondary BMS, and pyroxenite melt, all assuming that the Re–Os characteristics of the replaced peridotite were completely erased.

The three case studies just described represent the current state of the art with regard to what has been achieved with pyroxenite-hosted BMS. While the geochronology of these rocks must be interpreted with care, detailed grain-scale analyses have the potential to provide unique constraints on the timing and nature of melt–rock reaction events.

Diamond-hosted sulfides

Around 1% of macrocrystalline, gem-quality diamonds contain inclusions large enough to identify with a hand lens or optical microscope. Of such inclusions, BMS grains are not uncommon (Harris 1992; Deines and Harris 1995). The association between diamond occurrences and cratonic mantle has been known since the 1960s (e.g., Clifford 1966; Gurney and Switzer 1973; Boyd and Gurney 1986; Janse 1992). As a result of this association, coupled with (i) cold geotherms derived from geothermobarometry on peridotite xenoliths that pass through the diamond stability field, (ii) the actual presence of diamonds in xenoliths, and (iii) inclusions in diamonds that yield Archean ages, the hypothesis that diamonds reside in ancient lithospheric keels beneath continental interiors has gained wide acceptance (e.g., Richardson et al. 1984; Boyd et al. 1985; Boyd and Gurney 1986; Haggerty 1986). Compared to their low abundance in the mantle in general, BMS inclusions in diamonds from some kimberlites are unusually common (Gurney 1989), making them of particular interest to those who are interested in diamond paragenesis (Meyer 1987) and absolute ages of diamond formation (Pearson and Shirey 1999; Gurney et al. 2010; Shirey and Shigley 2013; Shirey et al. 2013).

Once enclosed in their chemically inert host, inclusions in diamonds are shielded from interaction with transiting melts and fluids, meaning that their chemical composition and the age of diamond formation can be preserved for >3 Ga (Richardson et al. 1984, 1993, 2001; Smith et al. 1991). Just like the peridotite-hosted BMS discussed above, diamond-hosted sulfide mineralogy is dominated by pyrrhotite ($Fe_{1-x}S$) and/ or pentlandite (($Fe,Ni)_9S_8$), with lesser amounts of Cu- or Co-rich sulfides such as chalcopyrite (Deines and Harris 1995; Fig. 4). Diamond-hosted BMS have been interpreted as precipitating from a C-O-S-H-rich fluid associated with Archean mantle melting (Deines and Harris 1995) and suggested to be syngenetic with the host diamonds (Bulanova et al. 1996). However, recent work (e.g., Howarth et al. 2014a,b) has shown that diamonds can also be found in metasomatic veins in eclogite and bear no particular spatial association with BMS grains. Furthermore, some diamonds host multiple BMS inclusions that are not in sulfur isotope equilibrium (e.g., Thomassot et al. 2009). In these cases the sulfides must be protogenetic (growing before the diamond). Protogenetic versus syngenetic distinctions are mineralogical in nature and may not compromise the use of BMS for age determination if the age difference between protogenetic inclusion growth and host diamond growth is within the resolution of the age dating method. Nonetheless, the similarity of BMS inclusions to peridotite-hosted BMS is demonstrated by their identical experimentally determined paragenesis i.e., derivation from sulfide/silicate immiscibility in the $FeS–FeO–Fe_3O_4–SiO_2$ system at around 1100 °C (Maclean 1969).

Base metal sulfide inclusions are distinguished from silicate and oxide inclusions by the presence of large rosette fractures surrounding each sulfide (Fig. 4). The rosette fractures result from rapid decompression during transport of the host diamond to the surface, commonly in a kimberlitic eruption. Silicate inclusions in diamond can be subdivided into eclogitic (E-type diamonds) and peridotitic (P-type diamonds; see Meyer 1987; Stachel and Harris 2008), More

recent work has added lherzolitic and wehrlitic parageneses to the classification scheme. Diamond-hosted BMS can be also be categorized by the presence or absence of peridotitic or eclogitic silicate and / or oxide mineral inclusions in the same diamond (e.g., Bulanova 1995), but the co-occurence of BMS and silicate inclusions in the same diamond is so rare that it is hardly a workable classification method for BMS inclusions. Sulfide composition can itself be used, but this classification can only be made after the inclusion is broken out of the diamond as the reflectivity and color differences between different BMS are hard to observe through the diamond.

Major element discriminators for peridotitic versus eclogitic BMS inclusions, such as Ni wt%, were used early in the 1980s in Siberian diamonds (Yefimova et al. 1983). However, with increasing numbers of analyses, the distinction between these two groups of Siberian diamonds became less clear (Deines and Harris 1995; Bulanova et al. 1996). Some studies (e.g., Smit et al. 2010) have observed a pyroxenitic BMS paragenesis compositionally in between eclogitic and peridotitic, which perhaps may explain the less clear distinction for some BMS inclusions. Subsequent studies have found that a combination of Ni and Os abundances is a more robust discriminator (Pearson et al. 1998). Osmium abundances range by a factor of 10^3 between eclogitic and peridotitic BMS inclusions and provide a more sensitive means of discrimination. Although 12% Ni content was the original identifier for peridotitic BMS, defined by Yefimova et al. (1983) and further refined by Deines and Harris (1995) and Pearson et al. (1999a,b), this scheme of classification does not work as well for BMS inclusions in Siberian diamonds (Sobolev 1974; Gurney 1989). As discussed in the following section, eclogitic (as opposed to peridotitic) BMS were originally defined as containing <8 wt% Ni (Yefimova et al. 1983), but the two-fold classification was found not to be appropriate for all sulfide inclusions. For example, BMS inclusions containing 11–18 wt % Ni in several Yakutian diamonds (Bulanova et al. 1996) left the provenance of Siberian diamonds in doubt. Consequently, a third sulfide-based paragenesis was proposed for BMS inclusions with intermediate Ni contents between 8 and 12%; a pyroxenitic paragenesis (Deines and Harris 1995; Pearson et al. 1998; Smit et al. 2010).

As with peridotite-hosted BMS, the relatively high Re and Os concentrations in diamond-hosted BMS mean that the Re–Os isotope system is ideal for the analysis of individual inclusions (Pearson et al. 1998; Pearson and Shirey 1999; Richardson et al. 2001). Single grain analysis of BMS has an advantage over the use of lithophile element-based isotope systems, e.g., Sm–Nd, in the analysis of silicate inclusions, as in these instances several inclusions may need to be pooled in order to provide enough material for an adequately precise measurement. However, the advent of a new generation of stable, high-ohmic input resistors on TIMS instruments is likely to change this story in the near future and allow single silicate grains to be analyzed. The strength of single BMS grain Re–Os measurements comes from the observation that not only can a single BMS grain give a model age for its formation, but also multiple non-touching sulfides with a range of Re/Os elemental ratios, closed to diffusive exchange between each other by the intervening inert diamond, have the potential to yield an isochron age if they grew during the same generation of diamond growth. Combined with the Sm–Nd system in lherzolitic and eclogitic garnet and clinopyroxene, for example (e.g., Richardson et al. 1990) or perhaps Pb–Pb if there is enough in BMS, it may be possible to generate complimentary age results by using two or more independent chronometers on silicate and BMS inclusions.

Peridotitic sulfides. Peridotitic diamonds are identified mainly by the peridotite mineral inclusions that they contain. These include diopside, olivine, enstatite, chromite and Cr-pyrope, (Meyer and Boyd 1972; Gurney and Switzer 1973; Harris and Gurney 1979; Fig. 4). Peridotitic diamond paragenesis can also be subdivided into harzburgitic or lherzolitic on the basis of the melt depletion signature of the inclusions. For example, this may be determined by olivine and / or orthopyroxene composition, the presence or absence of diopside or the CaO and Cr_2O_3 content of included garnet (Sobolev et al. 1973; Harris and Gurney 1979). As discussed in the previous section, unequivocal diamond paragenesis becomes more problematic in the absence of silicate inclusions.

Peridotitic BMS are likely to be residual after low to moderate degrees of partial melting (<25%; Keays 1995), where the basalts produced will almost certainly be sulfur saturated at the source of melting. In contrast, at the higher degrees of partial melting (>25%) necessary for the production of picrites or komatiites, the exhaustion of sulfur at the source of melting is much more likely to occur, leaving little or no residual sulfur for the formation of BMS that could ultimately become enclosed in diamond (e.g., Keays 1995; Mavrogenes and O'Neill 1999). Therefore, highly depleted portions of the SCLM that are associated with komatiite formation seem to be unlikely hosts for peridotitic BMS inclusions (e.g., Aulbach et al. 2009a). Nickel concentrations of diamond-hosted BMS grains provide some insights into diamond paragenesis, in the absence of co-genetic silicate inclusions. A minimum, cut-off value of 12 wt% Ni for BMS was suggested to be appropriate for peridotitic diamond formation (Yefimova et al. 1983; Deines and Harris 1995; Pearson et al. 1999a,b). More recently, Aulbach et al. (2009a) used (Ni+Co)/Fe ratios for BMS, rather than absolute abundances, in order to determine diamond paragenesis. Rather than analyzing the sulfide major element abundances using *in situ* methods—and the possible difficulties in reconstructing sulfide major element geochemistry from a number of phases that exsolved from a high temperature MSS (cf. Griffin et al. 2002)—Richardson et al. (2001), Westerlund et al. (2006), and Aulbach et al. (2009b) obtained the sulfide major element abundances from the eluent produced during the purification procedures for Re–Os isotope analysis. As the major metals are removed in a single aliquot, their relative abundance can be determined by mixing the eluent with appropriate gravimetric standards and then analyzing by ICPMS.

Peridotitic BMS share geochemical and isotopic similarities with Type-1 peridotite-hosted BMS, and in some respects can be thought of as extreme versions of those BMS found in non-cratonic SCLM. Osmium concentrations tend to be high (up to $\mu g \cdot g^{-1}$ levels) compared to BMS derived from the other diamond parageneses (Figs. 9 and 11). Rhenium concentrations are low,
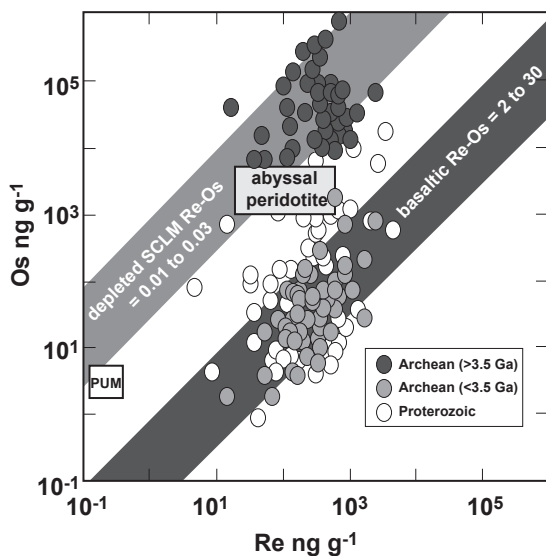
Figure 11. Rhenium and osmium abundances in parts per billion for diamond-hosted BMS grains. Sulfides grouped according to age: Early Archean (>3.5 Ga), late Archean (<3.5 Ga) and Proterozoic. Fertile mantle abundances (PUM; Morgan 1986) are for whole-rock peridotites. Field labeled "abyssal peridotite" encloses data for BMS in present-day abyssal peridotites (from Harvey et al. 2006). Modified after Shirey and Richardson (2011).

and with high Os concentrations lead to extremely unradiogenic $^{187}Os/^{188}Os$ ratios in BMS older than 2 Gyr (see below). Although the Re–Os isotope systematics of cratonic diamonds will be discussed in greater detail below (see section titled "The utility of Re–Os and Pb isotope geochronology"), typical Os abundances range from 10s–100s of $\mu g \cdot g^{-1}$ in peridotitic BMS from the Siberian craton, Russia (Griffin et al. 2002), and the Slave Craton, Canada (Westerlund et al. 2006; Aulbach et al. 2011, respectively). Exceptionally, several thousand $\mu g \cdot g^{-1}$ and even up to $2 \times 10^4 \ \mu g \cdot g^{-1}$ have been reported in one Siberian BMS grain (Griffin et al. 2002). The abundance of Re in Slave Craton peridotitc BMS grains tend to be $<1 \ \mu g \cdot g^{-1}$ (e.g., Aulbach et al. 2011) and, while studies using LA MC ICPMS to obtain Os isotope ratios do not report Re abundances because of the isobaric interference on ^{187}Os (e.g., Griffin et al. 2002, 2004; Beyer et al. 2004; González-Jiménez et al. 2014), $^{187}Re/^{188}Os$ ratios in peridotitic BMS are very low, i.e., significantly less than the mean for chondrites ($^{187}Re/^{188}Os = 0.40186$; Shirey and Walker 1998; see also Day et al. 2016, this volume), and often much lower, e.g., $^{187}Re/^{188}Os = 0.002$ in sulfide LT98/10-5 from the Kaapvaal craton (Griffin et al. 2004) and DA36 peridotitic sulfide from Diavik, Slave craton, Canada (Aulbach et al. 2011). In general, undisturbed peridotitic BMS grains possess $^{187}Os/^{188}Os$ ratios that are less radiogenic than mean chondrite and PUM (i.e., $^{187}Os/^{188}Os \leq 0.1270$ and 0.1296; Shirey and Walker 1998 and Meisel et al. 2001, respectively). A consequence of these sulfides evolving for several billion years, trapped as inclusions in diamond, and hence in a low-Re environment, is that peridotitic BMS tend to have very unradiogenic Os isotope ratios; typically $^{187}Os/^{188}Os < 0.110$ in sulfides with the lowest $^{187}Re/^{188}Os$.

Eclogitic sulfides. Unlike the high degree of melt depletion associated with komatiite and picrite formation, subduction of oceanic crust provides more favorable conditions for growth of diamonds with BMS inclusions. Not only may there be an adequate supply of carbon, but also sulfur, as oceanic crust formation occurs under S-saturated conditions. In addition, the low Ni content of most eclogitic BMS leads to low Ni/Fe ratios (0.1–0.2), which are too low to be in equilibrium with mantle olivine and suggest a basaltic precursor (Deines and Harris 1995; Richardson et al 2001). Although a subduction origin for the carbon from which some diamonds form may be controversial (cf. Cartigny et al. 2001), a subduction-related origin for diamond formation and for the supply of material to Archean SCLM roots is independently supported by (i) both S and Pb isotope systematics of BMS grains in eclogitic diamonds (Eldridge et al. 1991; Rudnick et al. 1993b; Farquhar et al. 2002; Thomassot et al. 2009), (ii) by diamond-bearing eclogite xenoliths whose oxygen isotopic systematics are not consistent with a mantle origin (e.g., Jacob 1994; Shirey et al. 2001, 2004a, 2008), and (iii) by the correlation between isotopically light C in diamond and the isotopically heavy O in eclogitic silicate inclusions (Ickert et al. 2013, 2015; Schulze et al. 2013). The S-saturated nature of the eclogitic protolith is less controversial and is based on the occurrence of BMS globules in MORB (e.g., Roy-Barman et al. 1998) and the absence of evidence for wholesale melting of the eclogitic protolith that would have removed the sulfur during subduction. A consequence of the mafic nature of the subducted material is that ultimately this will experience eclogite facies metamorphism, form eclogite and hence supply material that may become encapsulated within diamonds as eclogitic inclusions.

Diamonds are classified as eclogitic when they contain pyrope–almandine garnet ±coesite ±kyanite±omphacite or sulfide with low Ni contents. In contrast to the high Ni content of peridotitic BMS, eclogitic BMS grains are defined as containing predominantly Fe-sulfide, with less than 8 wt% Ni. Eclogitic BMS mineralogy is dominated by a low-Ni, pyrrhotite–pentlandite–chalcopyrite assemblage derived from cooling of MSS and ISS precursors. Pyrrhotite is usually the dominant phase, but the proportions of chalcopyrite and pentlandite may vary considerably within an individual sulfide. Chalcopyrite is concentrated on exterior surfaces of inclusions (Richardson et al. 2001), as a result of exsolution during kimberlite emplacement. Because Re is preferentially concentrated in chalcopyrite relative to pyrrhotite and/or pentlandite (Richardson et al. 2001; Brenan 2002; Brenan et al. 2016, this volume), incomplete recovery of a diamond

enclosed inclusion may preferentially skew the Re–Os elemental ratio to lower or higher values than the true ratio. If no significant exsolution of chalcopyrite occurred, for example if the sulfide was molten during extrusion into the surrounding fractures, then this is unlikely to be a problem. However, the observation that chalcopyrite is preferentially concentrated around the edges of a wide range of sulfides suggests that great care should be taken to exclude exsolution as a potential source of bias from Re–Os geochronological measurements. This exsolution problem and the high Re content make these grains unsuitable for LA MC ICPMS.

Rhenium–osmium isotope systematics of eclogitic BMS differ from those of peridotitic BMS. Osmium concentrations are often several orders of magnitude lower than peridotitic BMS, e.g., <1.5 µg·g^{-1} (e.g., Pearson et al. 1998; Pearson and Shirey 1999; Richardson et al. 2001, 2004; Aulbach et al. 2009a), while rhenium contents are only moderately lower in eclogitic BMS than peridotitic BMS (≤ 2.2 µg·g^{-1}; Aulbach et al. 2009a), as shown in Figure 9. Consequently Re/Os are also higher (eclogitic mostly >1 versus peridotitic <1; Pearson et al. 1998) and ^{187}Re/^{188}Os are also high (often >100; e.g., Pearson et al. 1998, Aulbach et al. 2009a) and sometimes exceptionally high (>1500; Richardson et al. 2004). Again, like pyroxenitic BMS, ^{187}Os/^{188}Os of eclogitic samples are all suprachondritic and often very high in old BMS grains, which contrasts with the dominantly unradiogenic Os isotope signature of undisturbed peridotitic BMS. This is predominantly because of the high ^{187}Re/^{188}Os and, especially in the case of diamond-hosted eclogitic BMS recovered from cratons, time integrated decay of ^{187}Re to ^{187}Os. Interestingly, in a recent study of eclogitic BMS inclusions recovered from Yakutian diamonds in the Siberian craton (Wiggers de Vries et al. 2013), Re–Os isotope dating demonstrated that individual diamonds may have protracted timescales of growth, with vastly different ages for cores and rims. For example, eclogitic BMS recovered from individual growth zones in diamonds from Mir and 23rd Party Congress kimberlite pipes were demonstrated to have crystallized over intervals lasting <200 Ma, but separated by up to ca. 1 Ga.

Re–Os–Pb MASS BALANCE IN ULTRAMAFIC SAMPLES

Osmium mass balance

The preferential partitioning of HSE into sulfide versus silicate was demonstrated experimentally in the early 1990s (e.g., Peach et al. 1990) and was well-known in ore-forming sulfide systems (see Shirey and Walker 1998 for an early review). But the investigation of HSE concentrations in natural sulfides in non-ore systems has lagged behind by several years. It was not until the investigation of Os abundances in handpicked mineral separates from a picrite from Mauna Loa, Hawaii, an ankaramite from Pico, Azores, and a Kilbourne Hole lherzolite (Hart and Ravizza 1996) that an Os mass balance was estimated for sulfides in equilibrium with silicate melt. This early study demonstrated that in the Kilbourne Hole peridotite, a mineral separate of BMS grains contained 3 orders of magnitude more Os than the bulk rock, and 4–5 orders of magnitude more Os than silicate and spinel mineral separates. Moreover, leaching an aliquot of the powdered lherzolite (in 2.5 M HCl for 1 hour) removed almost 75% of the Os (and all of the S) compared to an unleached aliquot, suggesting that the majority of the Os was hosted by sulfide. Leaching of a finely powdered bulk-rock lherzolite clearly does not provide direct constraints on sulfide Os compositions in the context of their Type-1 or Type-2 assemblage, but can serve as a rough guide to where the phases may be in the rock. In this study, the distribution of Os amongst the other constituent phases of the lherzolite was determined, resulting in calculated K_d^{Os} $_{sulfide/silicate}$ ($\leq 10^5$) that were comparable to those determined experimentally.

Working on a different Kilbourne Hole lherzolite, Burton et al. (1999) analyzed the Re–Os isotopic and elemental composition of inclusion-free silicates, spinel and BMS. By careful handpicking and sulfide selection, they were able to separate both enclosed and interstitial BMS and analyze them separately. In addition, they separated and analyzed clinopyroxene and

orthopyroxene fractions that were visibly contaminated by sulfide inclusions. The inclusion-free silicate phases contained very small amounts of Os (104–136 pg·g^{-1}), whereas spinel contained an order of magnitude more Os (1.2 ng·g^{-1}). However, Type-1 and Type-2 BMS contained 3.9 and 3.7 µg·g^{-1} Os, respectively, unlike several later studies (Alard et al. 2002; Harvey et al. 2010, 2011) where Type-2 BMS were described as containing significantly less Os. Critically, Burton et al. (1999) reported that the sulfide-contaminated pyroxenes had significantly higher Os concentrations than the uncontaminated equivalent, with both orthopyroxene and clinopyroxene containing 1.9 ng·g^{-1} Os compared to ca. 130 pg·g^{-1} in the clean mineral separates. Moreover, the pyroxenes that were contaminated by sulfide inclusions yielded ^{187}Os/^{188}Os that were remarkably close to that of the enclosed BMS (included sulfide and contaminated orthopyroxene ^{187}Os/^{188}Os = 0.11719 ± 11; contaminated clinopyroxene ^{187}Os/^{188}Os = 0.11790 ± 28), which were all significantly less radiogenic than the bulk-rock (^{187}Os/^{188}Os = 0.12076 ± 62 to 0.12126 ± 64), the interstitial BMS (^{187}Os/^{188}Os = 0.12086 ± 20), and the uncontaminated silicates (^{187}Os/^{188}Os = 0.12066 ± 11 to 0.12131 ± 22). For this particular Kilbourne Hole lherzolite, this not only confirmed that the Os elemental (and therefore ^{187}Os/^{188}Os) budget is controlled by BMS, but also suggested that the bulk-rock budget was likely dominated by Type-2 BMS in equilibrium with the silicates (Fig. 12) that
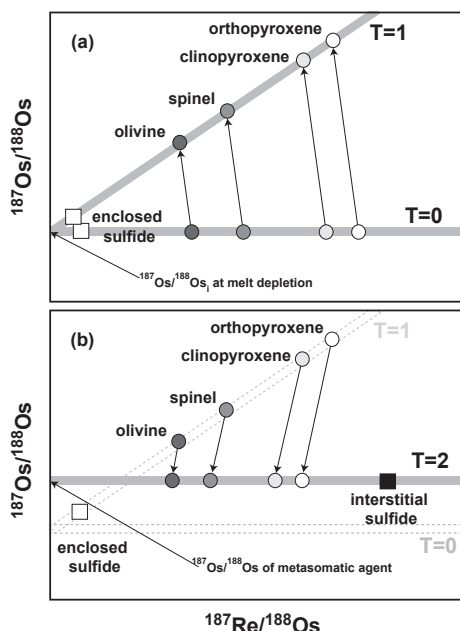

Figure 12. Evolution of Re–Os isotope systematics amongst peridotitic phases as a result of melting and metasomatism. (a) At the time of melt depletion and the enclosure of an immiscible sulfide, in isotopic equilibrium with co-existing silicate phases, all phases will share a common Os isotope ratio but have varying ^{187}Re/^{188}Os at T=0. Over time each phase will evolve according to its ^{187}Re/^{188}Os and the Re decay constant ($\lambda = 1.666 \times 10^{-11}$ yr^{-1} (T=1). The enclosed sulfide, with very low ^{187}Re/^{188}Os retains the ^{187}Os/^{188}Os$_i$. (b) At T=2 the mineral assemblage interacts with a metasomatic melt with a higher ^{187}Os/^{188}Os than the original residual solid. This melt may also be sulfur saturated and precipitate metasomatic, interstitial BMS with a high ^{187}Re/^{188}Os. Interaction of the residual silicates with the metasomatic melt may re-set the Os isotope ratio to that of the metasomatic melt (and interstitial BMS) but the enclosed BMS, buffered against re-equilibration by a high Os content and armored within its host silicate grain, is unaffected, thus preserving Os isotope disequilibrium between the enclosed BMS and the other phases. Modified after Burton et al. (1999).

were slightly more radiogenic than the Type-1 BMS. However, the bulk-rock $^{187}Os/^{188}Os$ was still significantly less radiogenic than PUM (Meisel et al. 2001) and mean chondrite (Shirey and Walker 1998; Day et al. 2016, this volume).

More recently, Harvey et al. (2010, 2011) revisited the issue of Os mass balance in SCLM lherzolites (Fig. 13), examining Os elemental and $^{187}Os/^{188}Os$ systematics in four lherzolites from Mont Briançon, French Massif Central (Harvey et al. 2010) and two harzburgites and a further two lherzolites from Kilbourne Hole, NM USA (Harvey et al. 2011). The harzburgites tended to have silicates that were more radiogenic than the bulk rock ($^{187}Os/^{188}Os = 0.11600$ to 0.12131) with low Os concentrations (≤ 142 pg·g^{-1}). Enclosed BMS grains were unradiogenic ($^{187}Os/^{188}Os = 0.1185$ to 0.1235) with high Os concentrations (6–25 µg·g^{-1}), while interstitial BMS grains were radiogenic ($^{187}Os/^{188}Os = 0.1304$ to 0.2163) with generally low Os concentrations (0.001–6 µg·g^{-1}, but with one exceptional grain containing 21 µg·g^{-1}). This suggests that enclosed BMS dominates the Os mass balance of these harzburgites, as confirmed by a quantitative Os elemental and isotopic mass balance (Fig. 13). In total, less than 5% of bulk-rock Os was hosted by the silicates, while the contribution from interstitial BMS was no more than 17% (and as low as 3%) and the remainder (up to 95%) of Os was hosted by Type-1 BMS (Harvey et al. 2011).

One of the two Kilbourne Hole lherzolites in the Harvey et al. (2011) study was similar to the harzburgites, with the same Os elemental and isotope distributions, but requiring an even smaller contribution of Os from interstitial BMS in order to balance the bulk-rock budget (Fig. 13). In the other Kilbourne Hole lherzolite, both the bulk-rock and silicate phases were supra-chondritic, as were most of the interstitial BMS ($^{187}Os/^{188}Os = 0.1291$ to 0.1694), even though some sub-chondritic BMS grains were recovered. In this example, the Os mass balance was controlled more by the interstitial BMS, although Harvey et al. (2011) were unable to calculate an unequivocal Os mass balance in this sample. The lherzolites from Mont Briançon (Harvey et al. 2010) shared many of the Os mass balance characteristics of the Kilbourne Hole peridotites dominated by enclosed BMS (Fig. 13) but, as discussed below, the $^{187}Re/^{188}Os$ and Re/Os signatures of these lherzolites are more difficult to interpret than a simple enclosed versus interstitial BMS division.
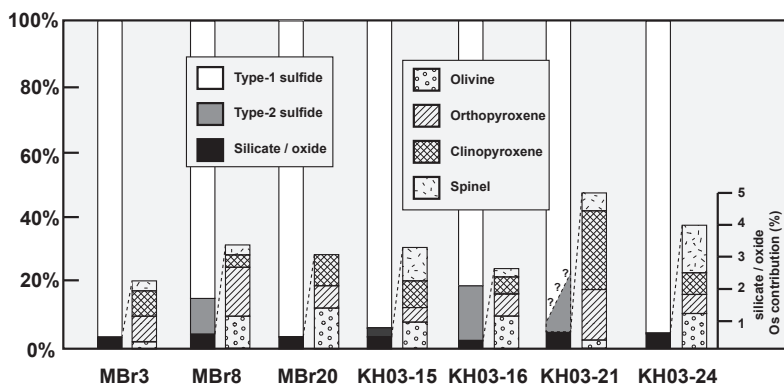
Figure 13. Osmium mass balance calculations for peridotite xenoliths from Mont Briançon, French Massif Central, and Kilbourne Hole New Mexico, USA. Silicates and spinel account for <5% of bulk-rock Os budgets, the remainder being accounted for by a balance between the two populations of BMS grains. The difference in Os concentration between enclosed and interstitial BMS is sufficiently large in MBr 3 that interstitial BMS contributes no more than 1% to the whole rock budget whilst maintaining the measured whole rock isotopic ratio. Similarly, in MBr 8 interstitial BMS can contribute no more than 11%. The contribution from interstitial BMS, in the case of KH03-24, is insignificant, and in KH03-15 and KH03-21 account for 3.5–17.5% respectively of the Os present. The relative contributions of the two BMS populations in KH03-16 is less clear but is probably dominated by the enclosed population. The contribution of the interstitial component in KH03-16 is calculated to be less than 17.5% of the total. Modified after Harvey et al. (2010, 2011).

Overall, the studies of Hart and Ravizza (1996), Burton et al. (1999) and Harvey et al. (2010, 2011) demonstrate that: (i) it is possible to quantify the contributions to bulk-rock peridotite Os mass balance from its constituent phases; (ii) in peridotites where enclosed BMS dominates the Os mass balance, melt depletion is sometimes ancient; and (iii) where interstitial BMS dominates the Os mass balance, bulk-rock Os isotope ratios are not likely to reveal any significant information pertaining to melt depletion. However, this contrasts with the information recorded in interstitial PGM, thought to have formed from extreme melt depletion in spinel lherzolites from Lherz (Luguet et al. 2007). But, as was demonstrated by the radiogenic Kilbourne Hole lherzolite of Harvey et al. (2011), analysis of enclosed BMS from otherwise metasomatized peridotites has the potential to "see through" the late events that precipitated radiogenic interstitial BMS and / or PGM and alloys.

Rhenium mass balance

Rhenium has high $K_{d,\text{sulfide/silicate}}$, but estimated values are significantly lower than the equivalent partition coefficient for Os. For example, the results of experiments designed to measure partitioning of Re and Os between sulfide and silicate melt (Brenan 2008; Brenan et al. 2016 this volume) produced values of $K_d^{\text{Os}}{}_{\text{sulfide/silicate}}$ / $K_d^{\text{Re}}{}_{\text{sulfide/silicate}}$ >150, which is the minimum required to produce the Re/Os fractionation observed in mantle derived magmas. However, the absolute value for $K_d^{\text{Re}}{}_{\text{sulfide/silicate}}$ varies over a wide range, from >20,000 to ~20, depending on f_{O_2}–f_{S_2} conditions imposed during an experiment (Fonseca et al. 2007; Brenan et al. 2016 this volume). This suggests that Re mass balance in peridotites should also be strongly controlled by BMS and, given the strong partitioning of Re into chalcopyrite and hence interstitial BMS, this phase should dominate the Re bulk-rock mass balance. However, a quantitative Re elemental mass balance that is consistent with observed [187]Re/[188]Os in peridotites is still lacking. Achievement of this mass balance is difficult due to the low abundance of Re reported in silicates (typically <100 pg·g⁻¹) combined with difficulties in obtaining low Re analytical blanks. In addition, the partial lithophile character of Re compared to the other HSE (Handler and Bennett 1999; Burton et al. 1999; Harvey et al. 2010, 2011) and associated implications for Re–Os fractionation during mantle melting (e.g., Righter and Hauri 1998; Mallmann and O'Neill 2007) make Re behavior with melting more difficult to predict, especially in the presence of residual sulfide. Rhenium is easily removed from a peridotite source during partial melting as it has a low bulk $K_{d\,\text{peridotite/basaltic melt}}$ (Brenan et al. 2003). The bulk-rock incompatibility of Re in the mantle leads to its high concentration in melt (Alard et al. 2002; Harvey et al. 2010, 2011; Warren and Shirey 2012), especially as BMS dissolve into undersaturated silicate melt during partial melting.

This first order interpretation of Re mass balance is not sufficient to interpret the Re–Os isotope systematics of peridotites with complicated histories such as those from Mont Briançon (Harvey et al. 2010), as the two distinct populations of BMS are difficult to distinguish based on [187]Re/[188]Os, Re and Os concentrations. Similar to the Griffin et al. (2002) study of Siberian xenoliths, Mont Briançon has different populations of BMS that were interpreted as having interacted with each other (see the section on peridotite-hosted BMS above). In both studies, unradiogenic Os isotope ratios have often been preserved in sulfides that at least originated as enclosed BMS, but [187]Re/[188]Os ratios were elevated and high Re concentrations often accompanied high Os concentrations. The original low Re/Os elemental ratio of enclosed BMS may have become elevated through melting and mixing with interstitial BMS melt, but the immediate effect on [187]Os/[188]Os was negligible because of the low Os concentration in interstitial BMS. It is only with the addition of time-integrated [187]Os from [187]Re decay that the original [187]Os/[188]Os of the hybrid BMS becomes progressively obscured.

Lead mass balance

Although the Pb isotope composition of the mantle has been of interest to geochemists for over half a century (e.g., Holmes 1946; Patterson 1956; Allègre 1969), the role that BMS play in the Pb mass balance of the mantle has been less well explored. Recent interest in the Pb elemental and isotopic composition of mantle sulfides stems from a potential solution to the first Pb paradox (i.e., the position of oceanic Pb isotopic compositions in the "future" Pb position, to the right of the geochron; Allègre 1969), as discussed in the final section of this chapter. A quantitative Pb mass balance (elemental and isotopic) based upon individual peridotites has yet to be accomplished, despite studies that have suggested that mantle Pb resides predominantly in BMS (Meijer et al. 1990; Hart and Gaetani 2006). Hart and Gaetani (2006) predicted that if BMS are the main mantle Pb reservoir they should represent c. 0.05% of the mantle to be consistent with PUM sulfur concentration estimates (Lorand 1990; O'Neill 1991; Palme and O'Neill 2003) and contain ca. 75 µg·g^{-1} Pb. More recently, Pb concentrations in individual BMS grains extracted from abyssal peridotites from the MAR, Gakkel and SWIR were measured by Burton et al. (2012) and Warren and Shirey (2012). Warren and Shirey (2012) found concentrations that ranged from 0.12–12 µg·g^{-1} (mean 4 µg·g^{-1}) whereas those in Burton et al. (2012) ranged from 1.5–52 µg·g^{-1} (mean 19 µg·g^{-1}). These values possibly over-estimate the average Pb concentration as data becomes increasingly difficult to obtain at abundances below about 1 µg·g^{-1}, due to the minute quantities involved in an individual BMS grain analysis.

Using these estimates for BMS Pb concentrations yields a significant deficit of Pb in many abyssal peridotites (Warren and Shirey 2012). For example, using the average Pb concentration of 4 µg·g^{-1} Pb found in Gakkel and SWIR BMS (Warren and Shirey 2012) and the average abyssal peridotite BMS modal abundance of 0.02% (Luguet et al. 2001 2003) gives a bulk peridotite Pb concentration of 0.8 ng·g^{-1}, significantly lower than the estimate of 150 ng·g^{-1} for PUM (McDonough and Sun 1995) and also lower than the estimate of 21 ng·g^{-1} for depleted MORB mantle (DMM; Salters and Stracke 2004; Workman and Hart 2005). Using the maximum modal estimate of 0.06% for mantle BMS in abyssal peridotite (Luguet et al. 2003) and the maximum BMS Pb concentration observed by Warren and Shirey (2012) of 12 µg·g^{-1}, only about 40% of Pb in DMM can be accounted for. Using the mean value of Pb in BMS analyzed by laser ablation (Burton et al. 2012) from the 15° 20' Fracture Zone, MAR (19 µg·g^{-1}) can account for approximately 60% of DMM Pb. Using the maximum value of 52 µg·g^{-1} and the maximum modal abundance of 0.06 % can account for the mean DMM Pb abundance of 21 µg·g^{-1}, but would still only represent ca. 25% of the estimated PUM Pb abundance. However, these maximum estimates of BMS Pb concentration and abundance are not representative of the oceanic mantle.

Observations of xenoliths suggest that Pb is present in the silicate phases at concentrations <1 µg·g^{-1} (e.g., Meijer et al. 1990; Hauri et al. 1994; Carignan et al. 1996; Eggins et al. 1998; Norman 1998; Ionov et al. 2002), but given their modal abundance this can account for a significant proportion of the bulk Pb. For example, Carignan et al. (1996) measured the Pb concentrations of the main silicate phases (olivine 11 ng·g^{-1}; orthopyroxene 20 ng·g^{-1}; clinopyroxene 470 ng·g^{-1}) in two peridotite xenoliths and calculated their bulk-rock Pb abundances to be 21 and 29 ng·g^{-1}, without the inclusion of peridotite-hosted BMS. These values were remarkably close to the measured bulk-rock Pb concentrations of 16 and 40 ng·g^{-1}, respectively. In this instance the three main silicate phases in peridotites can account for 73–100% of mantle Pb concentrations. Overall, it would appear that mantle BMS contain much less Pb than that predicted by Hart and Gaetani (2006).

The major difficulty with a Pb elemental and isotopic mass balance for the oceanic mantle is a lack of data on Pb in the silicate phases and bulk rock. Warren and Shirey (2012) provided an elemental mass balance for a single SWIR sample based on Pb concentration data for pyroxenes

and bulk peridotite. They found reasonable agreement between the measured bulk-rock concentration of 31 µg·g^{-1} and the reconstructed concentration of 22 µg·g^{-1} (excluding sulfides), as olivine would only need to contain 13 µg·g^{-1} to fully match the measured value. However, the measured bulk-rock concentration of 31 µg·g^{-1} is higher than the current estimate of 21 µg·g^{-1} for Pb in DMM, indicating the need for more systematic analysis of Pb concentrations in abyssal peridotite, particularly as studies of peridotite xenoliths have shown that bulk Pb concentrations can be highly variable (e.g., Carignan et al. 1996). This will also require improved constraints on the effect of alteration on peridotite Pb concentrations. Clearly several fundamental unknowns remain to be investigated with respect to the Pb isotopic and elemental mass balance in the mantle, most importantly, the contribution that mantle BMS make to solving the first Pb paradox.

GEOCHRONOLOGICAL METHODS, MODEL AGES, AND POTENTIAL PITFALLS.

### Sulfide Re–Os isochrons, T_{MA}, T_{RD}, and γOs.

An isochron is the "gold standard" in geochronology, notwithstanding the possiblility that an isochron may in fact represent a mixing line. For sulfides, Re–Os isochrons (Fig. 14) can be generated when a selection of co-genetic BMS in chemical equilibrium at the time of system closure, but with a range of Re–Os, evolve over time, under closed-system conditions. This, in theory at least, allows their isochronous relationship to be used as a precise measure of the time elapsed since they were isolated from open-system conditions. Isochrons also have the advantage of providing both age and initial isotopic composition. By projecting the slope of the isochron back to the intercept on the *y*-axis, i.e., at zero ^{187}Re/^{188}Os, this allows the ^{187}Os/^{188}Os at the time the system closed to be calculated, and hence inferences about the source of the sulfides and petrogenetic history can be made. Figure 14 shows examples of true isochrons among diamond-hosted BMS populations from Aulbach et al. (2004a) and Westerlund et al. (2006). Harvey et al. (2006) came close to a true isochron with a population of enclosed serpentinite-hosted BMS from the 15° 20' N Fracture Zone on the MAR (mean
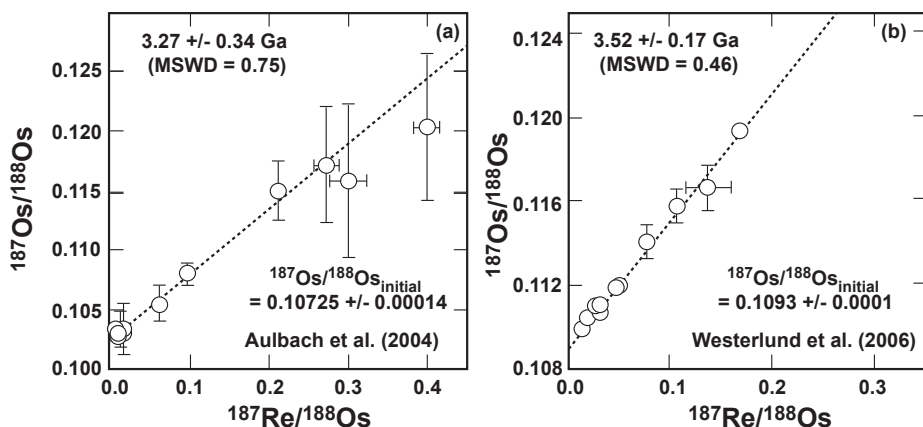
Figure 14. Rare examples of true Re–Os isochrons (MSWD<2.4) derived from diamond-hosted BMS grains recovered from the Slave Craton, Canada. (a) Re–Os isochron age of 3.27±0.34 Ga (MSWD=0.75) for BMS grains recovered from xenocrystic olivine and pyroxenes from kimberlites in the Lac de Gras area, central Slave Craton (modified after Aulbach et al. 2004a). (b) Re–Os isochron age of 3.52±0.17 (MSWD=0.46) derived from diamonds in harzburgitic host rocks from the 53 Ma Panda kimberlite pipe, Ekati Mine, North West Territories, Canada (modified after Westerlund et al 2006).

square weighted deviation or MSWD of 3.3), as shown in Figure 15. For this same location, Burton et al. (2012), in a plot of $^{207}Pb/^{204}Pb$ versus $^{206}Pb/^{204}Pb$ (Fig. 16), determined an isochron age of 1.83 ± 0.23 Ga (MSWD = 0.18) for enclosed serpentinite-hosted BMS. This value agrees, within analytical uncertainty, with the Re–Os age of 2.06 ± 0.26 Ga from Harvey et al. (2006); i.e., compare Figs. 15 and 16.

Unfortunately, many arrays of data derived for non-diamond related sulfides have MSWD values that are >2.4, indicating poor statistics for the data regression (Faure 2001), and cannot meet the conditions for a precise Re–Os geochronometer. Instead, isotopic data for these BMS can be compared to reference isochrons as an alternative to actual isochron regressions. In many instances, this is the closest to an isochron age that many studies are able to achieve. In BMS from diamonds, such data arrays can give a useful indication of the general age for the diamonds in question. That such BMS grains might not fall on a strict isochron is understandable given that diamonds are xenocrysts whose spatial relationship to each other in the lithosphere is not known and thus may be too far apart to have achieved strict chemical equilibrium.
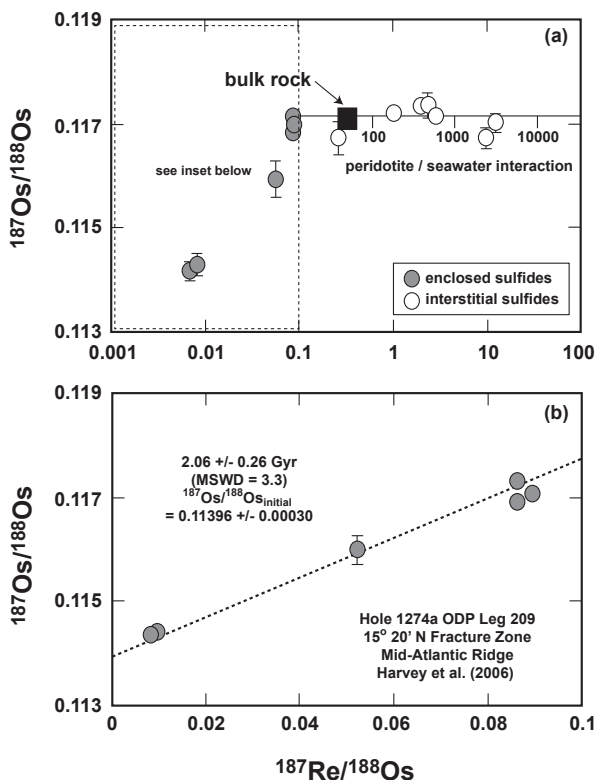
Figure 15. (a) $^{187}Re–^{187}Os$ isotope evolution diagram for serpentinite-hosted BMS grains from sample 2R1 31–37, Hole 1274A, 15° 20' N Fracture zone, Mid-Atlantic Ridge. Most of the BMS grains yield an indistinguishable $^{187}Os/^{188}Os$ isotope composition from that of the whole-rock, but possess a wide range of $^{187}Re/^{188}Os$. The solid curve illustrates the calculated trajectory for mixing of the low $^{187}Re/^{188}Os$ sulfides with seawater, and shows that even for sulfide/seawater ratios of 10^4 there is no measurable shift in $^{187}Os/^{188}Os$ ratio. (b) Regression of high-Os sulfides, with a rounded morphology, yields a best-fit line corresponding to an age of 2.06 ± 0.26 Gyr (MSWD = 3.3) using Model 3 of Ludwig (1997). Modified after Harvey et al. (2006).
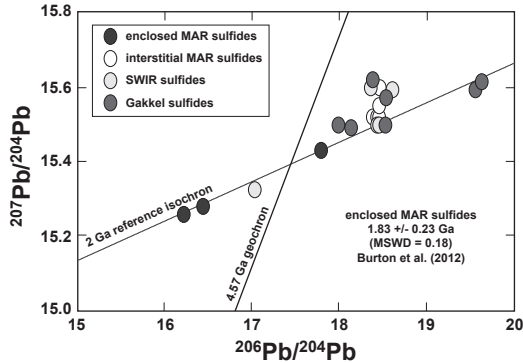
Figure 16. ^{207}Pb-^{206}Pb/^{204}Pb isotope diagram for BMS grains from abyssal peridotites from a single MAR abyssal peridotite (Burton et al. 2012) and from multiple Gakkel and SWIR peridotites (Warren and Shirey 2012). For the MAR sample, interstitial BMS (white circles) possess radiogenic Pb isotope compositions consistent with recent seawater interaction. In contrast, included MAR BMS grains (black circles) are unradiogenic, yielding a ^{207}Pb–^{206}Pb age of 1.83 ± 0.23 Gyr (MSWD = 0.18, model 2; Ludwig 1997). Base metal sulfide grains from the Gakkel (5 samples) and SWIR (7 BMS grains from 5 samples) show no clear distinction in Pb composition between included and interstitial BMS. Two standard error bars are smaller than the symbol sizes in all cases. Modified after Burton et al. (2012) and Warren and Shirey (2012).

The complexity of melt depletion and subsequent metasomatism, tectonism and metamorphism often obscures any meaningful information that could have been extracted from a population of BMS grains prior to their disturbance. Diamond-hosted BMS are less susceptible to these complexities because they are encapsulated and protected from secondary melts and fluids, but they do have xenocrystic-related uncertainties. As a consequence of these difficulties in producing Re–Os isochron ages, model ages are often employed instead. A model age represents a time when the isotopic growth curve for a mineral coincides with the isotopic evolution of a reference reservoir such as the mantle. A model age is an attempt to derive meaningful geochronological information with imperfect knowledge of the sequence of events that have affected the samples, or when there is simply an insufficient number of samples with which to construct an isochron. For example, they allow an "age" to be derived from a single data point.

In the case of the Re–Os isotope system, two types of model age calculations are in common use (Fig. 17). Both calculations compare ^{187}Os/^{188}Os in an unknown to the ^{187}Os/^{188}Os evolution curve for mantle with chondritic Re/Os. The evolution of ^{187}Os/^{188}Os from the initial osmium isotope ratio of IIIA iron meteorites (the most primitive Solar system initial value: ^{187}Os/^{188}Os$_i$ = 0.09531; Smoliar et al. 1996) is used to estimate the average composition of chondritic meteorites for the present day (Fig. 17a). A ^{187}Re decay constant (λ) of 1.666×10^{-11} yr^{-1} is used for this and all other age-dependent calculations:

$$^{187}\text{Os}/^{188}\text{Os}_t = {}^{187}\text{Os}/^{188}\text{Os}_i + {}^{187}\text{Re}/^{188}\text{Os}_{\text{chon}}(e^{\lambda(4.558 \times 10^9)} - e^{\lambda t}). \tag{1}$$

The measured composition for chondrites includes early measurements that gave 0.1262 ± 0.0005 (Allègre and Luck 1980; Luck et al. 1980; Walker and Morgan 1989). Meisel et al (1996) reported a narrow range of present-day ^{187}Os/^{188}Os ratios for 11 ordinary chondrites of 0.1289 ± 0.0022 (2σ) and a similar present-day ^{187}Os/^{188}Os ratio of 0.1283 ± 0.0008 (2σ) for 8 enstatite chondrites. The latter was later refined by Walker et al. (2002a) and termed the enstatite chondritic reservoir (ECR), with present-day ^{187}Os/^{188}Os = 0.1281 and ^{187}Re/^{188}Os = 0.421. In contrast, a suite of 4 carbonaceous chondrites defined a 1–2% lower ^{187}Os/^{188}Os ratio of 0.1263 ± 0.0008. A detailed discussion of the variability of chondrite ^{187}Os/^{188}Os can be found in this volume in the chapter on HSE in planetary bodies (Day et al. 2016, this volume).
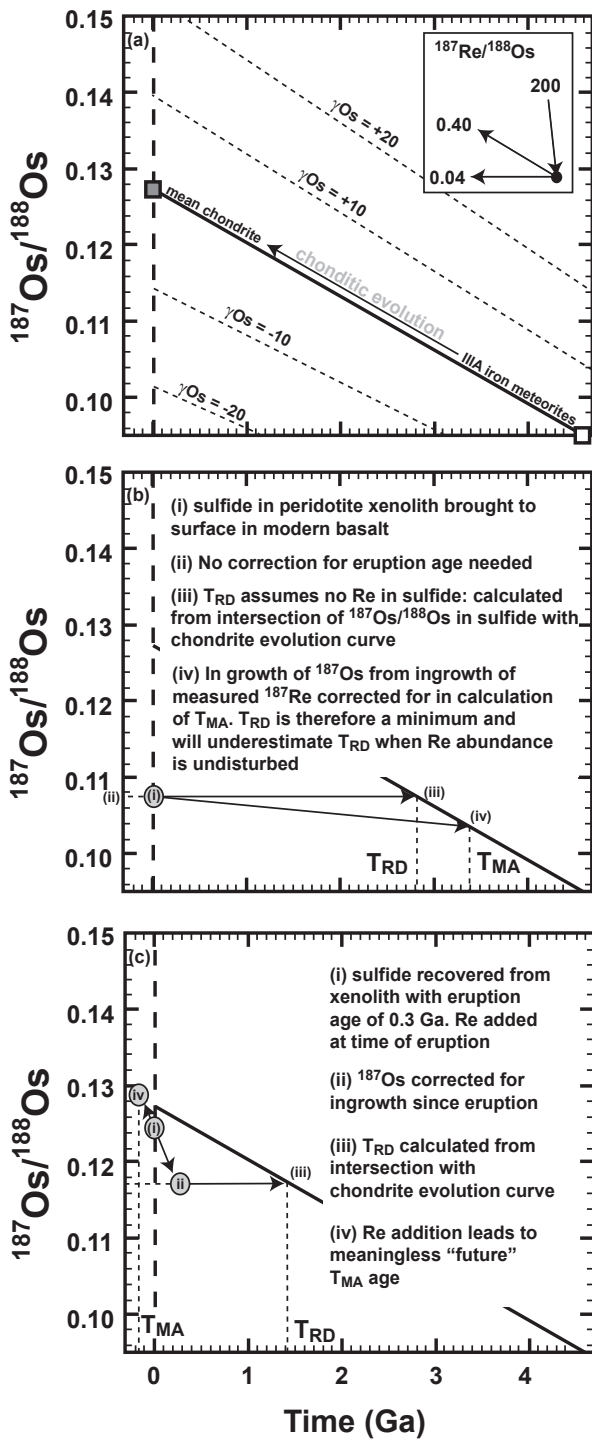
Figure 17. Graphical representation of (a) the chondrite evolution curve over the course of Earth history and materials with higher and lower γOs (from −20 to +20). Starting composition for chondrite evolution curve is ^{187}Os/^{188}Os=0.09531 (Smoliar et al. 1996). Present day mean chondrite ^{187}Os/^{188}Os=0.1270 (Shirey and Walker 1998). (b) Graphical representation of the difference between T_{MA} and T_{RD} derived from a BMS grain recently erupted in a peridotite xenolith (and no perturbation of original Re). This contrasts with (c) where the sulfide experienced Re-enrichment from the host lava en-route to the surface. Recent Re addition does not materially affect the ^{187}Os/^{188}Os of the sulfide but gives meaningless "future" ages. Modified after Shirey and Walker (1998).

The two commonly employed model age calculations (Walker et al. 1989; Shirey and Walker 1998) are T_{MA} (Eqn. 2) and T_{RD} (Eqn. 3), where both model ages use Equation (1) to calculate a mantle evolution curve. For T_{MA}, both the $^{187}Re/^{188}Os$ and $^{187}Os/^{188}Os$ ratios in the unknown are used to calculate the time of separation from asthenospheric mantle:

$$T_{MA} = \frac{1}{\lambda} \ln\left\{ \frac{(^{187}Os/^{188}Os_{chon} - ^{187}Os/^{188}Os_{sample})}{\left(^{187}Re/^{188}Os_{chon} - ^{187}Re/^{188}Os_{sample} \right)} + 1 \right\}. \tag{2}$$

This model age can be used both for BMS with low Re/Os (e.g., peridotite-hosted Type-1 BMS and diamond-hosted peridotitic BMS) and for BMS with much higher Re/Os (e.g., pyroxenite-hosted BMS, peridotite-hosted Type-2 BMS, and diamond-hosted eclogitic BMS). It assumes that the Re/Os measured today in a sample is representative of its long-term history in the mantle. If this assumption is correct, this implies that the geochronometer started at the time that the sulfide cystallized and no subsequent gain or loss of Re occurred. As such, T_{MA} ages can provide robust geochronological information regarding the age of an individual BMS grain (Fig. 17b). It is not always safe to assume that undisturbed Re/Os systematics have been preserved. For example, where an elevated Re/Os elemental ratio accompanies an unradiogenic $^{187}Os/^{188}Os$, or the converse, where an unsupported radiogenic $^{187}Os/^{188}Os$ (i.e., high $^{187}Os/^{188}Os$ with low Re/Os) is observed, a T_{MA} calculation will yield an erroneous number that likely bears no resemblance to any actual event in the history of the sulfide (Fig. 17c). Such a situation can occur when Re from the host lava (such as a kimberlite) is added to a xenocryst or xenolith during transport to the surface. Under these circumstances a T_{MA} age might yield a nonsense or "future" age and in this case a T_{RD}, or rhenium depletion age, is likely to be the most appropriate model age calculation.

T_{RD} is calculated as an intersection time with chondritic mantle growth, assuming a melt-depletion event previously removed all Re from the sample. It is calculated using the following equation:

$$T_{RD} = \frac{1}{\lambda} \ln\left\{ \frac{\left(^{187}Os/^{188}Os_{chon} - ^{187}Os/^{188}Os_{sample\,(EA)} \right)}{^{187}Re/^{188}Os_{chon}} + 1 \right\}, \tag{3}$$

where $^{187}Os/^{188}Os_{sample\,(EA)}$ is the ratio at the time of separation from the mantle:

$$^{187}Os/^{188}Os_{sample(EA)} = ^{187}Os/^{188}Os_{sample} - ^{187}Re/^{188}Os_{sample} \left(e^{\lambda t} - 1 \right). \tag{4}$$

For a xenolith-hosted BMS (Fig. 17c), $^{187}Os/^{188}Os_{sample\,(EA)}$ represents the osmium isotope ratio at the time the host xenolith was entrained and brought to the surface in a lava. However, the correction in the sample's isotopic composition defined by $^{187}Os/^{188}Os_{sample(EA)}$ is only necessary if the eruption of the host lava is far enough in the past or enough Re has been added by the host lava to dramatically change the $^{187}Re/^{188}Os$ such that sufficient ingrowth of ^{187}Os could be anticipated. With T_{RD}, the assumption is made that Re was completely removed from the sulfide during the event that isolated it from the convecting mantle. Therefore, in the absence of any ingrowth of ^{187}Os from ^{187}Re, the measured $^{187}Os/^{188}Os$ of the sulfide has remained unchanged since the sulfide crystallized. This is clearly an oversimplification, as even undisturbed diamond-hosted peridotitic BMS and Type-1 peridotite-hosted BMS contain some Re and some ^{187}Os ingrowth is inevitable. Hence the measured $^{187}Os/^{188}Os$ used in a T_{RD} age calculation will only yield a minimum age (Fig. 17) but one that could nonetheless be useful if the Re concentration is low.

A quick examination of equation (3) reveals that relying entirely upon a measured $^{187}Os/^{188}Os$ ratio for a model age may not yield the most accurate geochronological information and that, in examples where the measured $^{187}Os/^{188}Os$ exceeds that of the chondritic reference value, it is not possible to obtain any useful geochronological information. Meaningless T_{RD} ages in the future

and T_{MA} ages older than 4.5 Ga reflect derivation of Os from a source more radiogenic than PUM and / or the local disturbance of the Re–Os system. Fortunately, most host lavas have very low Os content and thus their ability to modify the Os isotopic composition of a mantle peridotite or a BMS grain is very limited (e.g., Walker et al. 1989; Shirey and Walker 1998).

An additional method has been developed to handle datasets produced by LA MC ICPMS as a consequence of the relative ease with which large numbers of $^{187}Re/^{188}Os$ and $^{187}Os/^{188}Os$ ratios can be generated (e.g., Griffin et al. 2002, 2004; Marchesi et al. 2010; González-Jiménez et al. 2014). Calculating model ages for these sulfides can give a high density of "ages" for a given region, allowing model ages to be plotted on histograms. This in turn allows peaks in the frequency of ages to be determined. More recently, large datasets of model ages have been presented as relative probability plots. For example, the model ages generated from BMS inclusions in olivines from Udachnya, Siberia (Griffin et al. 2002, using the models of Ludwig 2000) were incorporated into a relative density plot and used to suggest that most of the lithospheric mantle beneath the Daldyn kimberlite field formed during the period 3–3.5 Ga.

Bulk-rock data and BMS data generated by TIMS could also be used for this type of analysis, but the time taken to acquire sufficient data using TIMS is considerably longer. A case in point are the relative probability plots for the Kaapvaal and Slave cratons presented in Pearson and Wittig (2008), which are each comprised of TIMS data compiled from measurements acquired over several years (Kaapvaal: Pearson et al. 1995a; Carlson et al. 1999; Menzies et al. 1999; Irvine et al. 2001; Carlson and Moore 2004; Simon et al. 2008; Slave craton: Irvine et al. 2003; Aulbach et al. 2004a; Westerlund et al. 2006). In addition to a large peak in BMS Re–Os model ages at 2.5–3.0 Ga for the Kaapvaal craton (Fig. 18), the relative probability plots of Pearson and Wittig (2008) also demonstrated a main peak in BMS model ages around 2.8–2.9 Ga (see also Aulbach et al. 2004a) and subsidiary peaks at 1.3 Ga, 2.2 Ga, and 3.9 Ga for the Slave Craton (Fig. 18). These examples demonstrate the power of large numbers of Re–Os model ages to constrain the timing of regional scale events and the link, or lack thereof, between ages preserved in the SCLM and crust forming events (i.e., large-scale partial melting). Aulbach et al. (2016, this volume) discuss the significance of relative probability plots in more detail, including the use of HSE in dating cratons.

Finally, often quoted alongside Re–Os model ages, although not a model age itself, is the concept of γOs (gamma osmium), where the Os isotope ratio of an unknown is compared to that of a chondritic reference, with the difference at a specific time between the unknown and the chondritic reference (γOs) reported as either a positive or negative percentage (Fig. 17a). The underlying concept is exactly the same as the delta notation (δ) commonly used for many stable isotope systems (per mil deviations from a known standard) and the epsilon notation (ε) for Nd and Hf isotope ratios (parts per 10,000 deviation from a known standard):

$$\gamma Os_{(t)} = \left\{ \frac{\left(^{187}Os/^{188}Os_{sample(t)} \right)}{\left(^{187}Os/^{188}Os_{chon(t)} \right)} - 1 \right\} \times 100. \tag{5}$$

Samples with positive γOs often are described as enriched, radiogenic or suprachondritic and imply long-term elevated $^{187}Re/^{188}Os$. Samples with negative γOs often are described as depleted or unradiogenic and imply long-term lowered $^{187}Re/^{188}Os$.

Potential pitfalls with sulfide geochronology.

The fractionation of Re and Os during mantle melting preserves distinct Re/Os and $^{187}Os/^{188}Os$ systematics in primary BMS grains enclosed within either a silicate or diamond host (i.e., Type-1). These contrast with Type-2 BMS that are associated with metasomatism, which makes the Re–Os isotope system an ideal tool for dating melt depletion in the former and metasomatism in the latter. However, as with all isotope systems, there are limits to the utility of the Re–Os isotope system.
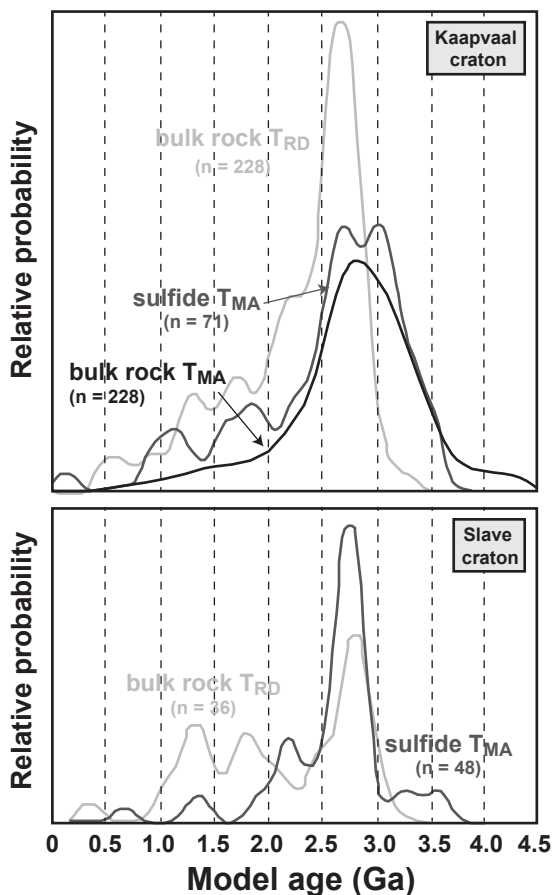
Figure 18. Probability density plots of Re–Os model ages for bulk-rock peridotites and BMS grains for the Kaapvaal and Slave cratons. Kaapvaal: Pearson et al. (1995a), Carlson et al. (1999), Menzies et al. (1999), Irvine et al. (2001), Carlson and Moore (2004) and Simon et al. (2008); Slave: Irvine et al. (2003), Aulbach et al. (2004a) and Westerlund et al. (2006); T_{RD} ages are corrected to the eruption age of the host kimberlite. Model age equations for T_{RD} and T_{MA} of Walker et al. (1989) and Pearson and Shirey (1999) are calculated using for $^{187}Os/^{188}Os= 0.1283$ and $^{187}Re/^{188}Os=0.422$ chondritic mantle. Modified after Pearson and Wittig (2008).

Ages calculated from sulfide isotopic compositions are subject to a number of potential pitfalls, including uncertainties in model age calculations, modifications induced during sample preparation or analysis, and changes to original Re–Os isotope systematics that derive from mantle processes. All of these modifications may obscure or even render useless model age information preserved in mantle BMS.

Uncertainties in model age calculations. Although the sulfides which are the subject of this chapter are mantle-derived, to obtain geologically meaningful T_{RD} and T_{MA} ages a choice of the reference reservoir for $^{187}Os/^{188}Os$ at time in the past must be made. The range and heterogeneity of published mantle values and, in particular, the wide disparity between mean $^{187}Os/^{188}Os$ for abyssal peridotite versus that of PUM (ca. 4% difference in $^{187}Os/^{188}Os$ between these two reservoirs, discussed in detail in Rudnick and Walker 2009; cf. Gannoun et al. 2016, this volume) means that a wide range of model ages for a single BMS grain could be derived depending upon

which mantle value was chosen for normalization. Using abyssal peridotite or PUM as a basis for calculating T_{MA} and T_{RD} ages yields younger and older model ages, respectively, than using mean chondrite. The main problem with PUM estimates is that PUM is an artificial construct designed to predict the composition of a notional pristine mantle by projecting back from samples that have been modified over the course of Earth's history. The disparity in the evolution models for the mantle impacts model ages by ca. 300 Ma (e.g., Pearson and Wittig 2008; Rudnick and Walker 2009). These differences are relatively unimportant for ancient systems but can be significant when attempting to date Phanerozoic events using the Re–Os geochronometer. Therefore model age calculations relative to PUM are probably not appropriate (Rudnick and Walker 2009). The carbonaceous chondrite average $^{187}Os/^{188}Os$ of 0.1262 ± 0.0005 (see Day et al. 2016, this volume) is probably still the best, and is the most commonly used reference for calculating model ages. In general, however, model ages rarely can carry a precision better than several hundred million years and this imprecision will offset some of the need for an accurate knowledge of the compositional evolution of the reference reservoir (e.g., the mantle).

Sample preparation issues. Some diamond-hosted BMS break up during the process of removing them which can result in skewed Re/Os ratios (Richardson et al. 2009). This is because Re is preferentially partitioned into chalcopyrite relative to pyrrhotite and/or pentlandite whereas the reverse is true for Os (e.g., Craig and Kullerud 1969; Li et al. 1996; Piña et al. 2012). The separation of chalcopyrite from pyrrhotite or former MSS will typically occur at a much later time (e.g kimberlite eruption) relative to the time averaged Re/Os that was established for the whole sulphide grain. This can introduce a different measured $^{187}Re/^{188}Os$ if chalcopyrite or pyrrhotite makes up a disproportionate part of the analysis. For example, Richardson et al. (2001) reported up to 30% difference in $^{187}Re/^{188}Os$ amongst fragments of chalcopyrite, pentlandite and pyrrhotite recovered from eclogitic diamonds. An artificial lowering of $^{187}Re/^{188}Os$ will skew the calculated T_{MA} of an affected sulfide to an artificially young model age (see Eqn. (2); Fig. 19). Consequently, Richardson et al. (2001) attributed scatter on Re–Os isochrons to the possible incomplete recovery of sulfide inclusions, in particular chalcopyrite-rich rims. The absence of well correlated linear arrays for BMS Re–Os isotope data was also attributed by Beyer et al. (2004) to the potential loss of Re-rich chalcopyrite rims during the preparation of polished sections for *in situ* analysis by LA MC ICPMS. With careful sample preparation, these artificially induced Re/Os fractionations and potential corruptions of model age calculations may be avoided, or at least minimized.

Mantle-derived changes to Re–Os systematics. Negative model ages, often meaninglessly referred to as "future ages", along with model age calculations that return "ages" that are greater than the age of the Earth are the result of a departure away from the idealized Re–Os isotope systematics of Type-1 peridotite-hosted (or diamond-hosted peridotitic) BMS grains. Examination of Equations (2) and (3) reveals that if melts with Re or Os interact with a population of BMS grains, the original geochronological information that was contained within that population may be obscured. Hence, BMS model ages should not be used indiscriminately, as their compositions may reflect cumulative effects of several events. Of particularly importance are the addition of Re (both recent and ancient) and radiogenic Os, and the implications of these on T_{MA} and T_{RD} are summarized in Figure 19.

Osmium enrichment. Unsupported radiogenic Os (i.e., insufficient ^{187}Re to account for the ^{187}Os present in a geologically reasonable time, also referred to as suprachondritic; Fig. 19) can be attributed to subduction-related processes. Subduction can involve sulfides equilibrated with the slab (the crustal portion of which is basaltic with a high Re/Os) and fluids in the wedge which can move Os. Highly oxidising subduction-related fluid liberates radiogenic Os, but not Re, from the downgoing slab (Brandon et al. 1996), resulting in a higher $^{187}Os/^{188}Os$ that suggests derivation from a time-integrated high-Re/Os reservoir. This elevated Os isotopic composition appears to be a general feature of arc peridotite whole rocks (e.g., Widom et al
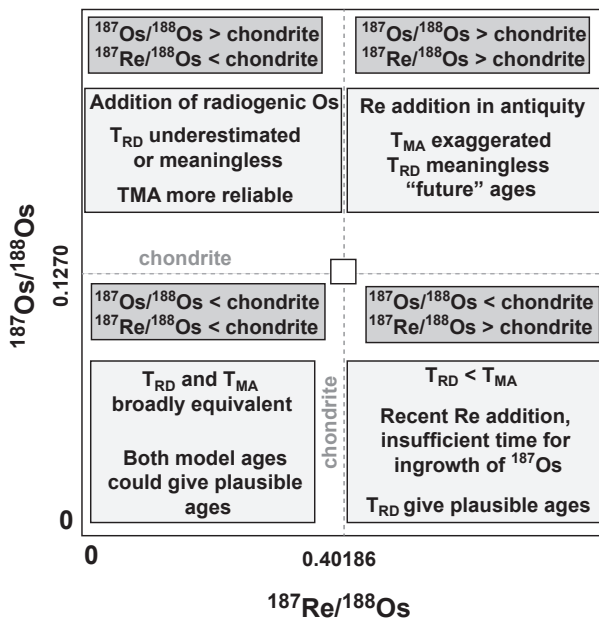
Figure 19. The effects of recent and ancient Re addition on sulfide T_{MA} and T_{RD} compared to seemingly undisturbed $^{187}Os/^{188}Os$ and $^{187}Re/^{188}Os$ (i.e., both <mean chondrite). Values which plot in the lower left quadrant do not necessarily preclude any metasomatism since early melt depletion (cf. Wang et al. 2009, where interaction with modest amounts of silicate melts may still yield plausible T_{MA} and T_{RD}), but may be considered the least likely to be seriously compromised.

2003). For this to be observed in an individual BMS grain requires a multistage history for that grain, which may have crystallized as an unradiogenic MSS with a low Re/Os ratio, followed by interaction with a melt or fluid that contains radiogenic Os, but relatively little Re (e.g., Wang et al. 2009). This process has the effect of raising the $^{187}Os/^{188}Os$, but suppressing still further the originally low Re/Os ratio of the sulfide. These features were evident in the peridotitic BMS inclusion suite studied from the Ekati Mine, in the Panda kimberlite pipe, Slave craton, where low Re/Os BMS grains were enriched in radiogenic Os associated with specific zones of diamond growth (Westerlund et al. 2006). Complicated, multistage scenarios are not as common in sulfide inclusions in diamond as they are in sulfides from mantle peridotites (see below), because the encapsulation in diamond gives the sulfide an impervious host. While a detailed appraisal of subduction-related HSE behavior is beyond the scope of this chapter, some selected examples that are specific to BMS Re–Os isotope systematics are highlighted here.

Gonzáles-Jiménez et al. (2014) reported suprachondritic $^{187}Os/^{188}Os$ in a population of BMS grains analyzed *in situ* in a suite of peridotite xenoliths from Calatrava, Spain (Fig. 20). As a consequence of elevated $^{187}Os/^{188}Os$, none of the disturbed BMS Re–Os isotopic ratios yielded geologically reasonable T_{MA} or T_{RD} model ages. They attributed these perturbed Re–Os isotope systematics to interaction with fluids originating in a supra-subduction zone environment where dehydration produces a fluid enriched in radiogenic Os (e.g., Brandon et al. 1996; Reisberg et al. 2004; Walker et al. 2002b). Beyer et al. (2004) also reported radiogenic initial $^{187}Os/^{188}Os$ (0.1282±0.0061) in BMS grains from the Western Gneiss Region of Norway and implicated the introduction of Os derived from sources with higher long-term Re/Os than the peridotites, likely local garnet pyroxenite and eclogite dykes. Similarly, in a study of diamond-hosted BMS
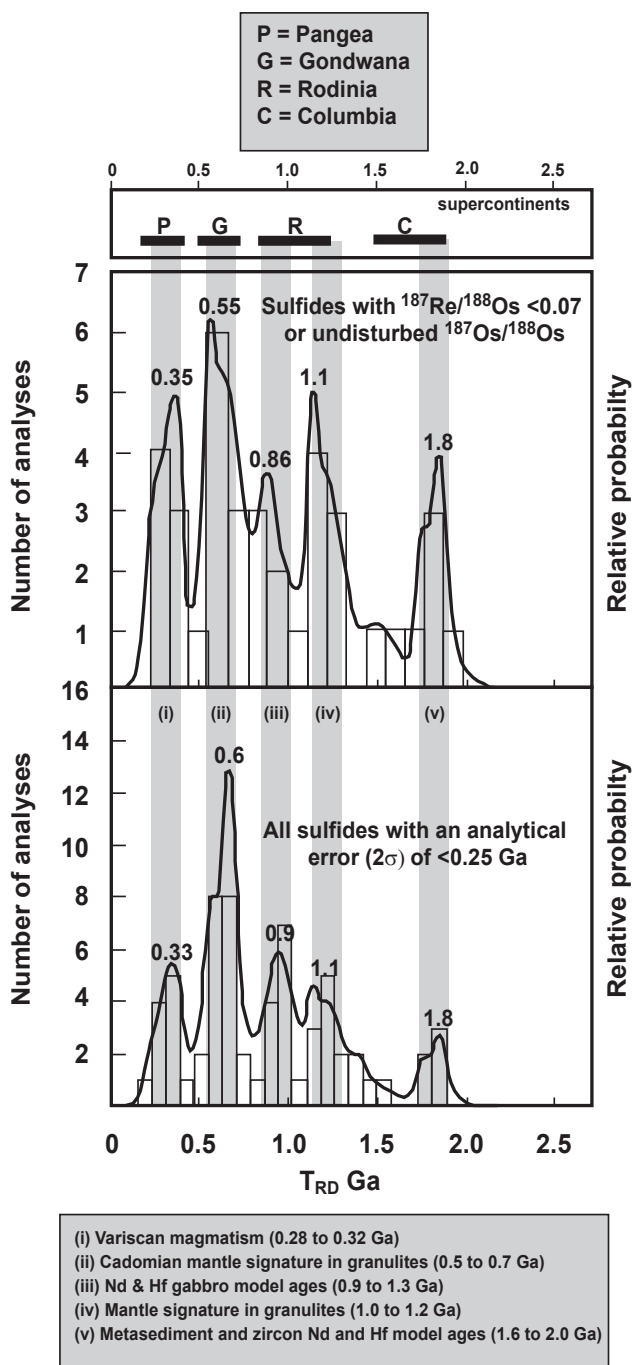
Figure 20. Relative probability plot of rhenium depletion ages of BMS grains from Calatrava peridotite xenoliths, Spain. Binned histograms of calculated model ages are used to produce relative probabilities that coincide with major crust-forming events and supercontinent assemblage outlined in the box. Rhenium depletion ages calculated according to Equation (3). Modified after González-Jiménez et al. (2013, 2014).

grains from the Slave Craton, Canada by Westerlund et al. (2006), sulfides with unsupported radiogenic $^{187}Os/^{188}Os$, which yielded future model ages, incorporated evolved radiogenic Os, thought to have been derived from fluids in an Eoarchean subduction setting.

Some independent evidence for a subduction zone origin is preserved in the metal/sulfur ratios of BMS that possess unsupported radiogenic Os isotope ratios. Wang et al. (2009) reported a negative correlation between metal/sulfur ratios and $^{187}Os/^{188}Os$ ratios of BMS that bore the signature of unsupported radiogenic Os. They suggested that as oxygen is added to a sulfide melt in the oxidizing environment of a subduction zone, magnetite appears as an early crystallizing phase and subsequent MSS will therefore be metal-deficient (Ballhaus et al. 2001). Thus, sulfides that have interacted with subduction-like oxidizing conditions are more likely to have low metal/sulfur ratios than those that do not display evidence for unsupported radiogenic Os. However, an alternative to subduction-related transport of radiogenic Os was recently postulated in the study of Gonzáles-Jiménez et al. (2014), who ascribed suprachrondritic $^{187}Os/^{188}Os$ and low Re/Os to a carbonate-like metasomatic overprint where volatile-rich fluids with elevated CO_2 were the likely source of the radiogenic $^{187}Os/^{188}Os$ signature (see also Reisberg et al. 2004; Lorand et al. 2004; Powell and O'Reilly 2007; Alard et al. 2011).

Rhenium enrichment. Rhenium enrichment results in elevated Re/Os elemental ratios and, consequently, raised $^{187}Re/^{188}Os$ (Fig. 19). Where this has occurred recently, i.e., there has been little opportunity for ^{187}Re to produce ingrown ^{187}Os in significant amounts, this may be accompanied by unradiogenic $^{187}Os/^{188}Os$. However, the effect on T_{MA} model age calculations will be to decrease the calculated age—potentially producing a "future" age (Fig. 17c)—whereas T_{RD} model ages will be unaffected. Gonzáles-Jiménez et al. (2014) attributed a horizontal trend in one of their Re–Os isotope plots to Re addition. Similarly, Archean model ages observed by Marchesi et al. (2010) in BMS from the Ronda peridotite, southern Spain, are only evident in the T_{MA} age calculations and not in T_{RD} model ages; a feature that does not represent any real magmatic event and indicates the secondary uptake of Re.

In a study of peridotite- and pyroxenite-hosted sulfides from the Penghu Islands, Taiwan, Wang et al. (2009) reported Re–Os isotope systematics of BMS grains that originally formed as residual MSS or by crystallization of sulfide melts after an ancient melting event, which later reacted with percolating metasomatic melts. Wang et al. (2009) suggested that these BMS grains may have been variably affected by one or more of up to three separate metasomatic episodes, which modified the Re–Os isotopic compositions of the sulfides. They attributed positive co-variations on Re–Os isochron style plots to interaction of BMS with an asthenosphere-derived silicate melt, whereas negative co-variations on the same plot were attributed to interaction with a fluid or melt that carried a radiogenic Os signature, but no significant Re (cf. Westerlund et al. 2006 and González-Jiménez et al. 2014, outlined above). In addition, several of the BMS grains analyzed by Wang et al. (2009) showed elevated $^{187}Re/^{188}Os$ with little or no concomitant increase in $^{187}Os/^{188}Os$, which are characteristics of recent Re-addition. In the case of those Penghu Island sulfides where positive correlation trends are apparent in $^{187}Os/^{188}Os$–$^{187}Re/^{188}Os$ plots, the apparent "isochron" ages are likely to be the result of mixing of pre-existing BMS with percolating basaltic melts and therefore have no age significance.

Griffin et al. (2002) also commented extensively on the necessity for an addition of unsupported radiogenic Os for many of their cratonic Group 3 BMS grains (broadly analogous to the Type-2 BMS of Alard et al. 2002) from Udachnya, Siberia, and a requirement for a multistage evolution. Critically, it led them to scrutinize the other sulfides that they had analyzed and conclude that these also may have experienced multistage, but not as intensive, metasomatic histories. This resulted in model ages that may at first sight seem plausible but are erroneous and simply mixing trends (cf. Wang et al. 2009). For example, a comparison of T_{RD} and T_{MA} model ages revealed that some of the Group 3 BMS grains yield $T_{MA} > 0$, but $T_{RD} < 0$, which implies recent Re addition.

Mixing between primary and metasomatic populations of BMS, or pre-existing BMS grains and sulfide-bearing melts and / or fluids, can occur in mantle much younger than cratonic mantle. Harvey et al. (2010) reported similar, although less complex interactions between BMS associated with melt depletion and secondary, metasomatic BMS in a suite of harzburgites and lherzolites from the French Massif Central. While many of these BMS grains had sub-chondritic Os isotope ratios, their Re and Os concentrations were not consistent with a simple sub-division between Type-1 and Type-2 peridotite-hosted BMS (cf. Alard et al. 2002). For example, most of the BMS grains with sub-chondritic $^{187}Os/^{188}Os$ ratios had Re abundances (up to 412 µg·g^{-1}) far in excess of their Os concentrations (maximum 41 µg·g^{-1}), consistent with Re addition. For these BMS grains to retain sub-chondritic $^{187}Os/^{188}Os$, Re addition must have occurred shortly before or during the entrainment of the host xenolith in the lava that brought it to the surface. Moreover, as in earlier studies of cratonic peridotites (Griffin et al. 2002; Beyer et al. 2004; Wang et al. 2009), not all of the BMS grains with supra-chondritic Os isotope ratios have a corresponding high Re abundance. BMS grains that have Re abundances as low as 0.01 µg·g^{-1}, but retain suprachondritic Os isotope ratios, can neither be accounted for by melt depletion nor ingrowth of Os. While the radiogenic Os for the Massif Central lherzolites and harzburgites could have been sourced during Variscan subduction, the addition of radiogenic Os from subduction-related fluxing of the Variscan mantle wedge was largely discounted by Harvey et al. (2010) on the basis of insufficient S and modal BMS abundances to accommodate a significant influx of "new" BMS. Harvey et al. (2010) concluded that overall, the Re–Os isotope systematics of these BMS were most likely the result of limited physical mixing, when interstitial melts and melt inclusions were added. Mixing has therefore occurred between originally unradiogenic BMS grains with high Os concentrations and metasomatic BMS grains with high Re/Os and low Os concentrations. An alternative suggestion made by Harvey et al. (2010) was a scenario involving the partitioning of Re into pre-existing BMS from a transient silicate melt, but that would have required a mechanism whereby a formerly enclosed BMS was exposed to a Re-rich percolating melt and then subsequently re-enclosed in a silicate grain.

Given the role that BMS clearly plays in the distribution (and redistribution) of the HSE, it seems likely that information hard won from the analysis of individual BMS grains will pay dividends in the interpretation of bulk-rock Re–Os isotope systematics that range from straightforward (e.g., Alard et al. 2002) to otherwise unfathomable. In several case studies, the Re–Os isotope systematics of BMS have revealed critical information regarding mantle evolution, geodynamic processes and the relationship between the upper mantle and the crust that it is inferred to have produced. Although these mixing and metasomatic scenarios may appear convoluted, there are a finite number of reservoirs from which melts and fluids can interact with pre-existing BMS grains. However, just like the silicate-hosted isotope systems, where early melt depletion events are easily obscured by subsequent metasomatism, a limit must exist in the number of metasomatic events the Re–Os isotope system will be able to "see through" before becoming of little use in determining the history of melt depletion in suites of mantle-derived rocks.

THE UTILITY OF Re–Os AND Pb ISOTOPE GEOCHONOLOGY

Dating the formation of diamonds

Diamonds are rare minerals in the mantle that crystallize in the deeper portions of the lithosphere and in the convecting mantle as deep as the top of the lower mantle, at pressures as high as ~25 GPa (Harte 2010; Shirey et al. 2013; Stachel and Luth 2015). Until the 1980s and the publication of the first accurate diamond ages (Kramers 1979; Richardson et al. 1984), the crystallization ages of diamonds was one of the least understood aspects of diamond petrogenesis. Direct dating of diamond itself using radiogenic isotope systems is not practical currently, and still relies on mineral inclusions because diamond does not contain

enough atoms of radiogenically decaying nuclides (e.g., ^{87}Rb, ^{147}Sm, ^{187}Re, ^{235}U, ^{238}U,^{232}Th) to produce enough daughter nuclides to be analyzed at current mass spectrometer sensitivity.

Diamonds can include silicate and / or sulfide phases that either grew synchronously with the diamonds themselves (syngenetic; Sobolev 1977; Meyer 1987; Stachel and Harris 2008) or mineralogically predate diamond growth (protogenetic; e.g., Thomassot et al. 2009). Many early studies involving the dating of inclusions stated that inclusions in diamonds can be clearly identified as being syngenetic with diamond growth based upon (i) their relationship to the internal growth structures of the host diamond, (ii) the relationship between inclusions and the nitrogen aggregation state of the host diamond, and (iii) the morphology of the inclusions themselves (Richardson et al. 1984, 1993; Richardson 1986; Smith et al. 1991; Bulanova 1995; Pearson and Shirey 1999). However, with new crystallographic CT-scans and stable isotopic studies, other workers maintain that most inclusions are pre-existing and become encapsulated by a growing diamond (Anand et al. 2004; Thomassot et al. 2009). In either case, if the mineral inclusion grew at a time close to diamond growth, these inclusions provide an opportunity to date diamonds using radiogenic isotope systems that are present in greater abundance in these inclusions than in the diamonds themselves.

In detail, silicate minerals that were included within the diamond as the diamonds grew (either syngenetic or protogenetic diamond inclusions) can be dated by Pb–Pb (Kramers 1979) and Sm–Nd isotopes (Richardson et al. 1984, 1993; Richardson 1986; Richardson and Harris 1997; see Pearson and Shirey 1999 and Gurney et al. 2010 for summaries) and have yielded Archean and Proterozoic ages, although some recent ages that are similar to kimberlite eruption ages have also been reported (Pearson et al. 1998; Shirey et al. 2001). The low abundance of Sr and Nd in the garnets and pyroxenes used by Richardson and coworkers for age dating, combined with their small size, meant that multiple inclusions were often combined to make a single age estimate. Often, grains were combined not just from a single diamond, but from several tens to hundreds of diamonds (Pearson and Shirey 1999). This necessitates the assumption that all of the silicate growth and encapsulating diamond genesis happened synchronously at a given locality.

Secondary ion mass spectrometry of Pb-isotopes in BMS from discrete diamond growth zones in a diamond from Yakutia, Siberia, suggested that diamond may grow sporadically with intervals of no growth that may extend for 1 Ga (Rudnick et al. 1993b). Inclusions in the centre of the Yakutian diamond generated Pb–Pb model ages of >2 Ga, whereas inclusions in the outer portions of the diamond yielded much younger ages that approached the age of the kimberlite eruption that brought the diamonds to the surface. A consequence of the uncertainties associated with the Pb isotope evolution of the mantle was that early Pb–Pb model ages (Rudnick et al. 1993b) were associated with large uncertainties. In Siberian diamonds, small BMS grains are frequently found in the innermost zones of diamonds and it has been suggested that these inclusions acted as seeds for the nucleation of the diamonds (Bulanova et al. 1996), although how long these BMS grains exist before the actual growth of the diamond is uncertain. Pearson et al. (1998) use this line of evidence to argue for syngenetic growth of diamond and BMS, which implies that BMS growth was effectively isochronous with the host diamond. Shirey and Richardson (2011) suggested that although there is evidence for silicate inclusions often being 500 to 1500 million years older than the diamond crystallization age, BMS inclusions tend to preserve ages that are only 10–100 million years older than the diamond that hosts them, making BMS inclusions a much more reliable measure of the age of diamond formation.

To improve upon Sm–Nd isochron ages derived from composites of silicate inclusions (e.g., Richardson and Harris 1997), a means of accurately and precisely dating individual BMS inclusions was sought in order to better elucidate the timing of diamond growth. Bulanova et al. (1996), using a proton probe, determined that many diamond-hosted BMS contained substantial Os that, in retrospect, would have been high enough to date with the Re–Os isotope system,

either to produce model ages on individual grains or to generate isochron style Re–Os plots with multiple cogenetic BMS grains. A modified version of the Os micro-distillation method of Roy-Barman and Allègre (1995) was used to obtain total procedural blanks approaching 10^{-15} g (Pearson et al. 1998; Pearson and Shirey 1999). This level of blank, which had previously been precluded by the conventional Carius tube digestion method (Shirey and Walker 1995), permitted the analysis of sulfides containing sub-$\mu g \cdot g^{-1}$ to $\mu g \cdot g^{-1}$ concentrations of Os (corresponding to an absolute amount of Os ranging from 0.1 to 10 pg). This technique produced the first successful date on a suite of diamonds from Koffiefontein, South Africa (Pearson et al. 1998). Since then this has been the preferred method for the dating of diamond formation (e.g., Pearson et al. 1999a,b; Pearson and Shirey 1999; Richardson et al. 2001, 2004, 2009; Shirey et al. 2001, 2002; Aulbach et al. 2004a,b, 2009a,b,c, 2011; Westerlund et al. 2004, 2006; Smit et al. 2010).

Diamond formation through time

Peridotitic diamond protoliths mostly date from the Paleoarchean and silicate inclusions in these diamonds have the depleted major element composition expected for refractory continental mantle (Richardson et al. 1984; Westerlund et al. 2006). These paleoarchean BMS grains have low Re/Os because they formed in equilibrium with mantle peridotite that was residual after melt extraction, consistent with their observed low Re concentrations (<10 pg$\cdot g^{-1}$ Re). Eclogitic BMS, in general, forms from protoliths that have a systematically higher initial Os isotopic composition than peridotitic BMS, implying that some degree of prior Re/Os enrichment must have occurred, i.e., they are derived from metamorphosed basaltic or komatiitic lavas.

Isochron and mantle model ages for peridotitic BMS grains extend to older ages (>3.2 Ga; Gurney et al. 2010; Shirey and Richardson 2011) than those of eclogitic BMS. To date, no Paleoarchean BMS inclusions with high, eclogitic Re/Os ratios have been found (Shirey and Richardson 2011). Consequently, eclogitic diamonds are only commonplace after 3.0 Ga, which Shirey and Richardson (2011) used to suggest represents the age of the earliest slab subduction and thus the establishment of modern plate tectonics. In their model, eclogitic diamonds usually occur where lithospheric mantle has been subject to continental collision. For example, the collision of two continental blocks of the Kaapvaal craton, the Witwatersrand and Kimberley blocks at 3.1–2.9 Ga (Moser et al. 2001; Schmitz et al. 2004), is suggested to have resulted in underthrusting of oceanic lithosphere and eclogite capture (Shirey and Richardson 2011).

The absence of Paleoarchean eclogite xenoliths and eclogitic BMS in diamonds from cratonic lithospheric mantle suggests that the earliest continental nuclei may have formed by processes that were different to what today are recognized as the Wilson cycle. The absence of a true Wilson cycle in the Palaeoarchean does not rule out the presence of some form of recycling or even shallow plate subduction, but the style of subduction observable today had not been initiated at this point. The earliest detected geochemical signatures consistent with some form of recycling of hydrated oceanic lithosphere date back as far as 3.9 Ga and perhaps even 4.2 Ga, based upon the changing Nb/Th (Jochum et al. 1991) and Th/U ratios in basaltic and ultramafic rocks (Collerson and Kamber 1999; Zartman and Richardson 2005), and their trace and major element systematics (O'Neil et al. 2011). Crustal rocks with a signature consistent with derivation from depleted mantle (ϵNd : ϵHf$=1$:2) became apparent after 3.6 Ga (Shirey et al. 2008). The appearance of subduction-related imprints on the stable keels of cratons supports the hypothesis that the generation of continental crust was progressively depleting the mantle from 3.6 Ga onwards. By the Neoarchean (after ca. 2.8 Ga), recycling processes more strongly resembled the style of subduction consistent with the Wilson cycle (Shirey et al. 2008).

The age of the continental lithospheric mantle and the assembly of its domains

The timing of diamond formation and the conditions of their formation are invaluable in unravelling the series of events that together resulted in the assembly of the cratons. Moreover, the geochronological information preserved in BMS grains that become isolated within the

SCLM as a result of melt depletion can help to constrain the timings of melt depletion and the inherent link between the formation of continental crust and the stabilization of the SCLM. With specific regard to mantle BMS geochronology, three cratons in particular have been studied in detail: the Kaapvaal craton, South Africa, the Siberian craton, Russia, and the Slave Craton, Canada. A detailed discussion of the HSE systematics of cratonic mantle is covered in depth in Aulbach et al. (2016, this volume) and only the role of BMS in the determination of cratonic structure and history will be briefly discussed here.

The history of the Kaapvaal craton, from the perspective of BMS inclusions in diamonds, was summarized by Shirey et al. (2004) and more recently by Aulbach et al. (2016, this volume). Briefly, the southern African cratonic keel, comprising the Kaapvaal–Zimbabwe cratons, separated by the Limpopo mobile belt, is underlain by Archean mantle peridotite and subordinate quantities of eclogite, which host multiple generations of diamonds of Archean to Proterozoic age (Kramers 1979; Richardson et al. 1984, 1993, 2001; Navon 1999; Pearson and Shirey 1999; Shirey et al. 2002). Some parts of the craton are underlain by portions of the mantle keel that probably relate to the generation of the oldest crust observed in the Kaapvaal. This hypothesis in entirely consistent with the numerous bulk-rock Re–Os model ages derived from xenolith studies of the region (e.g., Walker et al. 1989; Carlson et al. 1999, 2000; Janney at al. 2010) and more recently *in situ* Re–Os model ages on silicate-hosted BMS grains derived by LA MC ICPMS (e.g., Griffin et al. 2003a,b).

Of the suites of eclogitic diamonds associated with the Kaapvaal craton, four (De Beers Pool, Jwaneng, Koffiefontein, and Orapa) preserve Archean ages that overlap the average Neoarchean Re–Os mantle model ages of cratonic peridotite (Carlson et al. 1999; Irvine et al. 2001; Shirey et al. 2001). The eclogitic BMS grains form an array in $^{187}Re/^{188}Os$–$^{187}Os/^{188}Os$ space that highlights two general groups of ages. A large number of inclusions from the De Beers Pool, Jwaneng and Orapa plot on a 2.9 Ga isochron (Richardson et al. 2001), with the remainder displaying more scatter (Shirey et al. 2001). At Koffiefontein, only two inclusions correspond to a ca. 2.9 Ga age, while the majority yield much younger ages of 1 Ga (Pearson et al. 1998). The younger Proterozoic diamond ages vary from locality to locality within the Kaapvaal (Pearson et al. 1998; Richardson et al. 2001; Shirey et al. 2004).

The sequence of events proposed for the formation of the Kaapvaal craton begins with formation of the nucleus of the craton at ca. 3.7–3.3 Ga (Aulbach et al. 2009a). This would have been accompanied by hot, large melting intervals, such as those inferred to have been responsible for the 3.5 Ga Barberton komatiites. This process would have left a highly depleted residue with refractory olivine and garnet compositions (Stachel et al. 2003; Stachel and Harris 2008) and a sulfide-free residuum (e.g., Keays 1995). In this hot, volatile-poor peridotitic environment, diamond formation would be difficult. Percolation of S-undersaturated melts during secondary processes at this time may also have worked to strip the SCLM of its sulfide content (Reisberg et al. 2005). Those diamonds that could form may have been able to trap refractory silicate inclusions, but the sulfur-undersaturated nature of the protolith may have impeded the encapsulation of large numbers of peridotitic-BMS grains despite the abundance of peridotitic silicate inclusions (Aulbach et al. 2009a). Continental collision of the eastern and western blocks of the Kaapvaal craton at 2.9 Ga allowed for incorporation of volatile bearing and sulfur rich oceanic lithosphere into the mantle keel peridotite. BMS added at this time were eclogitic and preferentially added in the west, explaining both the timing and distribution of 2.9 Ga eclogitic diamond growth (Shirey et al. 2004a, 2013; Aulbach et al. 2009a). Subsequent repeated episodes of sulfide re-introduction into the lithosphere accompanying metasomatism and marginal subduction are documented by peridotitic BMS grains in mantle xenoliths and xenocrysts (Griffin et al. 2004) and multiple episodes of Proterozoic diamonds with eclogitic sulphides (e.g., Pearson et al. 1998; Richardson et al. 2004; Aulbach et al. 2009b). The few examples of peridotitic BMS-containing diamonds in the Kaapvaal craton have proved to be young. (Pearson et al. 1998; Aulbach et al. 2009b).

Archean peridotitic BMS inclusion-bearing diamonds are more abundant in the central Slave craton, where diamond formation appears to have been coeval with lithosphere formation (Aulbach et al. 2009a, 2011). The Slave craton comprises a juvenile eastern and an ancient central to western domain that may have become amalgamated as a result of east-oriented subduction at ca. 2.7 Ga ago (Kusky 1989; Bleeker et al. 1999a,b). The formation of shallow lithosphere beneath the Slave craton is thought to have commenced through accretionary processes as early as ca. 3.5 Ga (Aulbach et al. 2011). Several peridotitic diamond-hosted BMS grains derived from Diavik plot along a 3.3 Ga isochron, whereas 11 similar inclusions yield an isochron age of 3.52 Ga i.e., from the Palaeoarchean (Westerlund et al. 2006). This early generation of peridotitic BMS that is predominant in the Slave craton is completely missing in the Kaapvaal craton. In contrast to the Kaapvaal craton, the less depleted deep lithospheric mantle beneath the central Slave craton is proposed to have formed as a result of plume-related underplating, but with a lower overall degree of melt depletion because of the presence of a pre-existing lithospheric mantle lid. This smaller degree of melt depletion did not result in a complete exhaustion of the SCLM sulfur supply and hence permitted the formation of peridotitic BMS inclusions coeval with diamond formation (Aulbach et al. 2009a). However, like the Kaapvaal craton, the subsequent evolution of the Slave craton has been dominated by a series of collision and subduction-related events recorded in the multiple generations of diamond-hosted eclogite- and pyroxenite-hosted BMS (Aulbach et al. 2009a,c).

The relationship between the age of the SCLM and the overlying crust

In regions where the overlying crustal record is preserved, ages derived for crust generation from the crust itself can be compared to peaks in model ages preserved in SCLM-derived BMS grains derived from peridotite xenoliths (e.g., Pearson et al. 2007; González-Jiménez et al. 2013, 2014). Where the crustal record is imperfect, for example when ancient crust has been eroded or has become obscured through burial or tectonism, the geochronological evidence preserved in relative probability plots of BMS model ages still provides valuable information regarding the history of crust formation and SCLM stabilization. Peaks in model ages on relative probability diagrams of Re–Os T_{RD} or T_{MA} (e.g., Figs. 18, 20) are attributed significance as corresponding to the stabilization of SCLM, which may have been coupled to major crust formation events. Both bulk-rock and BMS Re–Os ages frequently show a correspondence between the crust and the underlying mantle, sampled as xenoliths, from which it is inferred to be derived (Pearson et al. 1995a,b 2002; Handler et al. 1997; Carlson et al. 1999; Chesley et al. 1999; Menzies et al. 1999; Hanghøj et al. 2001; Irvine et al. 2001 2003; Lee et al. 2001; Griffin et al. 2002; Schmidt and Snow 2002; Carlson and Moore 2004; Marchesi et al. 2010; González-Jiménez et al. 2013, 2014). However, there are some examples where underlying mantle is apparently older than the overlying crust (Parkinson and Pearce 1998; Peslier et al. 2000; Handler et al. 2003; Smit et al. 2010).

In the Udachnaya kimberlite, Siberia, Griffin et al. (2002) used sulfide model ages to construct a relative probability plot to date the formation of the Siberian craton, though the BMS enclosed in olivine macrocrysts are complex in nature. Of the 53 BMS grains that had $^{187}Re/^{188}Os$ of <0.07 (the cut-off chosen by Griffin et al. 2002, as ensuring a model age that was not affected by Re-addition or mixing with Re-rich secondary sulfides) 45 of the BMS grains produced T_{MA} ages between 2.5 and 3.6 Ga, and 35 of the grains gave T_{MA} of >2.8 Ga. This lead Griffin et al. (2002) to conclude that the Siberian SCLM formed during the period 3–3.5 Ga, with a peak in lithosphere stabilization at around 2.9 Ga, and little evidence for significant additions to the lithosphere afterwards. However, the recent Re–Os isotope study of Yakutian diamond-hosted BMS by Wiggers de Vries et al. (2013) demonstrated that the assemblage of the Siberian craton is more protracted than the initial 2.9–3.5 Ga growth phase suggested by Griffin et al. (2002). The ages obtained by Wiggers de Vries et al. (2013) for the different diamond populations demonstrate two major periods of eclogitic and lherzolitic Yakutian

diamond formation at ca. 2.1–1.8 Ga (Mir, 23rd Party Congress and Udachnaya kimberlites) and at ca.1.0–0.9 Ga (Mir and 23rd Party Congress kimberlites). These correspond to the collision between different terranes of the Siberian Craton during the formation of a Palaeoproterozoic supercontinent at ca. 2.0–1.8 Ga and accretion leading to formation of the supercontinent Rodinia ca. 1.1 Ga. The very radiogenic initial Os isotope ratios of the eclogitic and lherzolitic BMS grains (^{187}Os/^{188}Os = 0.14–2.22) imply the incorporation of radiogenic Os from subducted oceanic lithosphere, a conclusion that is also relevant to the Kaapvaal and Slave cratons.

However, more recently, the age of the Siberian craton as a whole has been called into question, as the vast majority of Re–Os dates for the region have been derived from a single kimberlite province, i.e., Udachnaya. Doucet et al. (2015) argue that although the Siberian SCLM contains components of material that retain an Archean signature, a wide range of Re-depletion ages have been derived (3.4–1 Ga and commonly ≤2 Ga for peridotite xenoliths), consistent with craton-forming activity not limited to the Archean. Using data derived from a second Siberian kimberlite, Obnazhennaya, Ionov et al. (2015) have recently proposed that the lithospheric mantle beneath the Siberian craton was formed in at least two events, one in the late Archean and the other in the Paleoproterozoic.

An example of the utility of relative probability plots in coupling melt depletion and the crustal growth history of non-cratonic SCLM was recently published by González-Jiménez et al. (2013). Here, using a similar approach to that employed by Griffin et al. (2002) for olivine-hosted BMS, they determined T_{RD} of BMS grains from peridotite xenoliths recovered from the Calatrava volcanic field, Spain. Their study revealed that episodes of mantle magmatism and/or metasomatism in the Iberia microplate were linked to supercontinent assembly and/or breakup at ca. 1.8, 1.1, 0.9, 0.6, and 0.3 Ga (Fig. 20). In addition, they found that the mantle and crust constituting the Iberian microplate have coexisted since at least Paleozoic–Proterozoic time. Rhenium-depletion ages of 68 carefully screened BMS grains, either possessing ^{187}Re/^{188}Os < 0.07 (n = 12) or ^{187}Re/^{188}Os > 0.07 but with uncorrelated Re/Os, and hence no systematic ingrowth of ^{187}Os (n = 56), produced peaks on a relative probability plot coinciding with major tectonic events recorded in the crust (Fig. 20). The formation of the Iberian lithosphere at ca. 1.6–2.0 Ga coincides with crust-mantle differentiation that occurred during the assemblage of the Columbia supercontinent (ca. 1.8–1.5 Ga). Peaks in T_{RD} at 1.3–0.9 Ga coincided with the amalgamation of Rodinia at ca. 1.25 Ga and its breakup at ca. 0.75 Ga.

Peaks in T_{RD} at 0.6 Ga and 0.3 Ga were interpreted by González-Jiménez et al. (2013) as representing the beginning of continental collisions to form Gondwana and the initiation of the breakup of Pangea respectively (Orejana et al. 2009). These interpretations should be treated with some caution given the caveats associated with interpreting Phanerozoic T_{RD} in peridotites. The interpretation of the older sulfide T_{RD} are broadly consistent with the earlier study of Marchesi et al. (2010), which examined individual BMS grains recovered from the Ronda orogenic massif, Spain. This earlier study also considered the possibility that residual BMS grains with Os model ages of ca. 1.2–1.4 Ga may represent the reworking of older SCLM in the Mesoproterozoic. Critically, if the massif became part of the lithosphere at about 1.2–1.4 Ga, the preferred interpretation of whole-rock Os isotopic data (Reisberg et al. 1991; Reisberg and Lorand 1995), then the residual BMS grains with Os model ages of ~1.6–1.8 Ga from Marchesi et al. (2010) could be interpreted as inherited grains that survived within the convecting mantle for hundreds of millions of years. The studies of Marchesi et al. (2010) and González-Jiménez et al. (2013) agree that the Proterozoic Os model ages exhibited by BMS grains in the Iberian SCLM tend to correspond to different stages of generation of crust, which was later recycled in the Gondwana supercontinent.

Evidence for ancient lithospheric mantle pre-dating the oldest exposed cratonic crust has also been found in the Kimberley craton, north-western Australia in BMS-bearing diamonds recovered from the ca. 20 Ma Ellendale lamproite pipes (Smit et al. 2010). Lherzolitic

diamond–hosted BMS grains yield an age of 1426 ± 130 Ma, with an initial $^{187}Os/^{188}Os$ ratio of 0.1042 ± 0.0034. The upper limit on the $^{187}Os/^{188}Os$ initial ratio suggests a Re depletion age of 2.96 Ga, indicating the presence of SCLM beneath Ellendale since at least the Mesoarchaean. This is supported by independent evidence for the presence of deep SCLM below the King Leopold Orogen and the Kimberley craton by seismic tomography (van der Hilst et al. 1998; Kennett 2003; Fishwick et al. 2005) and cool cratonic geotherms for the West Kimberley province (Griffin and Ryan 1995). Archean SCLM also extends to the south-east of the Kimberley craton, with mantle xenolith T_{RD} ages as old as the Neoarchean (2.2–2.9 Ga; Luguet et al. 2009) or possibly even older, as suggested by an imprecise Re–Os isochron age of 3.4 Ga (Graham et al. 1999). However, the age of the mantle below the Kimberley craton is significantly older than the oldest exposed crust within the North Australian Craton (ca. 2 Ga; Page et al. 1995; Tyler et al. 1999; Worden et al. 2008). Therefore, despite early Proterozoic convergent margins and new crust formation (Tyler et al. 1999; Griffin et al. 2000), remnants of the underlying continental mantle were preserved (Smit et al. 2010). This indicates that crust and mantle in the Kimberley region were decoupled (Luguet et al. 2009), with preservation of the pre-existing lithosphere during accretion (Smit et al. 2010).

The generation of BMS grains during ancient melt-depletion events that no longer represent any known event recorded in the overlying crust is the most likely explanation for some populations of BMS. These could either be related to domains where ancient crust is not exposed, either because it has been removed or because newer mantle, containing an old heterogeneous component has become part of the lithosphere. This is particularly pertinent to the subject of osmium and lead isotope heterogeneity in the oceanic mantle.

The inherent heterogeneity within the oceanic mantle

Isotopic studies of oceanic samples have long demonstrated the occurrence of isotopic variations in the mantle that must have been created by geologic processes much older than the 180 My age of the oldest ocean floor (e.g., Gast et al. 1964; Sun and Hanson 1975; O'Nions et al. 1977). In addition, compositional heterogeneities in the oceanic mantle at length scales of thousands of kilometres (e.g., Hart 1984; Meyzen et al. 2007) to sub-km scales have often been reported (e.g., Shirey et al. 1987; Dosso et al. 1999; Meibom et al. 2002; Standish et al. 2002; Warren et al. 2009). These observations contrast with studies of the SCLM, where Re–Os ages for the mantle often show a correspondence to the age of the overlying crust (e.g., Griffin et al. 2002; Pearson et al. 2002), though examples exist of the SCLM having ages older than the overlying crust (e.g., Peslier et al. 2000; and discussion above).

Although the Pb isotope composition of the oceanic mantle has been of interest to geochemists for nearly half a century (e.g., Allègre 1969), the role that BMS plays as a reservoir for mantle Pb has been less well explored, despite the early realization that Pb isotope heterogeneity may be present at a small scale (e.g., Saal et al. 1998, and more recently Maclennan 2008). Recent interest in the Pb elemental and isotopic composition of mantle BMS stems from a potential solution to the first Pb paradox (Allègre 1969), which is the observation that global basalts have ubiquitously radiogenic Pb isotope compositions (Hofmann 1997) that fall at much higher $^{206}Pb/^{204}Pb$ than the geochron. If estimates of the bulk silicate Earth Pb isotope composition are correct (i.e., broadly chondritic for U, Th, and Pb; e.g., Palme and Jones 2003) and that the U/Pb ratio was set at ~4.50 Ga when core formation ended (Kleine and Rudge 2011), then there must be a reservoir of unradiogenic Pb. Observations of Pb isotopes in both bulk-rock peridotite and individual BMS grains suggest that the mantle may represent one of the reservoirs for unradiogenic Pb based upon isotopic measurements of peridotites and their minerals (e.g., Malaviarachchi et al. 2008; Burton et al. 2012; Warren and Shirey 2012), and predictions based upon trace element depletion (Godard et al. 2005; Kelemen et al. 2007; Hanghøj et al. 2010).

The first hint that the unradiogenic Pb reservoir was at least partially hosted in the mantle came from a Pb isotope study of the Horoman peridotite (Malaviarachchi et al. 2008). Here, bulk-rock plagioclase lherzolites were analyzed for their Pb isotope ratios and some plotted to the unradiogenic side of the 4.5 Ga geochron. Among abyssal peridotites, one clinopyroxene analysis out of three samples analyzed has yielded an unradiogenic composition (Warren et al. 2009). To date, further Pb isotope data on pyroxene mineral separates from abyssal peridotites are not available due to the analytical difficulties of working at Pb concentrations of $\sim 10 \, \mathrm{ng \cdot g^{-1}}$.

More recently, Burton et al. (2012) and Warren and Shirey (2012) measured Pb isotope compositions in individual BMS grains extracted from abyssal peridotites recovered from the MAR, Gakkel Ridge and SWIR (Fig. 16). For the MAR, Burton et al (2012) found that $^{206}\mathrm{Pb}/^{204}\mathrm{Pb}$ ratios ranged from 18.4063 to 18.4672 for interstitial BMS, i.e., all radiogenic compared to the geochron. In contrast, enclosed BMS ranged from 16.2276 to 17.7839, i.e., extending to values considerably less radiogenic than the geochron. Similarly, Warren and Shirey (2012) reported BMS $^{206}\mathrm{Pb}/^{204}\mathrm{Pb}$ ratios ranging from 17.034 (less radiogenic than the geochron) to 19.640 (considerably more radiogenic than the BMS grains of Burton et al. 2012). As seen in Os isotope ratios of abyssal peridotite BMS grains (e.g., Alard et al. 2005; Harvey et al. 2006), Pb isotope ratios of abyssal peridotite BMS show little systematic covariation with basalt Pb isotopic compositions from the area of the ridge from which they were recovered. For example, BMS grains from Gakkel abyssal peridotites span the full range of Gakkel Ridge basalt compositions (Warren and Shirey 2012; Blusztajn et al. 2014), but do not show the break in Pb isotope ratios at 15° E observed among basalts (Goldstein et al. 2008).

The recent discoveries of ancient Pb isotope signatures preserved in BMS grains recovered from abyssal peridotites (Fig. 16) suggests that at least some of the missing unradiogenic Pb resides in the upper mantle. This conclusion is supported by the observation that the Pb isotope composition of bulk-rock peridotites from a variety of continental settings also spans both sides of the geochron (Warren and Shirey 2012). In addition, Os and Pb isotopic compositions are correlated (Fig. 21), with both isotope systems yielding similar model ages. For the combined dataset from the MAR, Gakkel and SWIR, the Pb isotopic composition of mantle BMS grains aligns along the ~2 Ga data array for oceanic basalts and peridotite mineral separates, while the Re–Os datasets plot along the 2 Ga Re–Os reference isochron (Harvey et al. 2006; Burton et al. 2012; Warren and Shirey 2012). This "age", combined with the observed Pb–Os isotopic correlation (Fig. 21) and a very small ($\ll 1$ km) length scale of peridotite compositional variability can be explained either by crustal extraction at 2 Ga or an average mixing age for the mantle. A single depletion event that can explain the isotope datasets from three widely separated ridges (Gakkel, SWIR and MAR) seems implausible and is inconsistent with episodes of peak crustal formation at 2.7, 1.0, 0.6, and 0.3 Ga (Condie and Aster 2010). In contrast, the mixing of ancient components back into the mantle by subduction has long been suggested as an explanation for the heterogeneity of the oceanic basalt array (e.g., Chase 1981; Hofmann and White 1982; Zindler and Hart 1986; Kellogg et al. 2007).

Analysis of the isotopic composition of individual BMS grains from abyssal peridotites allows mantle heterogeneity to be probed at very small length scales, which is particularly powerful when Pb and Os isotopes can be analyzed in the same grain (Fig. 21; Warren and Shirey 2012). Base metal sulfide grains recovered from the same drill core (Harvey et al. 2006; Burton et al. 2012) or dredge haul (Alard et al. 2005; Warren and Shirey 2012; Blusztajn et al. 2014) have large magnitude Os and Pb isotopic variations, demonstrating that these can be preserved in the oceanic mantle at length scales of significantly less than 1 km. For example, the Os and Pb isotope heterogeneity in BMS from serpentinized peridotite, reported by Harvey et al. (2006) and Burton et al. (2012) came from a single 6 cm section of quarter-core from Hole 1274a on the 15° 20' N Fracture Zone, MAR. Blusztajn et al. (2014) found considerable Pb isotope variation among BMS grains in some individual samples from the Gakkel Ridge and SWIR,
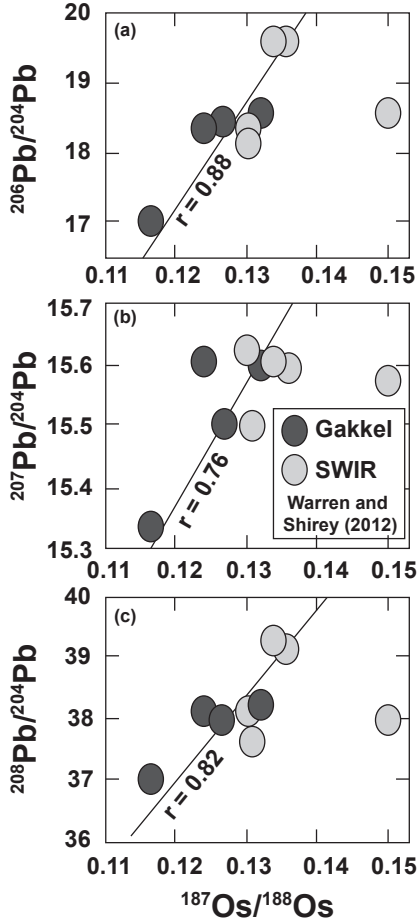
Figure 21. Co-variation of Pb isotopes with ^{187}Os/^{188}Os. The solid lines are regressions through the data (correlation coefficient given by r). PS86-6-38 is excluded from the regressions due to radiogenic Os, which reflects recent interaction with melts from Bouvet hotspot. After Warren and Shirey (2012).

including one sample with BMS grains that cover 25% of the Pb isotope range of oceanic basalts. Pyroxenes from abyssal peridotites have also been used to show considerable Nd (e.g., Cipriani et al. 2004), Sr (e.g., Warren et al. 2009) and Hf (e.g., Stracke et al. 2011) isotope variability, but these isotopes so far have only been measured in mineral separates and not individual grains.

The scale and magnitude of oceanic Pb and Os isotope heterogeneity will remain poorly constrained, especially compared to current knowledge of the SCLM, until a larger dataset for abyssal peridotite BMS becomes available. However, what is clear is that the composition of basalts alone cannot be relied upon to constrain either the extent of mantle depletion or the degree of small scale variations in the mantle from which they were derived. Sulfides indicate the occurrence of Os and Pb heterogeneities in the upper mantle with extreme compositions that are not resolvable in pooled basaltic melts. Either these anomalies reside in BMS within domains that are too refractory to contribute to the melting process or their size is such that more voluminous melts smooth out the most extreme isotopic signatures of the source (e.g., Warren and Shirey 2012).

CONCLUDING REMARKS AND FUTURE DIRECTIONS

Base metal sulfides in mantle peridotite and diamonds preserve evidence for a variety of processes, including melt depletion, re-fertilization, metasomatism, and alteration. The ability of sulfides in mantle rocks to preserve different processes has led to an unraveling of these different generations of processes in bulk mantle samples. Combined with new advances in analytical sensitivity and spatial resolution, an improved understanding of the geological history of mantle samples on all scales is being achieved. The emergence of improved amplifier resistors for TIMS and MC ICP-MS instruments has recently seen a leap in possible analytical resolution for silicates (e.g., Koornneef et al. 2015; Sarkar et al. 2015) and meteoritic material (Peters et al. 2015). It seems likely that these methods will be applied to problems where high precision analyses of micro-metric BMS grain and / or alloys are required in the near future.

Base metal sulfides hosted in peridotites and pyroxenites of the oceanic lithosphere carry a memory of melt depletion and melt infiltration that is an evident effect of the plate tectonic cycle of ridge melting and slab subduction. For the first time, isotopic ages can be anchored to their mineral hosts. By looking at primary BMS grains, we can peer through the prevalent alteration that masks much of the work done on the bulk-rock scale. Future work will increase the now sparse sites on the ocean floor that have been studied and will allow us to approach a global understanding of specific episodes of depletion and melting, with the ultimate goal to relate these episodes to specific plate geometries and geodynamic cycles.

Geochronology on BMS grains in diamonds has achieved the long-held goal of producing ages for every diamond locality that carries amenable BMS inclusions. With the caveat that all diamonds in kimberlite are xenocrysts, age arrays that have geological significance emerge from the diamond suites in many well-mined kimberlites. These arrays are being used to identify when portions of the deep continental lithosphere have been added and reworked, giving a new and deep dimension—one not evident from the surface—to the evolution of the continents. Future work will more solidly anchor these deep mantle lithosphere ages to crustal tectonothermal histories, so that we can achieve a thorough picture of crustal differentiation through time and the nature of the earliest stable crust forming processes.

ACKNOWLEDGMENTS

REFERENCES

Ackerman L, Pitcher L, Strnad L, Puchtel IS, Jelínek E, Walker RJ, Rohovec J (2013) Highly siderophile element geochemistry of peridotites and pyroxenites from Horní Bory, Bohemian Massif: Implications for HSE behaviour in subduction-related upper mantle. Geochim Cosmochim Acta 100:158–175

Alard O, Griffin WL, Lorand JP (2000) Non-chondritic distribution of the highly siderophile elements in mantle sulphides. Nature 497:891–894

Alard O, Griffin WL, Pearson NJ, Lorand J-P, O'Reilly SY (2002) New insights into the Re–Os systematics of subcontinental lithospheric mantle from in-situ analysis of sulphides. Earth Planet Sci Lett 203:651–663

Alard O, Luguet A, Pearson NJ, Griffin WL, Lorand J-P, Gannoun A, Burton KW, O'Reilly SY (2005) In-situ Os isotopes in abyssal peridotites bridge the isotopic gap between MORBs and their source mantle. Nature 436:1005–1008

Alard O, Lorand J-P, Reisberg L, Bodinier J-L, Dautria J-M, O'Reilly SY (2011) Volatile-rich metasomatism in Montferrier xenoliths (Southern France): Implications for the abundances of chalcophile and highly siderophile elements in the subcontinental mantle. J Petrol 52 :2009–2045

Allègre CJ (1969) Comportement des systèmes U–Th–Pb dans le manteau supérieur et modèle d'évolution de ce dernier au cours des temps géologiques. Earth Planet Sci Lett 5:261–269

Allègre C-J, Luck JM (1980) Osmium isotopes as petrogenetic and geological tracers. Earth Planet Sci Lett 48:148–54

Alt JC, Shanks WC (2003) Serpentinization of abyssal peridotites from the MARK area, Mid-Atlantic Ridge: sulfur geochemistry and reaction modeling. Geochim Cosmochim Acta 67:641–653

Alt JC, Shanks WC, Bach W, Paulick H, Garrido CJ, Beaudoin G (2007) Hydrothermal alteration and microbial sulfate reduction in peridotite and gabbro exposed by detachment faulting at the Mid-Atlantic Ridge, 15º 20′ N (ODP Leg 209): a sulfur and oxygen isotope study. Geochem Geophys Geosyst 8:Q08002, doi:10.1029/2007GC001617

Amundsen HEF (1987) Evidence for liquid immiscibility in the upper mantle. Nature 327:692–695

Anand M, Taylor L, Misra K, Carlson W (2004) Nature of diamonds in Yakutian eclogites: views from eclogite tomography and mineral inclusions in diamonds: Lithos 77:333–348

Anbar AD, Creaser RA, Papanastassiou DA, Wasserberg GJ (1992) Rhenium in seawater: confirmation of generally conservative behaviour. Geochim Cosmochim Acta 56:4009–4103

Andersen T, Griffin WL, O'Reilly SY (1987) Primary sulfide melt inclusions in mantle derived megacrysts and pyroxenites. Lithos 20:279–294

Aulbach S, Griffin WL, Pearson NJ, O'Reilly SY, Kivic K, Doyle BJ (2004a) Mantle formation and evolution, Slave Craton: constraints from HSE abundances and Re–Os isotope systematics of sulfide inclusions in mantle xenocrysts. Chem Geol 208:61– 88

Aulbach S, Griffin WL, O'Reilly SY, McCandless TE (2004b) Genesis and evolution of the lithospheric mantle beneath the Buffalo Head Terrane, Alberta (Canada). Lithos 77:413–451

Aulbach S, Stachel T, Creaser RA, Heaman LM, Shirey SB, Muehlenbachs K, Eichenberg D, Harris JW (2009a) Sulphide survival and diamond genesis during formation and evolution of Archaean subcontinental lithosphere: a comparison between the Slave and Kaapvaal cratons. Lithos 112:747–757

Aulbach S, Shirey SB, Stachel T, Creighton S, Muehlenbachs K, Harris JW (2009b) Diamond formation episodes at the southern margin of the Kaapvaal Craton: Re–Os systematics of sulfide inclusions from the Jagersfontein Mine. Contrib Mineral Petrol 157:525–540

Aulbach S, Creaser RA, Pearson NJ, Simonetti SS, Heaman LM, Griffin WL, Stachel T (2009c) Sulfide and whole rock Re–Os systematics of eclogite and pyroxenite xenoliths from the Slave Craton, Canada. Earth Planet Sci Lett 283:48–58

Aulbach S, Stachel T, Heaman LM, Creaser RA, Shirey SB (2011) Formation of cratonic subcontinental lithospheric mantle and complementary komatiite from hybrid plume sources. Contrib Mineral Petrol 161:947–960

Aulbach S, Mungall JE, Pearson DG (2016) Distribution and processing of highly siderophile elements in cratonic mantle lithosphere. Rev Mineral Geochem 81:239–304

Bach W, Garrido CJ, Paulick H, Harvey J, Rosner M (2004) Seawater–peridotite interactions: first insights from ODP Leg 209, MAR 15ºN. Geochem Geophys Geosyst 5:Q09F26. doi:10.1029/2004GC000744

Ballhaus C, Sylvester P (2000) Noble metals enrichment processes in the Merensky Reef, Bushveld Complex. J Petrol 41:546–561

Ballhaus C, Tredoux M, Spaeth A (2001) Phase relations in the Fe–Ni-Cu-PGE-S system at magmatic temperature and application to massive sulfide ores of the Sudbury Igneous Complex. J Petrol 42:1911–1926

Ballhaus C, Bockrath C, Wohlgemuth-Ueberwasser C, Laurenz V, Berndt J (2006) Fractionation of the noble metals by physical processes. Contrib Mineral Petrol 152:667–684

Barnes S-J, Ripley EM (2016) Highly siderophile and strongly chalcophile elements in magmatic ore deposits. Rev Mineral Geochem 81:725–774

Barnes SJ, Mungall JE, Maier WD (2015) Platinum group elements in mantle melts and mantle samples. Lithos 232:395–417

Becker H, Dale CW (2016) Re–Pt–Os isotopic and highly siderophile element behavior in oceanic and continental mantle tectonite. Rev Mineral Geochem 81:369–440

Bedini RM, Bodinier J-L, Dautria J-M, Morten L (1997) Evolution of LILE-enriched small melt fractions in the lithospheric mantle: a case study from the East African Rift. Earth Planet Sci Lett 153:67–83

Behrens H, Johannes W, Schmalzreid H (1990) On the mechanisms of cation diffusion processes in ternary feldspars. Phys Chem Mineral 17:62–78

Bell PM, England JL, Kullerud G (1964) Pentlandite: pressure effect on breakdown. Carnegie Institution of Washington Yearbook 63:206–207

Bell AS, Simon A, Guillong M (2009) Experimental constraints on Pt, Pd and Au partitioning and fractionation in silicate melt–sulfide oxide–aqueous fluid systems at 800 °C, 150 MPa and variable sulfur fugacity. Geochim Cosmochim Acta 73:5778–5792

Beyer EE, Brueckner HK, Griffin WL, O'Reilly SY, Graham S (2004) Archean mantle fragments in Proterozoic crust, Western Gneiss Region, Norway. Geology 32:609–612, doi: 10.1130/G20366.1

Beyer EE, Griffin WL, O'Reilly S (2006) Transformation of Archaean lithospheric mantle by refertilization: evidence from exposed Peridotites in the Western Gneiss Region, Norway. J Petrol 47:1611–1636

Bischoff JL, Seyfried WE (1978) Hydrothermal chemistry of seawater from 25 degrees to 350 degrees C. Am J Sci 278:838–860

Bishop FC, Smith JV, Dawson JB (1975) Pentlandite–magnetite intergrowth in De Beers spinel lherzolite: review of sulfide in nodules. Phys Chem Earth 9:323–337

Bleeker W, Ketchum JWF, Jackson VA, Villeneuve M (1999a) The Central Slave Basement Complex. Part I: its structural topology and autochthonous core. Can J Earth Sci 36:1083–1109

Bleeker W, Ketchum JWF, Davis WJ (1999b) The Central Slave Basement Complex. Part II: age and tectonic significance of high-strain zones along the basement-cover contact. Can J Earth Sci 36:1111–1130

Blusztajn JS, Shimizu N, Warren JM, Dick HJB (2014) In-situ Pb isotopic analysis of sulfides in abyssal peridotites: New insights into heterogeneity and evolution of the oceanic upper mantle, Geology 42:159–162. doi:10.1130/G34966.1

Bockrath C, Ballhaus C, Holzheid A (2004) Fractionation of the Platinum-group elements during mantle melting. Science 305:1951–1953

Bodinier J-L, Godard M (2014) Orogenic, Ophiolitic, and Abyssal Peridotites. *In:* The Mantle and Core. Treatise on Geochemistry. Carlson, R.W. (ed.), Elsevier, Amsterdam. 3 p. 103–167

Bodnar RJ (2003) Reequilibration of fluid inclusions. *In:* Fluid Inclusions: Analysis and Interpretation. Samson I, Anderson A, Marshall D (eds) Mineral Assoc Canada, Short Course 32:213–230

Borisov A, Palme H, Spettel B (1994) Solubility of palladium in silicate melts: implications for core formation in the Earth. Geochim Cosmochim Acta 58:705–716

Boschi C, Dini A, Früh-Green GL, Kelley DS (2008) Isotopic and element exchange during serpentinization and metasomatism at the Atlantis Massif (MAR 30°N): insights from B and Sr isotope data. Geochim Cosmochim Acta 72:1801–1823

Boudier F, Nicholas A (1991) High-Temperature Hydrothermal Alteration of Peridotite, Zabargad Island (Red Sea). J Petrol Spec Vol 2:243–253

Boyd FR, Gurney JJ (1986) Diamonds and the African Lithosphere. Science 232:472–477

Boyd FR, Gurney JJ, Richardson SH (1985) Evidence for a 150–200 km thick Archaean lithosphere from diamond inclusion thermobarometry. Nature 315:387–389

Brandon AD, Creaser RA, Shirey SB, Carlson RW (1996) Osmium recycling in subduction zones. Science 272:861–864

Brenan JM, Cherniak DJ, Rose LA (2000) Diffusion of osmium in pyrrhotite and pyrite: implications for closure of the Re–Os isotopic system. Earth Planet. Sci. Lett. 180: 399–413

Brenan JM (2002) Re–Os fractionation in magmatic sulfide melt by monosulfide solid solution. Earth Planet Sci Lett 199:257–268

Brenan JM (2008) Re–Os fractionation by sulfide melt–silicate melt partitioning: A new spin. Chem Geol 248:140–165

Brenan JM, McDonough WF, Dalpé C (2003) Experimental constraints on the partitioning of rhenium and some platinum group elements between olivine and silicate melt. Earth Planet Sci Lett 212:135–150

Brenan JM, Bennett NR, Zajacz Z (2016) Experimental results on fractionation of the highly siderophile elements (HSE) at variable pressures and temperatures during planetary and magmatic differentiation. Rev Mineral Geochem 81:1–87

Buchanan DL, Nolan J (1979) Solubility of sulfur and sulfide immiscibility in synthetic tholeiitic melts and their relevance to Bushveld-Complex rocks. Can Mineral 17:483–494

Büchl A, Brügmann G, Batanova VG, Münker C, Hofmann AW (2002) Melt percolation monitored by Os isotopes and HSE abundances: a case study from the mantle section of the Troodos Ophiolite. Earth Planet Sci Lett 204:385–402

Büchl A, Brügmann G, Batanova VG, Hofmann AW (2004) Os mobilization during melt percolation: the evolution of Os isotope heterogeneities in the mantle sequence of the Troodos Ophiolite, Cyprus. Geochim Cosmochim Acta 68:3397–3408

Bulanova GP (1995) The formation of diamond. J Geochem Explor 53:1–23

Bulanova GP, Griffin WL, Ryan CG, Shestakova OY, Barnes S-J (1996) Trace elements in sulfide inclusions from Yakutian diamonds. Contrib Mineral Petrol 124:111–125

Burnham OM, Rogers NW, Pearson DG, van Calsteren P, Hawkesworth CJ (1998) The petrogenesis of the eastern Pyrrenian peridotites: an integrated study of their whole-rock geochemistry and Re–Os isotope composition. Geochim Cosmochim Acta 62:2293–2310

Burton KW, Schiano P, Birck J-L, Allègre CJ (1999) Osmium isotope disequilibrium between mantle minerals in a spinel-lherzolite. Earth Planet Sci Lett 172:311–322

Burton KW, Cenki-Tok B, Mokadem F, Harvey J, Gannoun A, Alard O, Parkinson IJ (2012) Unradiogenic lead in Earth's upper mantle. Nature Geosci 5:570–573

Basaltic Volcanism Study Project (BVSP) (1981) Basalt Volcanism on the Terrestrial Planets. New York: Pergamon Press

Cabri LJ (1973) New data on phase relations in the Cu–Fe–S system. Econ Geol 68:443–454

Cabri L (1992) The distribution of trace metals in minerals and mineral products. Mineral Mag 56:289–308

Carignan J, Ludden JN, Francis D (1996) On the recent enrichment of sub-continental lithosphere: a detailed U–Pb study of spinel lherzolite xenoliths, Yukon, Canada. Geochim Cosmochim Acta 60:4241–4252

Carlson RW (2005) Application of the Pt–Re–Os isotopic systems to mantle geochemistry and geochronology. Lithos 82:249–272

Carlson RW, Moore RO (2004) Age of the Eastern Kaapvaal mantle: Re–Os isotope data for peridotite xenoliths from the Monastery mine. S Afr J Geol 107:81–90

Carlson RW, Pearson DG, Boyd FR, Shirey SB, Irvine G, Menzies AH, Gurney JJ (1999) Re–Os systematics of lithospheric peridotites: Implications for lithosphere formation and preservation. *In:* Proceedings of the VIIth International Kimberlite Conference. Gurney, JJ, Gurney JL, Pascoe MD, Richardson SH (eds). Red Roof Designs, Cape Town, 99–108

Carlson RW, Boyd FR, Shirey SB, Janney PE, Grove TL, Bowring SA, Schmitz MD, Dann JC, Bell DR, Gurney JJ, Richardson SH, Tredoux M, Menzies AH, Pearson DG, Hart RJ, Wilson AH, Moser D (2000) Continental growth, preservation, and modification in southern Africa. GSA Today 10:1–7

Cartigny P, Harris JW, Javoy M (2001) Diamond genesis, mantle fractionations and mantle nitrogen content: a study of δ^{13}C–N concentrations in diamonds. Earth Planet Sci Lett 185:85–98

Chakraborty S (1997) Rates and mechanisms of Fe–Mg interdiffusion in olivine at 980º–1300ºC. J Geophys Res 102:12317–12331

Chase CG (1981) Oceanic island Pb: two-stage histories and mantle evolution. Earth Planet Sci Lett 52:277–284

Cherniak DJ (1995) Diffusion of lead in plagioclase and K-feldspar: an investigation using Rutherford backscattering and resonant nuclear reaction analysis. Contrib Mineral Petrol 120:358–371

Chesley JT, Rudnick RL, Lee C-T (1999) Re–Os systematics of mantle xenoliths from the East African rift: age, structure, and history of the Tanzanian craton. Geochim Cosmochim Acta 63:1203–1217

Chou CL (1978) Fractionation of siderophile elements in the Earth's upper mantle. Proc Lunar Planet Sci Conf 9th, p 219–230

Cipriani A, Brueckner HK, Bonatti E, Brunelli D (2004) Oceanic crust generated by elusive parents: Sr and Nd isotopes in basalt-peridotite pairs from the Mid-Atlantic Ridge. Geology 32:657–660

Clifford TN (1966) Tectono-metallogenic units and metallogenic provinces. Earth Planet Sci Lett 1:421–434

Collerson KD, Kamber BS (1999) Evolution of the continents and the atmosphere inferred from Th–U–Nb systematics of the depleted mantle: Science 283:1519–1522

Condie KC, Aster RC (2010) Episodic zircon age spectra of orogenic granitoids: the super continent connection and continental growth. Precamb Res 180:227–236

Cooper JA, Green DH (1969) Lead isotope measurements on lherzolite inclusions and host basanites from western Victoria, Australia. Earth Planet Sci Lett 6:69–76

Craig JR (1973) Pyrite-pentlandite assemblages and other low temperature relations in the Fe–Ni-S system: Am J Sci 273-A: 496–510

Craig JR, Kullerud G (1969) Phase relations in the Cu–Fe–Ni–S system and their application to magmatic ore deposits. *In:* Magmatic Ore Deposit: A Symposium. Wilson HDB (ed) Econ Geol Monog 4, Soc Econ Geol, Colorado, U.S. p 344–358

Dalton CA, Langmuir CH, Gale A (2014) Geophysical and Geochemical Evidence for Deep Temperature Variations Beneath Mid-Ocean Ridges. Science 344:80–83, doi:10.1126/science.1249466

Dasch EJ, Green DH (1975) Strontium isotope geochemistry of lherzolite inclusions and host basaltic rocks, Victoria, Australia. Am J Sci 275:461–469

Day (2013) Hotspot volcanism and highly siderophile elements. Chem Geol 341: 50–74

Day JMD, Brandon AD, Walker RJ (2016) Highly siderophile elements in Earth, Mars, the Moon, and asteroids. Rev Mineral Geochem 81:161–238

Desborough GA, Czamanske GK (1973) Sulfides in eclogite nodules from a kimberlite pipe, South Africa, with comments on violarite stoichiometry. Am Mineral 58:195–202

Deines P, Harris JW (1995) Sulfide inclusion chemistry and carbon isotopes of African diamonds. Geochim Cosmochim Acta 59:3173–3188, doi:10.1016/0016–7037(95)00205-E

Delpech G, Lorand J-P, Grégoire M, O'Reilly SY (2012) In-situ geochemistry of chalcophile and highly siderophile elements in highly metasomatised Kerguelen mantle xenoliths (South Indian Ocean). Lithos 154:296–314 http://dx.doi.org/10.1016/j.lithos.2012.07.018

DeWaal SA, Calk LC (1975) The sulfides in the garnet pyroxenite xenoliths from Salt Lake Crater, Oahu: J Petrol 16:134–153

Dosso L, Bougault H, Langmuir C, Bollinger C, Bonnier O, Etoubleau J (1999) The age and distribution of mantle heterogeneity along the Mid-Atlantic Ridge (31–41°N). Earth Planet Sci Lett 170:269–286

Doucet LS, Ionov DA, Golovin AV (2015) Paleoproterozoic formation age for the Siberian cratonic mantle: Hf and Nd isotope data on refractory peridotite xenoliths from the Udachnaya kimberlite. Chem Geol 391:42–55

Dreibus G, Palme H, Spettel B, Zipfel J, Wanke H (1995) Sulfur and selenium in chondritic meteorites. Meteoritics 30:439–445

Dromgoole E, Pasteris J (1987) Interpretation of the sulfide assemblages in a suite of xenoliths from Kilbourne Hole and Potrillo Maar, New Mexico. *In:* Mantle Metasomatism and Alkaline Magmatism. Morros E, Pasteris J (eds) Geol Soc Amer Spec Paper p 25-46

Eggins SM, Rudnick RL, McDonough WF (1998) The composition of peridotites and their minerals: a laser-ablation ICP-MS study. Earth Planet Sci Lett 154:53–71

Eldridge CS, Compston W, Williams IS, Harris JW, Bristow JW (1991) Isotope evidence for the involvement of recycled sediments in diamond formation. Nature 353:649–653

Farquhar J, Wing BA, McKeegan KD, Harris JW, Cartigny P, Thiemens MH (2002) Mass-independent sulfur of inclusions in diamond and sulfur recycling on early Earth. Science 298:2369–2372

Faul UH (2001) Melt retention and segregation beneath mid-ocean ridges. Nature 410:920–923

Faure G (2001) Origin of igneous rocks. Springer, Berlin. p 496

Ferraris C, Lorand J-P (2008) An HRTEM study of platinum-group elements in mantlederived Cr-rich spinel Lherz; North-Eastern Pyrenees, France. Earth Planet Sci Lett 276:167–174

Fishwick S, Kennett BLN, Reading AM (2005) Contrasts in lithospheric structure within the Australian craton—insights from surface wave tomography. Earth Planet Sci Lett 231:163–176

Fleet ME (2006) Phase equilibria at high temperatures. Rev Mineral Geochem 61:365–419

Fleet ME, Pan Y (1994) Fractional crystallization of anhydrous sulfide liquid in the system Fe–Ni–Cu–S, with application to magmatic sulfide deposits. Geochim Cosmochim Acta 58:3369–3377

Fleet ME, Stone WE (1990) Nickeliferous sulfides in xenoliths, olivine megacrysts and basaltic glass. Contrib Mineral Petrol 105:629–636

Fleet ME, Wu T-W (1993) Volatile transport of platinum-group elements in sulfide-chloride assemblages at 1000° C. Geochim Cosmochim Acta 57:3519–3531

Fleet ME, Crocket JH, Stone WE (1996) Partitioning of platinum-group elements (Os, Ir, Ru, Pt, Pd) and gold between sulfide liquid and basalt melt. Geochim Cosmochim Acta 60:2397–2412

Fonseca ROC, Mallmann G, O'Neill HStC, Campbell IH (2007) How chalcophile is rhenium? An experimental study of the solubility of Re in sulphide mattes. Earth Planet. Sci. Lett. 260: 537–548

Fonseca ROC, Mallmann G, O'Neill HStC, Campbell IH, Laurenz V (2011) Solubility of Os and Ir in sulfide melt: implications for Re/Os fractionation during mantle melting. Earth Planet Sci Lett 311:339–350

Foustoukos DI, Bizimis M, Frisby C, Shirey SB (2015) Redox controls on Ni–Fe–PGE mineralization and Re/Os fractionation during serpentinization of abyssal peridotite. Geochim Cosmochim Acta 150:11–25

Frei R, Gervilla F, Meibom A, Proenza JA, Garrido CJ (2006) Os isotope heterogeneity of the upper mantle: evidence from the Mayarí-Baracoa ophiolite belt in eastern Cuba. Earth Planet Sci Lett 241:466–476

Frey FA, Green DH (1974) The mineralogy, geochemistry, and origin of lherzolite inclusions in Victorian basanites: Geochim Cosmochim Acta 38:1023–1059

Frey FA, Prinz M (1978) Ultramafic inclusions from San Carlos, Arizona: petrological and geochemical data bearing on their petrogenesis. Earth Planet Sci Lett 38:129–176

Frick C (1973) The sulphides in griquaite and garnet-peridotite xenoliths in kimberlite. Contrib Mineral Petrol 39:1–16

Galer SJG, O'Nions RK (1989) Chemical and isotopic studies of ultramafic inclusions from the San Carlos Volcanic Field, Arizona: a bearing on their petrogenesis. J Petrol 30:1033–1064

Gammons CH, Bloom MS (1993) Experimental investigation of the hydrothermal geochemistry of platinum and palladium: II. The solubility of PtS and PdS in aqueous sulfide solutions to 300°C. Geochim Cosmochim Acta 57:2451–2467

Ganguly J, Tirone M, Hervig RL (1998a) Diffusion kinetics of samarium and neodymium in garnet, and a method for determining cooling rates of rocks. Science 281:805–807

Ganguly J, Cheng W, Chakraborty S (1998b) Cation diffusion in aluminosilicate garnets: experimental determination in pyrope–almandine diffusion couples. Contrib Mineral Petrol 131:171–180

Gannoun A, Burton KW, Day JMD, Harvey J, Schiano P, Parkinson I (2016) Highly siderophile element and Os isotope systematics of volcanic rocks at divergent and convergent plate boundaries and in intraplate settings. Rev Mineral Geochem 81:651-724

Garuti G, Gorgoni C, Sighinolfi GP (1984) Sulfide mineralogy and chalcophile and siderophile element abundances in the Ivrea-Verbano mantle peridotites (Western Italian Alps). Earth Planet Sci Lett 70:69–87

Gast PW, Tilton GR, Hedge C (1964) Isotopic composition of lead and strontium from Ascension and Gough Islands. Science145:1181–1185

Godard M, Kelemen PB, Hart SR, Jackson MG, Hanghøj K (2005) High Pb/Ce reservoir in depleted, altered mantle peridotites. Eos Trans Am Geophys Union 86 : V23D–07

Goldstein SL, Soffer G, Langmuir CH, Lehnert KA, Graham DW, Michael PJ (2008) Origin of a 'Southern Hemisphere' geochemical signature in the Arctic upper mantle. Nature 453:89–93

González-Jiménez JM, Villaseca C, Griffin WL, Belousova E, Konc Z, Anochea E, O'Reilly SY, Pearson NJ, Garrido CJ, Gervilla F (2013) The architecture of the European-Mediterranean lithosphere: A synthesis of the Re–Os evidence. Geology 41:547–550

González-Jiménez JM, Villaseca C, Griffin WL, O'Reilly SY, Belousova E, Ancochea E, Pearson NJ (2014) Significance of ancient sulfide PGE and Re–Os signatures in the mantle beneath Calatrava, Central Spain. Contrib Mineral Petrol 168:1–24

Graham S, Lambert DD, Shee SR, Smith CB, Reeves S (1999) Re–Os isotopic evidence for Archean lithospheric mantle beneath the Kimberley block, Western Australia. Geology 27:431–434

Greau Y, Alard O, Griffin WL, Huang J-X, O'Reilly SY (2013) Sulfides and chalcofile elements in Roberts Victor eclogites: unravelling a sulfide-rich metasomatic event. Chem Geol 354:73–92

Green DH, Morgan JW, Heier KS (1968) Thorium, uranium and potassium abundances in peridotite inclusions and their host basalts. Earth Planet Sci Lett 4:155–166

Griffin WL, Ryan CG (1995) Trace elements in indicator minerals: area selection and target evaluation in diamond exploration. J Geochem Explor 53:311–337

Griffin TJ, Page RW, Sheppard S, Tyler IM (2000) Tectonic implications of Palaeoproterozoic post-collisional, high-K felsic igneous rocks from the Kimberley region of northwestern Australia. Precambrian Res 101:1–23

Griffin WL, Spetsius ZV, Pearson NJ, O'Reilly SY (2002) *In situ* Re–Os analysis of sulfide inclusions in kimberlitic olivine: new constraints on depletion events in the Siberian lithospheric mantle. Geochem Geophys Geosyst 3(11), doi:10.1029/ 2001GC000287

Griffin WL, Graham S, O'Reilly SY, Pearson NJ (2003a) Lithosphere evolution beneath the Kaapvaal Craton. *In:* Re–Os systematics of sulfides in mantle-derived peridotites. Carlson RW, Grutter H, Jones AG (eds.) Slave-Kaapvaal Workshop, Merrickville, Ontario

Griffin WL, O'Reilly SY, Abe N, Aulbach S, Davies RM, Pearson NJ, Doyle BJ, Kivi K (2003b) The origin and evolution of Archean lithospheric mantle. Precam Res 127:19–41

Griffin WL, Graham S, O'Reilly SY, Pearson NJ (2004) Lithosphere evolution beneath the Kaapvaal Craton: Re–Os systematics of sulfides in mantle-derived peridotites. Chem Geol 208:89–118

Guo J, Griffin WL, O'Reilly SY (1999) Geochemistry and Origin of Sulphide Minerals in Mantle Xenoliths: Qilin, Southeastern China. J Petrol 40:1125–1149

Gurney JJ (1989) Diamonds, Kimberlites and Related Rocks. Spec Publ Geol Soc Austral 14:935–965

Gurney JJ, Switzer GS (1973) The discovery of garnets closely related to diamonds in the Finsch pipe, South Africa. Contrib Mineral Petrol 39:103–116

Gurney JJ, Harris JW, Rickard RS (1984) Minerals associated with diamonds from the Roberts Victor Mine. *In:* Kimberlites II: The Mantle and Crust–Mantle Relationships. Kornprobst, J. (ed) Elsevier, Amsterdam p 25–32

Gurney JJ, Helmstaedt HH, Richardson SH, Shirey SB (2010) Diamonds through time. Econ Geol 105:689–712

Haggerty SE (1986) Diamond genesis in a multiply-constrained model. Nature 320:34–38

Hamlyn PR, Keays RR (1986) Sulfur saturation and second stage melts: application to the Bushveld platinum metal deposits. Econ Geol 81:1431–1445

Handler MR, Bennett VC (1999) Behaviour of platinum-group elements in the subcontinental mantle of eastern Australia during variable metasomatism and melt depletion. Geochim Cosmochim Acta 63:3597–3618

Handler MR, Bennett VC, Esat TM (1997) The persistence of off-cratonic lithospheric mantle: Os isotopic systematics of variably metasomatised southeast Australian xenoliths. Earth Planet Sci Lett 151:61–75

Handler MR, Wysoczanski RJ, Gamble JA (2003) Proterozoic lithosphere in Marie Byrd Land, West Antarctica: Re–Os systematics of spinel peridotite xenoliths. Chem Geol 196:131–145

Hanghøj K, Kelemen PB, Bernstein S, Blustztajn J, Frei R (2001) Osmium isotopes in the Wiedemann Fjord mantle xenoliths: A unique record of cratonic mantle formation by melt depletion in the Archean. Geochem Geophys Geosys 2:2000GC000085

Hanghøj K, Kelemen, PB, Hassler D, Godard M (2010) Composition and genesis of depleted mantle peridotites from the Wadi Tayin Massif, Oman Ophiolite: major and trace element geochemistry, and Os isotope and PGE systematics. J Petrol 51:201–227

Harris JW (1992) Diamond geology. *In:* The Properties of Natural and Synthetic Diamond. Field JE (ed). Academic Press, London, p 345–393

Harris JW, Gurney JJ (1979) Inclusions in diamond. *In:* The Properties of Diamond. Field JE (ed). Academic Press, New York. p 674

Hart SR (1984) A large-scale isotope anomaly in the Southern Hemisphere mantle. Nature 9:753–757

Hart SR, Gaetani GA (2006) Mantle Pb paradoxes: the sulfide solution. Contrib Mineral Petrol 152:295–308

Hart SR, Ravizza GE (1996) Os partitioning between phases in lherzolite and basalt. *In:* Earth Processes: Reading the Isotopic Code. Basu A, Hart S (eds). Geophys Monogr 95:123–134. Am Geophys Union

Harte B (2010) Diamond formation in the deep mantle: the record of mineral inclusions and their distribution in relation to mantle dehydration zones. Mineral Mag 74:189–215

Harvey J, Gannoun A, Burton KW, Rogers NW, Alard O, Parkinson IJ (2006) Ancient melt extraction from the oceanic upper mantle revealed by Re–Os isotopes from the Mid-Atlantic Ridge. Earth Planet Sci Lett 244:606–621

Harvey J, Gannoun A, Burton KW, Schiano P, Rogers NW, Alard O (2010) Unravelling the effects of melt depletion and secondary infiltration on mantle Re–Os isotopes beneath the French Massif Central. Geochim Cosmochim Acta 74:293–320

Harvey J, Dale CW, Gannoun A, Burton KW (2011) Osmium mass balance in peridotite and the effects of mantle-derived sulphides on basalt petrogenesis. Geochim Cosmochim Acta 75:5574–5596

Harvey J, Savov IP, Agostini S, Cliff RA, Walshaw R (2014) Si-metasomatism in serpentinized peridotite: The effects of talc-alteration on strontium and boron isotopes in abyssal serpentinites from Hole 1268a, ODP Leg 209. Geochim Cosmochim Acta 126:30–48

Harvey J, König S, Luguet A (2015) The effects of melt depletion and metasomatism on highly siderophile and strongly chalcophile elements: S-Se-Te-Re-PGE systematics of peridotite xenoliths from Kilbourne Hole, New Mexico. Geochim. Cosmochim. Acta 166:210–233

Haughton DR, Roeder PL, Skinner BJ (1974) Solubility of sulfur in mafic magmas. Econ Geol 69:451–467

Hauri EH, Wagner TP, Grove TL (1994) Experimental and natural partitioning of Th, U, Pb and other trace elements between garnet, clinopyroxene and basaltic melts. Chem Geol 117:149–166

Helz RT (1977) Determination of the P-T dependence of the first appearance of FeS-rich liquid in natural basalts to 20 kb. Eos Trans Am Geophys Union 58:533

Hirschmann MM, Stolper EM (1996) A possible role for garnet pyroxenite in the origin of the 'garnet signature' in MORB. Contrib Mineral Petrol 124:185–208

Hofmann AW (1997) Mantle geochemistry: the message from oceanic volcanism. Nature 385:219–229

Hofmann AW, White WM (1982) Mantle plumes from ancient oceanic crust. Earth Planet Sci Lett 57:421–436

Holmes A (1946) Lead isotopes and the age of the Earth. Nature 157:680

Holzheid A, Schmitz MD, Grove TL (2000) Textural equilibria of iron sulfide liquids in partly molten silicate aggregates and their relevance to core formation scenarios. J Geophys Res: Solid Earth 105(B6):13555–13567, doi: 10.1029/2000JB900046

Holzheid A (2010) Separation of sulfide melt droplets in sulfur saturated silicate liquids. Chem Geol 274:127–135

Howarth GH, Barry PH, Pernet-Fisher JF, Baziotis IP, Pokhilenko NP, Pokhilenko LN, Bodnar RJ, Taylor LA (2014a) Superplume metasomatism: Evidence from Siberian mantle xenoliths. Lithos. 184–187:209–224. http://dx.doi.org/10.1016/j.lithos.2013.09.006

Howarth GH, Sobolev NV, Pernet-Fisher JF, Barry PB, Penumadu D, Puplampu S, Ketcham RA, Maisano JA, Taylor D, Taylor LA (2014b) The secondary origin of diamonds: multi-modal radiation tomography of diamondiferous eclogites. Intl Geol Rev 56:1172–1180

Ickert RB, Stachel T, Stern RA, Harris JW (2013) Diamond from recycled crustal carbon documented by coupled $\delta^{18}O$–$\delta^{13}C$ measurements of diamonds and their inclusions. Earth Planet Sci Lett 364:85–97

Ickert RB, Stachel T, Stern RA, Harris JW (2015) Extreme ^{18}O enrichment in majorite constrains a crustal origin of transition zone diamonds. Geochem Perspectives Lett 1:65–74, doi: 10.7185/geochemlet.1507

Ionov DA, Mukasa SB, Bodinier J-L (2002) Sr-Nd-Pb Isotopic Compositions of Peridotite Xenoliths from Spitsbergen: Numerical Modelling Indicates Sr-Nd Decoupling in the Mantle by Melt Percolation Metasomatism. J Petrol 43:2261–2278

Ionov DA, Carlson RW, Doucet LS, Golovin AV, Oleinikov OB (2015) The age and history of the lithospheric mantle of the Siberian craton: Re–Os and PGE study of peridotite xenoliths from the Obnazhennaya kimberlite. Earth Planet Sci Lett 428: 118–129

Irvine GJ, Pearson DG, Carlson RW (2001) Lithospheric mantle evolution in the Kaapvaal craton: A Re–Os isotope study of peridotite xenoliths from Lesotho kimberlites. Geophys Res Lett 28:2505–2508

Irvine GJ, Pearson DG, Kjarsgaard BA, Carlson RW, Kopylova MG, Dreibus GE (2003) A Re–Os isotope and PGE study of kimberlite derived peridotite xenoliths from Somerset Island and a comparison to the Slave and Kaapvaal craton. Lithos 71:461–488

Irving AJ (1974) Geochemical and high-pressure experimental studies of garnet pyroxenite and pyroxene granulite xenoliths from the Delegate basaltic pipes, Australia: J Petrol 15:1–40

Irving AJ (1980) Petrology and geochemistry of composite ultramafic xenoliths in alkalic basalts and implications for magmatic processes in the mantle. Am J Sci 280A:389–426

Jacob D, Jagoutz E, Lowry D, Mattey D, Kudrjavtseva G (1994) Diamondiferous eclogites from Siberia; remnants of Archean ocean crust. Geochim Cosmochim Acta 58:5191–5207

Janecky DR, Seyfried Jr.WE (1986) Hydrothermal serpentinization of peridotite within the oceanic crust: experimental investigations of mineralogy and major element chemistry. Geochim Cosmochim Acta 50:1357–1378

Janney P, Shirey S, Carlson R, Pearson D, Bell D, le Roex A, Nixon P, Boyd F (2010) Age, composition and thermal characteristics of South African off-craton mantle lithosphere: Evidence for a multi-stage history: J Petrol 51:1849–1890

Janse AJA (1992) New ideas in subdividing cratonic areas. Russ Geol Geophys 33:9–25

Jochum KP, Arndt NT, Hofmann AW (1991) Nb–Th–La in komatiites and basalts: Constraints on komatiite petrogenesis and mantle evolution: Earth Planet Sci Lett 107:272–289

Karup-Møller S, Makovicky E (1995) The phase system Fe–Ni–S at 725°C. Neues Jahrb Mineral Monatshefte 1:1–10

Keays RR (1995) the role of komatiitic and picritic magmatism and S saturation in the formation of ore deposits. Lithos 34:1–18. doi: 10.1016/0024–4937(94)00029–2

Kelemen PB, Kikawa E, Miller DJ, Party SS (2007) Leg 209 summary: processes in a 20-km-thick conductive boundary layer beneath the Mid-Atlantic Ridge 14º–16ºN. *In:* Proceedings of the Ocean Drilling Program, Scientific Results, Vol. 209, Kelemen PB, Kikawa E, Miller DJ (Eds.). Ocean Drilling Program, College Station, TX, p 1–33

Kellogg JB, Jacobsen SB, O'Connell RJ (2007) Modeling lead isotopic heterogeneity in mid-ocean ridge basalts. Earth Planet Sci Lett 262:328–342

Kennett BLN (2003) Seismic structure in the mantle beneath Australia. *In:* Evolution and Dynamics of the Australian Plate. Hills R, Mueller R (eds). Geol Soc Austral Spec Pub 22, p 7–23

Kimura K, Lewis RS, Anders E (1974) Distribution of gold and rhenium between nickel–iron and silicate melts: implications for abundance of siderophile elements on the Earth and Moon. Geochim Cosmochim Acta 38:683–701

Kleeman JD, Green DH, Lovering JF (1969) Uranium distribution in ultramafic inclusions from Victorian basalts. Earth Planet Sci Lett 5:449–458

Klein F, Bach W (2009) Fe–Ni–Co–O–S phase relations in peridotite–seawater interactions. J Petrol 50:37–59

Kleine T, Rudge JF (2011) Chronometry of meteorites and the formation of the Earth and Moon (2011) Elements 7:41–46

Kohlstedt DL (1992) Structure, rheology and permeability of partially molten rocks at low melt fractions, *In:* Mantle Flow and Melt Generation at Mid-Ocean Ridges, Am Geophys Union Geophys Monogr 71:103–121

Komor SC, Elthon D, Casey JF (1985) Serpentinization of cumulate ultramafic rock from the North Arm Mountain massif of the Bay of Islands ophiolite. Geochim Cosmochim Acta 49:2331–2338

Koornneff JM, Nikogosian I, van Bergen MJ, Smeets R, Bouman C, Davies GR (2015) TIMS analysis of Sr and Nd isotopes in melt inclusions from Italian potassium-rich lavas using prototype 10^{13} Ω amplifiers. Chem Geol 397: 14–23

Kramers J (1979) Lead, uranium, strontium, potassium and rubidium in inclusion-bearing diamonds and mantle-derived xenoliths from southern Africa. Earth Planet Sci Lett 42:58–70

Kullerud G, Yund RA, Moh GH (1969) Phase relations in the Cu–Fe–S, Cu–Ni–S, and Fe–Ni–S systems. Econ Geol Monogr 4:323–343

Kusky TM (1989) Accretion of the Archean Slave province. Geology 17:63–67

Lassiter JC, Byerly BL, Snow JE, Hellebrand E (2014) Constraints from Os-isotope variations on the origin of Lena Trough abyssal peridotites and implications for the composition and evolution of the depleted upper mantle, Earth Planet Sci Lett 403:178–187

Lee CT (2002) Platinum-group element geochemsitry of peridotite xenoliths from the Sierra Nevada and the Basin and Range, California. Geochim Cosmochim Acta 66:3987–4006

Lee C-T, Yin Q, Rudnick RL, Jacobsen SB (2001) Preservation of ancient and fertile lithospheric mantle beneath the Southwestern United States. Nature 411:69–73

Levasseur S, Birck J-L, Allègre CJ (1998) Direct measurement of femtomoles of osmium and the ^{187}Os/^{188}Os ratio in seawater. Science 282:272–274

Li C, Barnes SJ, Makovicky E, Rose-Hansen J, Makovicky M (1996) Partitioning of nickel, copper, iridium, rhenium, platinum, and palladium between monosulfide solid solution and sulfide liquid: effects of composition and temperature. Geochim Cosmochim Acta 60:1231–1238

Liu C-Z, Snow JE, Hellebrand E, Brügmann GE, von der Handt AB, Hofmann AW (2008) Ancient highly heterogeneous mantle beneath Gakkel ridge, Arctic Ocean. Nature 452:311–316

Lorand J-P (1985) The behaviour of the upper mantle sulfide component during the incipient alteration of "Alpine-"type peridotites as illustrated by the Beni Bousera (Northern Morocco) and Ronda (Southern Spain) ultramafic bodies. Tschermaks Mi Per Mitt 34:183–209

Lorand J-P (1987) Caractères minéralogiques et chimiques généraux des microphases du système Cu–Fe–Ni–S dans les roches du manteau supérieur: exemples d'hétérogénéités en domaine sub-continental. B Soc Geol France 8:643–657

Lorand J-P (1990) Are spinel lherzolite xenoliths representative of the sulfur content of the upper mantle. Geochim Cosmochim Acta 54:1487–1492

Lorand J-P, Alard O (2001) Platinum-group element abundances in the upper mantle: new constraints from *in situ* and whole-rock analyses of Massif Central xenoliths (France). Geochim Cosmochim Acta 65:2789–2806

Lorand J-P, Conquéré F (1983) Contribution à l'étude des sulfures dans les enclaves de lherzolites a spinelle des basaltes alcalins (Massif Central et du Languedoc, France). B Mineral 106:585–606

Lorand J-P, Grégoire M (2006) Petrogenesis of base-metal sulfide of some peridotites of the Kaapvaal craton (South Africa). Contrib Mineral Petrol 151:521–538

Lorand J-P, Luguet A (2016) Chalcophile and siderophile elements in mantle rocks: Trace elements controlled by trace minerals. Rev Mineral Geochem 81:441–488

Lorand J-P, Alard O, Luguet A, Keays RR (2003a) S/Se systematics of the subcontinental lithospheric mantle beneath the Massif Central. Geochim Cosmochim Acta 67:4137–4153

Lorand J-P, Reisberg L, Bedini RM (2003b) Platinum-group elements and melt percolation processes in Sidamo spinel peridotite xenoliths, Ethiopia, East African Rift. *In:* Highly siderophile elements in the earth and meteorites; a volume in honour of John Morgan. Bennett V, Brandon A, Neal M, Horan M (eds). Chem Geol 196:57–76

Lorand J-P, Delpech G, Grégoire M, Moine B, O'Reilly SY, Cottin J-Y (2004) Platinum group elements and the multistage metasomatic history of Kerguelen lithospheric mantle South Indian Ocean. Chem Geol 208:195–215

Lorand J-P, Luguet A, Alard O, Bezos A, Meisel, T (2008) Distribution of platinum group elements in orogenic lherzolites: a case study in a Fontête Rouge lherzolite (French Pyrenees). Chem Geol 248:174–194

Lorand J-P, Luguet A, Alard O (2013) Platinum-group element systematics and petrogenetic processing of the continental upper mantle: A review. Lithos 164–167:1–21

Luck JM, Birck JL, Allègre CJ (1980) ^{187}Re-^{187}Os systematics in meteorites; early chronology of the solar system and age of the Galaxy. Nature 283:256–59

Ludwig KR (1997) Isoplot. Program and documentation, version 2.95. revised edition of U.S. Open-File report 91–445

Ludwig KR (2000) Isoplot/Ex version 2.3: A Geochronological Toolkit for Microsoft Excel, Spec Publ 1a, Berkeley Geochronology Cent., Berkeley, Calif

Luguet A, Lorand J-P (1998) Altération supergène et teneurs en soufre des xénolithes du manteau: une approche à partir des lherzolites des basaltes de Montferrier (Languedoc, France). C R Acad Paris II A 327:519–525

Luguet A, Reisberg L (2016) Highly siderophile element and ^{187}Os signatures in non–cratonic basalt–hosted peridotite xenoliths: Unravelling the origin and evolution of the post-Archean lithospheric mantle. Rev Mineral Geochem 81:305–367

Luguet A, Alard O, Lorand JP, Pearson NJ, Ryan CG, O'Reilly SY (2001) LAM-ICP-MS unravel the highly siderophile element geochemistry of abyssal peridotites. Earth Planet Sci Lett 189:285–294

Luguet A, Lorand J-P, Seyler M (2003) A coupled study of sulfide petrology and highly siderophile element geochemistry in abyssal peridotites from the Kane Fracture Zone (MARK area, Mid-Atlantic ridge). Geochim Cosmochim Acta 67:1553–1570

Luguet A, Lorand J-P, Alard O, Cottin JY (2004) A multi-technique study of platinum group element systematic in some Ligurian ophiolitic peridotites, Italy. Chem Geol 208:175–194

Luguet A, Shirey SB, Lorand J-P, Horan MF, Carlson RC (2007) Residual platinum-group minerals from highly depleted harzburgites of the Lherz massif (France) and their role in HSE fractionation of the mantle. Geochim Cosmochim Acta 71:3082–3097

Luguet A, Pearson DG, Nowell GM, Dreher ST, Coggan JA, Spetsius ZV, Parman SW (2008) Enriched Pt–Re–Os isotope systematics in plume lavas explained by metasomatic sulphides. Science 319:453–456

Luguet A, Jaques AL, Pearson DG, Smith CB, Bulanova GP, Roffey SL, Rayner MJ, Lorand J-P (2009) An integrated petrological, geochemical and Re–Os isotope study of peridotite xenoliths from the Argyle lamproite, Western Australia and implications for cratonic diamond occurrences. *In:* Proceedings of the Ninth International Kimberlite Conference. Lithos 112S:1096–1108

MacLean WH (1969) Liquidus phase relations in the FeS–FeO–Fe$_3$O$_4$–SiO$_2$ system, and their application in geology. Econ Geol 64:865–884

Maclennan J (2008) Lead isotope variability in olivine-hosted melt inclusions from Iceland. Geochim Cosmochim Acta 72: 4159–4176

Mackovicky M, Mackovick E, Rose-Hansen J (1986) Experimental studies on the solubility and distribution of platinum group elements in base-metal sulphides in platinum deposits. *In:* Metallogeny of Basic and Ultrabasic Rocks. Gallagher MJ, Ixer RA, Neary CR, Prichard HM (eds). Inst Mineral Metall p 415–425

MacRae ND (1979) Silicate glass and sulfides in ultramafic xenoliths, Newer Basalts, Victoria, Australia: Contrib Mineral Petrol 68:275–280

Malaviarachchi SPK, Makishima A, Tanimoto M, Kuritani T, Nakamura E (2008) Highly unradiogenic lead isotope ratios from the Horoman peridotite in Japan. Nat Geosci 1:859–863

Mallmann G, O'Neill HSC (2007) The effect of oxygen fugacity on the partitioning of Re between crystals and silicate melt during mantle melting. Geochim Cosmochim Acta 71:2837–2857

Marchesi C, Griffin WL, Garrido CJ, Bodinier J-L, O'Reilly SY, Pearson NJ (2010) Persistence of mantle lithospheric Re–Os signature during asthenospherization of the subcontinental lithospheric mantle: insights from *in situ* isotopic analysis of sulfides from the Ronda peridotite (Southern Spain). Contrib Mineral Petrol 159:315–330

Marchesi C, Garrido CJ, Harvey J, González-Jiménez J-M, Hidas K, Lorand J-P, Gervilla F (2013) Platinum-group elements, S, Se and Cu in highly depleted abyssal peridotites from the Mid-Atlantic Ocean Ridge (ODP Hole 1274A): Influence of hydrothermal and magmatic processes. Contrib Mineral Petrol 166:1521–1538

Mavrogenes J, O'Neill HStC (1999) The relative effects of pressure, temperature and oxygen fugacity on the solubility of sulfide in mafic magmas. Geochim Cosmochim Acta 63:1173–1180

McDonough WF, Sun S-s (1995) The composition of the Earth. Chem Geol 120:223–253

Meibom A, Sleep NH, Chamberlain CP, Coleman RG, Frei R, Hren MT, Wooden JL (2002) Re–Os isotopic evidence for long-lived heterogeneity and equilibration processes in the Earth's upper mantle. Nature 419:705–708

Meijer A, Kwon T-T, Tilton GR (1990) U-Th-Pb partitioning behavior during partial melting in the upper mantle: implications for the origin of high Mu components and the Pb Paradox. J Geophys Res 95(B1):433–448

Meisel T, Walker RJ, Morgan JW (1996) The osmium isotopic composition of the Earth's primitive upper mantle. Nature 383:517–20

Meisel T, Walker RJ, Irving AJ, Lorand JP (2001) Osmium isotopic composition of mantle xenoliths: a global perspective. Geochim Cosmochim Acta 65:1311–1323

Menzies MA, Dupuy C (1991) Orogenic massifs: protolith, process and provenance. J Petrol 1–16 (Special Lithosphere Issue)

Menzies MA, Hawkesworth CJ (1987) Mantle Metasomatism. Academic Press, London p 472

Menzies AH, Shirey SB, Carlson RW, Gurney JJ (1999) Re–Os systematics of Newlands peridotite xenoliths: implications for diamond and lithosphere formation. *In:* Proceedings of the 7th International Kimberlite Conference. Gurney JJ, Gurney JL, Pascoe MD, Richardson SH (eds) Red Roof Design, Cape Town. p 566–583

Mével C, Stamoudi C (1996) Hydrothermal alteration of the upper mantle at Hess Deep. *In:* Proc Ocean Drill Prog Scientific Results. Mével, C, Gillis, K.M., Allan, J.F., and Meyer, P.S. (eds).147:293–309. College Station, TX (Ocean Drilling Program)

Meyer HAO (1987) Inclusions in diamond. *In:* Mantle Xenoliths (ed) Nixon PH. John Wiley and Sons New York, NY. p 501-525

Meyer HOA, Boctor NZ (1975) Sulfide-oxide minerals in eclogite from Stockdale kimberlite, Kansas: Contrib Mineral and Petrol 52:57–68

Meyer HOA, Boyd FR (1972) Composition and origin of crystalline inclusions in natural diamonds. Geochim Cosmochim Acta 36:1255– 1273

Meyer HOA, Brookins DG (1971) Eclogite xenoliths from Stockdale Kimberlite, Kansas. Contrib Mineral Petrol 34:60–72

Meyer HOA, Tsai HM (1979) Inclusions in diamond and the mineral chemistry of the upper mantle. Phys Chem Earth 2: 631–644

Meyzen CM, Blichert-Toft J, Ludden JN, Humler E, Mével C, Albarède F (2007) Isotopic portrayal of the Earth's upper mantle flow field. Nature 447:1069–1074

Misra KC, Fleet ME (1973) The chemical composition of synthetic and natural pentlandite assemblages: Econ Geol 68:518–539

Mitchell RH, Keays RR (1981) Abundance and distribution of gold, palladium, and iridium in some spinel and garnet lherzolites: Implications for the nature and origin of precious metal-rich intergranular components in the upper mantle: Geochim Cosmochim Acta 45:2425–2442

Miyashiro A, Shido F, Ewing M (1969) Composition and origin of serpentinites from the Mid-Atlantic Ridge near 24° and 30° north latitude. Contrib Mineral Petrol 23:117–127

Moine BN, Grégoire M, O'Reilly SY, Delpech G, Sheppard SMF, Lorand J-P, Renac C, Giret A, Cottin JYC (2004) Carbonatite melt in oceanic upper mantle beneath the Kerguelen Archipelago. Lithos 75:239–252

Morgan JW (1986) Ultramafic xenoliths: clues to Earth's late accretionary history. J Geophys Res 91(B12):12375–12387

Moser DE, Flowers RM, Hart RJ (2001) Birth of the Kaapvaal tectosphere 3.08 Ga ago. Science 291:465–468

Mungall JE, Andrews DRA, Cabri LJ, Sylvester PJ, Tubrett M (2005) Partitioning of Cu, Ni, Au, and platinum-group elements between monosulfide solid solution and sulfide melt under controlled oxygen and sulfur fugacities. Geochim Cosmochim Acta 69:4349–4360

Naldrett AJ (1969) A portion of the system Fe-S-O between 900 and 1080°C and its application to sulfide ore magmas. J Petrol 10:171–201

Navon O (1999) Diamond formation in the Earth's mantle. *In:* The PH Nixon Volume—Proceedings of the Seventh International Kimberlite Conference. Gurney JJ, Gurney JL, Pascoe MD, Richardson SH (eds) Cape Town. Red Roof Design, Cape Town. p 584– 604

Norman MD (1998) Melting and metasomatism in the continental lithosphere: laser ablation ICPMS analysis of minerals in spinel lherzolites from eastern Australia. Contrib Mineral Petrol 130:240–255

Nowell GM, Pearson DG, Parman SW, Luguet A, Hanski E (2008) Precise and accurate $^{186}Os/^{188}Os$ and $^{187}Os/^{188}Os$ measurements by Multi-collector Plasma Ionisation Mass Spectrometry, part II: Laser ablation and its application to single-grain Pt–Os and Re–Os geochronology. Chem Geol 248:394–426

O'Driscoll B, González-Jiménez J (2016) Petrogenesis of the platinum-group minerals. Rev Mineral Geochem 81:489–578

O'Driscoll B, Day JMD, Walker RJ, Daly JS, McDonough WF, Piccoli PM (2012) Chemical heterogeneity in the upper mantle recorded by peridotites and chromitites from the Shetland Ophiolite Complex, Scotland. Earth Planet Sci Lett 333–334:226–237

O'Hanley DS (1996) Serpentinites—records of tectonic and petrological history. *In:* Oxford Monographs on Geology and Geophysics, 34. Oxford University Press

O'Neil J, Francis D, Carlson RW (2011) Implications of the Nuvvuagittuq Greenstone Belt for the Formation of Earth's Early Crust: J Petrol 52:985–1009

O'Neill HStC (1991) The origin of the Moon and early history of the Earth—a chemical model: Part 2. The Earth. Geochim Cosmochim Acta 55:1159–1172

O'Nions RK, Hamilton PJ, Evensen NM (1977) Variations in $^{143}Nd/^{144}Nd$ and $^{87}Sr/^{86}Sr$ ratios in oceanic basalts. Earth Planet Sci Lett 34:13–22

O'Reilly SY, Griffin WL (1987) Eastern Australia—4000 kilometres of mantle samples. *In:* Mantle Xenoliths Nixon, PH (ed.), John Wiley, Chichester, UK p 267–280

Orejana D, Villaseca C, Pérez-Soba C, López-García JA, Billström K (2009) The Variscan gabbros from the Spanish Central System: A case for crustal recycling in the subcontinental lithospheric mantle? Lithos 110:262–276

Page RW, Sun SS, Blake D, Edgecombe D, Pearcey D (1995) Geochronology of an exposed late Archean basement terrane in the Granites-Tamani Region. AGSO Res Newsl 22:19–20

Palme H, Jones A (2003) Solar system abundances of the elements. *In:* Treatise on Geochemistry, Meteorites and Comets (eds) Holland HD, Turekian KK. Elsevier, Amsterdam. p 41–61

Palme H, O'Neill HStC (2003) Cosmochemical estimates of mantle composition. *In:* Treatise on Geochemistry, The Mantle and Core (ed) Carlson RW. Elsevier, Amsterdam. p 1–38

Pan P, Wood SA (1994) Solubility of Pt and Pd sulfides and Au metal in aqueous bisulfide solutions II. Results at 200° to 350°C and saturated vapor pressure. Miner Depos 29:373–390

Parkinson IJ, Pearce JA (1998) Peridotites from the Izu–Bonin–Mariana Forearc (ODP Leg 125): Evidence for Mantle Melting and Melt–Mantle Interaction in a Supra-Subduction Zone Setting. J Petrol 39:1577–1618

Pasteris JD (1981) Significance of sulfide textures and mineralogy in mantle xenoliths. Geol Soc Am Abstr Prog 13:526

Patterson C (1956) Age of meteorites and the earth. Geochim Cosmochim.Acta 10:230–237

Paulick H, Bach W, Godard M, De Hoog JCM, Suhr G, Harvey J (2006) Geochemistry of abyssal peridotites (Mid-Atlantic Ridge, 15°20' N, ODP Leg 209): implications for fluid/rock interaction in slow spreading environments. Chem Geol 234:179–210

Peach CL, Mathez EA, Keays RR (1990) Sulphide melt—silicate melt distribution coefficients for nickel and iron and implications for the distribution of other chalcophile elements. Geochim Cosmochim Acta 57:3013–3021

Pearson DG, Shirey SB (1999) Isotopic dating of diamonds. *In:* Application of Radiogenic Isotopes to Ore Deposit Research and Exploration. Lambert DD, Ruiz J (eds). Soc Econ Geol, Denver p 143-172

Pearson DG, Wittig N (2008) Formation of Archaean continental lithosphere and its diamonds: the root of the problem. J Geol Soc London 165:895–914

Pearson DG, Shirey SB, Carlson RW, Boyd FR, Pokhilenko P, Shimizu N (1995a) Re–Os, Sm–Nd, and Rb–Sr isotope evidence for thick Archaean lithospheric mantle beneath the Siberian craton modified by multistage metasomatism. Geochim Cosmochim Acta 59:959– 977

Pearson DG, Carlson RW, Shirey SB, Boyd FR, Nixon PH (1995b) Stabilization of Archean lithospheric mantle: A Re–Os isotope study of peridotite xenoliths from the Kaapvaal craton, Earth Planet Sci Lett 134:341–357

Pearson DG, Shirey SB, Harris JW, Carlson RW (1998) Sulphide inclusions in diamonds from the Koffiefontein kimberlite, S Africa: constraints on diamond ages and mantle Re–Os systematics. Earth Planet Sci Lett 160:311–326

Pearson DG, Shirey SB, Bulanova, GP, Carlson RW, Milledge HJ (1999a) Re–Os isotope measurements of single sulfide inclusions in a Siberian diamond and its nitrogen aggregation systematics. Geochim Cosmochim Acta 63:703–711

Pearson DG, Shirey SB, Bulanova GP, Carlson RW, Milledge HJ (1999b) Dating and paragenetic distinction of diamonds using the Re–Os isotope system: application to some Siberian diamonds. *In:* The PH Nixon Volume. Proceedings of the International Kimberlite Conference,7. Gurney JJ, Gurney JL, Pascoe MD, Richardson S. (eds) Red Roof Design, Cape Town, p 637–643

Pearson DG, Irvine GJ, Carlson RW, Kopylova MG, Ionov DA (2002). The development of lithospheric keels beneath the earliest continents: time constraints using PGE and Re–Os isotope systematics. *In:* The Early Earth: Physical, Chemical and Biological Development. Fowler CMR, Ebinger CJ, Hawkesworth CJ (eds). Geol Soc London, Bath

Pearson NJ, Alard O, Griffin WL, Jackson SE, O'Reilly SY (2002) In situ measurement of Re–Os isotopes in mantle sulfides by laser ablation multicollector-inductively coupled plasma mass spectrometry: analytical methods and preliminary results. Geochim Cosmochim Acta 66:1037–1050

Pearson DG, Irvine GJ, Ionov DA, Boyd FR, Dreibus GE (2004) Re–Os isotope systematics and platinum group element fractionation during mantle melt extraction: A study of massif and xenolith peridotite suites. Chem Geol 208:29–59

Pearson DG, Parman SW, Nowell GM (2007) A link between large mantle melting events and continent growth seen in osmium isotopes. Nature, 449: 202–205

Pearson DG, Canil D, Shirey SB (2014) Mantle samples included in volcanic rocks: xenoliths and diamonds. *In:* Treatise on Geochemistry. Holland HD, Turekian KK (eds). Elsevier, Amsterdam, 3, p 169–253

Peslier AH, Reisberg L, Ludden J, Francis D (2000) Re–Os constraints on harzburgite and lherzolite formation in the lithospheric mantle; a study of northern Canadian Cordillera xenoliths. Geochim Cosmochim Acta 64:3061–3071

Peters STM, Münker C, Wombacher F, Elfers B-M (2015) Precise determination of low abundance isotopes (^{174}Hf, ^{180}W and ^{190}Pt) in terrestrial materials and meteorites using multiple collector ICP-MS equipped with 10^{12} Ω Faraday amplifiers. Chem Geol 413:132–145

Peterson R, Francis D (1977) The origin of sulfide inclusions in pyroxene megacrysts: Am Mineral 62:1049–1051

Piña R, Gervilla F, Barnes SJ, Ortega L, Lunar R (2012) Distribution of platinum-group and chalcophile elements in the Aguablanca Ni–Cu sulfide deposit (SW Spain): evidence from a LA-ICPMS study. Chem Geol 302–303:61–75

Powell W, O'Reilly SY (2007) Metasomatism and sulfide mobility in lithospheric mantle beneath eastern Australia: implications for mantle Re–Os chronology. Lithos 94:132–147

Rehkämper M, Halliday AN, Alt J, Fitton JG, Zipfel J, Takazawa E (1999) Non-chondritic platinum group element ratios in ocean mantle lithosphere: petrogenetic signature of melt percolation? Earth Planet Sci Lett 172:65–81

Reisberg L, Lorand J-P (1995) Longevity of sub-continental mantle lithosphere from osmium isotope systematics in orogenic peridotite massifs. Nature 376:159–162

Reisberg LC, Allègre CJ, Luck J-M (1991) The Re–Os systematics of the Ronda Ultramafic Complex of Southern Spain. Earth Planet Sci Lett 105:196–213

Reisberg L, Lorand J-P, Bedini RM (2004) Reliability of Os model ages in pervasively metasomatized continental mantle lithosphere: a case study of Sidamo spinel peridotite xenoliths (East African Rift, Ethiopia). Chem Geol 208:119–140

Reisberg L, Zhi X, Lorand J-P, Wagner C, Peng Z, Zimmermann C (2005) Re–Os and S systematics of spinel peridotite xenoliths from east central China: evidence for contrasting effects of melt percolation. Earth Planet Sci Lett 239:286–308

Rhyzenko B, Kennedy GC (1973) The effect of pressure on the eutectic in the system Fe–FeS*. Am J Sci 273:803:810

Richardson SH (1986) Latter-day origin of diamonds of eclogitic paragenesis. Nature 322:623–626

Richardson SH, Harris JW (1997) Antiquity of peridotitic diamonds from the Siberian craton. Earth Planet Sci Lett 151:271–277

Richardson SH, Gurney JJ, Erlank AJ, Harris JW (1984) Origin of diamonds in old enriched mantle. Nature 310:198–202

Richardson SH, Erlank AJ, Harris JW, Hart SR (1990) Eclogitic diamonds of Proterozoic age from Cretaceous kimberlites. Nature 346:54–56

Richardson SH, Harris JW, Gurney JJ (1993) Three generations of diamonds from old continental mantle. Nature 366:256–258

Richardson SH, Shirey SB, Harris JW, Carlson RW (2001) Archean subduction recorded by Re–Os isotopes in eclogitic sulfide inclusions in Kimberley diamonds. Earth Planet Sci Lett 191:257–266

Richardson SH, Shirey SB, Harris JW (2004) Episodic diamond genesis at Jwaneng, Botswana, and implications for Kaapvaal craton evolution. Lithos 77:143–154

Richardson SH, Pöml PF, Shirey SB, Harris JW (2009) Age and origin of peridotitic diamonds from Venetia, Limpopo Belt, Kaapvaal–Zimbabwe craton. Lithos 112S:785–792

Righter K, Hauri EH (1998) Compatibility of Re in garnet during mantle melting and magma genesis, Science 280: 1737–1741

Roy-Barman M, Allègre CJ (1995) ^{187}Os/^{186}Os in oceanic island basalts: tracing oceanic crust recycling in the mantle. Earth Planet Sci Lett 129:145–161

Roy-Barman M, Wasserburg GJ, Papanastassiou DA, Chaussidon M (1998) Osmium isotopic compositions and Re–Os concentrations in sulphide globules from basaltic glasses. Earth Planet Sci Lett 154:331–347

Rudnick RL, McDonough WF, Chappell W (1993a) Carbonatite metasomatism in the Northern Tanzanian mantle: petrographic and geochemical characteristics. Earth Planet Sci Lett 114:463–475

Rudnick RL, Eldridge CS, Bulanova GP (1993b) Diamond growth history from *in situ* measurement of Pb and S isotopic compositions of sulphide inclusions. Geology 21:13–16

Rudnick RL, Walker RJ (2009) Interpreting ages from Re–Os isotopes in peridotites. Lithos 112S:1083–1095, doi:10.1016/j.lithos.2009.04.042

Ryabchikov ID, Ntaflos T, Kurat G, Kogarko LN (1995) Glass-bearing xenoliths from Cape Verde: evidence for a hot rising mantle jet. Mineral Petrol 55:217–237

Saal AE, Hart SR, Shimizu N, Hauri EH, Layne GD (1998) Pb Isotopic Variability in Melt Inclusions from Oceanic Island Basalts, Polynesia. Science 282: 1481–1484

Salters VJM, Stracke A (2004) Composition of the depleted mantle. Geochem Geophys Geosys 5(5) Q05B07 doi:10.1029/2003GC000597

Sarkar C, Pearson DG, Heaman LM, Woodland SJ (2015) Precise Pb isotope ratio determination of picogram-size samples: A comparison between multiple Faraday collectors equipped with 10^{12} Ω amplifiers and multiple ion counters. Chem Geol 395: 27–40

Schmidt G, Snow J (2002) Os isotopes in mantle xenoliths from the Eifel volcanic field and the Vogelsberg (Germany): age constraints on the lithospheric mantle. Contrib Mineral Petrol 143:694–705

Schmitz M, Bowring S, de Wit M, Garz V (2004) Subduction and terrane collision stabilize the western Kaapvaal craton tectosphere 2.9 billion years ago. Earth Planet Sci Lett 222:363–376

Schulze DJ, Harte B, EIMF staff, Page FZ, Valley JW, Channer DMDR, Jaques AL (2013) Anticorrelation between low δ^{13}C of eclogitic diamonds and high δ^{18}O of their coesite and garnet inclusions requires a subduction origin. Geology 41:455–458

Schwarzenbach EM, Gazel E, Caddick MJ (2014) Hydrothermal processes in partially serpentinized peridotites from Costa Rica: evidence from native copper and complex sulfur assemblages. Contrib Mineral Petrol 168:1079

Selby D, Creaser RA, Stein HJ, Markey RJ, Hannah JL (2007) Assessment of the 187Re decay constant by cross calibration of Re–Os molybdenite and U-Pb zircon chronometers in magmatic ore systems. Geochim Cosmochim Acta 71:1999–2013

Sen IS, Bizimis M, Sen G, Huang S (2011) A radiogenic Os component in the oceanic lithosphere? Constraints from Hawaiian pyroxenite xenoliths. Geochim Cosmochim Acta 75:4899–4916

Seyfried WE, Dibble WEJ (1980) Sea water—peridotite interaction at 300° C and 500 bars: implications for the origin of oceanic serpentinites. Geochim Cosmochim Acta 44:309–321

Seyler M, Lorand J-P, Toplis MJ, Godard G (2004) Asthenospheric metasomatism beneath the mid-ocean ridge: Evidence from depleted abyssal peridotites. Geology 34:301–304

Shen JJ, Papanastassiou DA, Wasserburg GJ (1996) Precise Re–Os determinations and systematics of iron meteorites. Geochim Cosmochim Acta 60:2887–900

Shirey SB, Richardson SH (2011) Start of the Wilson Cycle at 3 Ga Shown by Diamonds from Subcontinental Mantle. Science 333:434–436, doi: 10.1126/science.1206275

Shirey SB, Shigley JE (2013) Recent dvances in understanding the geology of diamonds. Gems and Gemology 49:188–222

Shirey SB, Walker RJ (1995) Carius tube digestion for low blank rhenium–osmium analysis. Anal Chem 34:2134–2141

Shirey SB, Walker RJ (1998) The Re–Os isotope system in cosmochemistry and high-temperature geochemistry. Annu Rev Earth Planet Sci 26:423–500

Shirey SB, Bender JF, Langmuir CH (1987) Three-component isotopic heterogeneity near the Oceanographer transform, Mid-Atlantic Ridge. Nature 325:217–223

Shirey SB, Carlson RW, Richardson SH, Menzies A, Gurney JJ, Pearson DG, Harris JW, Wiechert U (2001) Archean emplacement of eclogitic components into the lithospheric mantle during formation of the Kaapvaal craton. Geophys Res Lett 28:2509–2512

Shirey SB, Harris JW, Richardson SH, Fouch MJ, James DE, Cartigny P, Deines P, Viljoen F (2002) Diamond genesis, seismic structure, and evolution of the Kaapvaal–Zimbabwe craton. Science 297:1683–1686

Shirey SB, Richardson SH, Harris JW (2004a) Integrated models of diamond formation and craton evolution. Lithos 77:923–944

Shirey SB, Richardson SH, Harris JW (2004b) Age, paragenesis and composition of diamonds and evolution of the Precambrian lithosphere of southern Africa. S Af J Geol 107:91–106

Shirey SB, Richardson SH, Harris JW (2008) Mesoarchean to Mesoproterozoic Re–Os ages for sulfide inclusions in Orapa diamonds and implications for Kaapvaal-Zimbabwe craton development. *In:* Extended abstract of 9th International Kimberlite conference, A-00365

Shirey SB, Cartigny P, Frost DJ, Keshav S, Nestola F, Nimis P, Pearson DG, Sobolev NV, Walter MJ (2013) Diamonds and the geology of mantle carbon. Rev Mineral Geochem 75:355–421

Simon NSC, Neumann E-R, Bonadiman C, Coltorti M, Delpech G, Gregoire M, Widom E (2008) Ultra-refactory Domains in the Oceanic Mantle Lithosphere Sampled as Mantle Xenoliths at Ocean Islands. J Petrol 49:1223–1251

Skinner BJ, Peck DL (1969) An immiscible sulfide melt from Hawaii, in Wilson HD (ed) Magmatic ore deposits: Econ Geol Monogr 4:310–322

Smit KV, Shirey SB, Richardson SH, le Roex AP, Gurney JJ (2010) Re–Os isotopic composition of peridotitic sulphide inclusions in diamonds from Ellendale, Australia: Age constraints on Kimberley cratonic lithosphere. Geochim Cosmochim Acta 74:3292–3306

Smith CB, Gurney JJ, Harris JW, Otter ML, Robinson DN, Kirkley MB, Jagoutz E (1991) Neodymium and strontium isotope systematics of eclogite and websterite paragenesis inclusions from single diamonds. Geochim Cosmochim Acta 55:2579–2590

Smoliar MI, Walker RJ, Morgan JW (1996) Re–Os ages of Group IIA, IIIA, IVA, and IVB iron meteorites. Science 271:1099–102

Snow JE, Dick HJB (1995) Pervasive magnesium loss by marine weathering of peridotite. Geochim Cosmochim Acta 59:4219–4235

Snow JE, Reisberg L (1995) Os isotopic systematics of the MORB mantle: results from altered abyssal peridotites. Earth Planet Sci Lett 133:411–421

Snow JE, Schmidt G (1998) Constraints on Earth accretion deduced from noble metals in the oceanic mantle. Nature 391:166–169

Sobolev NV (1974) Deep-seated Inclusions in Kimberlites and the Problem of the Composition of the Upper Mantle. Nauka, Novosibirsk. p 264 (in Russian)

Sobolev NV (1977) Deep-seated inclusions in kimberlites and the problem of the composition of the upper mantle, Am Geophys. Union, Washington

Sobolev NV, Laurent'ev Yu G, Pokhilenko NP (1973) Chrome rich garnets from the kimberlites of Yakutia and their paragenesis. Contrib Mineral Petrol 40:39–52

Sobolev AV, Hofmann AW, Sobolev SV, Nikokosian IK (2005) An olivine-free mantle source of Hawaiian shield basalts. Nature 434:590–597

Sobolev AV, Hofmann AW, Kuzmin DV, Yaxley GM, Arndt NT, Chung S-L, Danyushevsky LV, Elliott T, Frey FA, Garcia MO, Gurenko AA, Kamenetsky VS, Kerr AC, Krivolutskaya NA, Matvienkov VV, Nikogosian IK, Rocholl A, Sigurdsson IA, Sushchevskaya NM, Teklay M (2007) The amount of recycled crust in mantle derived melts. Science 316:412–417

Stachel T, Harris JW (2008) The origin of cratonic diamonds-constraints from mineral inclusions: the genesis of gem deposits. Ore Geology Rev 34:5–32

Stachel T, Luth RW (2015) Diamond Formation—Where, when and how? Lithos doi: 10.1016/j.lithos.2015.01.028

Stachel T, Harris JW, Tappert R, Brey GP (2003) Peridotitic diamonds from the Slave and the Kaapvaal cratons-similarities and differences based on a preliminary data set. Lithos 71:489–503

Standish JJ, Hart SR, Blusztajn J, Dick HJB, Lee KL (2002) Abyssal peridotite osmium isotopic compositions from Cr-spinel. Geochem Geophys Geosys 3(1) 10.1029/2001GC000161

Stixrude L, Lithgow-Bertelloni C (2012) Geophysics of chemical heterogeneity in the mantle, Annu Rev Earth Pl Sc 40:569–595, doi: 10.1146/annurev.earth.36.031207.124244

Stracke A, Snow JE, Hellebrand E, von der Handt A, Bourdon B, Birbaum K, Günther, D (2011) Abyssal peridotite Hf isotopes identify extreme mantle depletion. Earth Planet Sci Lett 308:359–368

Sun SS, Hanson GN (1975) Evolution of the mantle: geochemical evidence from alkali basalt. Geology 3:297–302

Szabó CS, Bodnar RJ (1995) Chemistry and origin of mantle sulfides in spinel peridotite xenoliths from alkaline basaltic lavas, Nògràd-Gömör volcanic field, northern Hungary and southern Slovakia. Geochim Cosmochim Acta 59:3917–3927

Thomassot E, Cartigny P, Harris RW, Lorand J-P, Rollion-Bard C, Chaussidon M (2009) Metasomatic diamond growth: A multi-isotope study (^{13}C, ^{15}N, ^{33}S, ^{34}S) of sulphide inclusions and their host diamonds from Jwaneng (Botswana). Earth Planet Sci Lett 282:79–90

Tyler I, Page R, Griffin T (1999) Depositional age and provenance of the Marboo Formation from SHRIMP U–Pb zircon geochronology: implications for the early Palaeoproterozoic tectonic evolution of the Kimberley region, Western Australia. Precamb Res 95:225–243

Usselman TM (1975) Experimental approach to the state of the core: Part I. The liquidus relations of the Fe-rich portion of the Fe–Ni–S system from 30 to 100 kb. Am J Sci 275:278–290

Vakhrushev VA, Prokoptsev NG (1972) Primary magmatic formations in basalts from oceanic crust and inclusions of ultrabasic rocks in basalts. Int Geol Rev 14: 125–135

Vakhrushev VA, Sobolev NV (1973) Sulfidic formations in deep xenoliths from kimberlite pipes in Yakutia. Int Geol Rev 15:103–110

van Acken D, Becker H, Walker RJ (2008) Refertilization of Jurassic oceanic peridotites from the Tethys Ocean—implications for the Re–Os systematics of the upper mantle. Earth Planet Sci Lett 268:171–181

van Acken D, Becker H, Walker RJ, McDonough WF, Wombacher F, Ash RD, Piccoli PM (2010a) Formation of pyroxenite layers in the Totalp ultramafic massif (Swiss Alps)—Insights from highly siderophile elements and Os isotopes. Geochim Cosmochim Acta 74:661–683

van Acken D, Becker H, Hammerschmidt K, Walker RJ, Wombacher F (2010b) Highly siderophile elements and Sr–Nd isotopes in refertilized mantle peridotites - A case study from the Totalp ultramafic body, Swiss Alps. Chem Geol 276:257–268

van Acken D, Humayun M, Brandon AD, Peslier AH (2012) Siderophile trace elements in metals and sulfides in enstatite achondrites record planetary differentiation in an enstatite chondritic parent body. Geochim Cosmochim Acta 83:272–291

van der Hilst R, Kennett B, Shibatani T (1998) Upper mantle structure beneath Australia from portable array deployment. *In:* Structure and Evolution of the Australian Continent. Doolet J, Goleby J, van der Hilst B, Klootwijk R (eds). Am Geophys Union, Washington, DC, p 39–57

Walker RJ (2009) Highly siderophile elements in the Earth, Moon and Mars: update and implications for planetary accretion and differentiation. Chemie der Erde 69:101–126

Walker RJ, Morgan JW (1989) Rhenium osmium isotope systematics of carbonaceous chondrites. Science 243:519–22

Walker RJ, Carlson RW, Shirey SB, Boyd FR (1989) Os, Sr, Nd, and Pb isotope systematics of Southern African peridotite xenoliths; implications for the chemical evolution of subcontinental mantle. Geochim. Cosmochim. Acta 53:1583–95

Walker RJ, Horan MF, Morgan JW, Becker H, Grossman JN, Rubin AE (2002a) Comparative ^{187}Re–^{187}Os systematics of chondrites: implications regarding early solar system processes. Geochim Cosmochim Acta 66:4187–4201

Walker RJ, Prichard HM, Ishiwatari A, Pimentel M (2002b) The osmium isotopic composition of convecting upper mantle deduced from ophiolite chromites. Geochim Cosmochim Acta 66:329–345

Wang KL, O'Reilly SY, Griffin WL, Pearson NJ, Zhang M (2009) Sulfides in mantle peridotites from Penghu Island, Taiwan: melt percolation, PGE fractionation, and the lithospheric evolution of the South China block. Geochim Cosmochim Acta 73:4531–4557

Warren JM (2015), Global Variations in Abyssal Peridotite Compositions, Lithos, submitted

Warren JM, Shirey SB (2012) Lead and osmium isotopic constraints on the oceanic mantle from single abyssal peridotite sulfides. Earth Planet Sci Lett 359–360:279–293

Warren JM, Shimizu N, Sakaguchi C, Dick HJB, Nakamura E (2009) An assessment of upper mantle heterogeneity based on abyssal peridotite isotopic compositions. J Geophys Res 114(B12203)

Westerlund KJ, Gurney JJ, Carlson RW, Shirey SB, Hauri EH, Richardson SH (2004) A metasomatic origin for late Archean eclogitic diamonds: implications from internal morphology of Klipspringer diamonds and Re –Os and S isotope characteristics of their sulfide inclusions. S Afr J Geol 107:119–130

Westerlund KJ, Shirey SB, Richardson SH, Carlson RW, Gurney JJ, Harris JW (2006) A subduction wedge origin for Paleoarchean peridotitic diamonds and harzburgites from the Panda kimberlite, Slave craton: evidence from Re–Os isotope systematics. Contrib Mineral Petrol 152:275–294. doi:10.1007/s00410-006-0101-8

White RW (1966) Ultramafic inclusions in basaltic rocks from Hawaii. Contrib Mineral Petrol 12: 245–314

Wicks FJ, Whittaker EJW (1977) Serpentinite textures and serpentinization. Can Mineral 15:459–488

Widom E, Kepezhinskas P, Defant M (2003) The nature of metasomatism in the sub-arc mantle wedge: evidence from Re–Os isotopes in Kamchatka peridotite xenoliths. Chem Geol 196:283–306

Wiggers de Vries DF, Pearson DG, Bulanova GP, Smelov AP, Pavlushin AD, Davies GR (2013) Re–Os dating of sulphide inclusions zonally distributed in single Yakutian diamonds: Evidence for multiple episodes of Proterozoic formation and protracted timescales of diamond growth. Geochim Cosmochim Acta 120:363–394

Wilshire HG, Meyer CE, Nakata JK, Calk LC, Shervais LW, Nielson JW, Schwarzman EG (1988) Mafic and Ultramafic Xenoliths from Volcanic Rocks of the Western United States. US Geological Survey Professional Paper 1443. p 1–179

Wood SA (1987) Thermodynamic calculations of the volatility of the platinum group elements (PGE): the PGE content of fluids at magmatic temperatures. Geochim Cosmochim Acta 51:3041–3050

Worden K, Carson C, Scrimgeour I, Lally J, Doyle N (2008) A revised Palaeoproterozoic chronostratigraphy for the Pine Creek Orogen, Northern Australia: evidence from SHRIMP U–Pb zircon geochronology. Precamb Res 166:122–144

Workman RK, Hart SR (2005) Major and trace element composition of the depleted MORB mantle (DMM). Earth Planet Sci Lett 231:53–72

Yaxley GM, Kamenetsky V (1999) *In situ* origin for glass in mantle xenoliths from south-eastern Australia: insights from the trace element compositions of glasses and metasomatic phases. Earth Planet Sci Lett 172:97–109

Yefimova ES, Sobolev NV, Pospelova LN (1983) Sulfide inclusions in diamonds and specific features of their paragenesis. Zap Vses Mineral Ova 112:300–310

Zangana NA, Downes H, Thirwall MF, Hegner E (1997) Relationship between deformation, equilibration temperatures, REE and radiogenic isotopes in mantle xenoliths (Ray Pic, Massif Central, France): an example of plume-lithosphere interaction? Contrib Mineral Petrol 127:187–203

Zartman RE, Richardson SH (2005) Evidence from kimberlitic zircon for a decreasing mantle Th/U since the Archean. Chem Geol 220:263–283

Zindler A, Hart S (1986) Chemical Geodynamics. Annu Rev Earth Planet Sci 14:493–571